DOCTOR OF PHILOSOPHY

Mathematical Modelling of Cancer Growth and Development
Adhesion, Stem Cells and Structure

Kelly, John

Award date:
2014

Mathematical Modelling of Cancer Growth and Development: Adhesion, Stem Cells and Structure

By

John Watson Kelly

Doctor of Philosophy

Division of Mathematics

University of Dundee

Dundee

September 2014

Contents

Acknowledgements

I would like to thank my supervisors Professor Mark Chaplain and Professor Inke Nathke for giving me the opportunity to carry out my PhD at the University of Dundee. Most importantly, I thank Professor Chaplain for his continuing support throughout the entire four years of my PhD. I could not have asked for a better or more understanding supervisor.

I would also like to thank everyone in the mathematics department that I have had the privilege of working with throughout my academic career. I will miss the coffee breaks, lunch times and trips to the pub that made my time here more enjoyable and I will miss the friendly culture within the department. I especially would like to thank Nick who was always available to help with IT problems, but also to chat about weird and wonderful subjects. I would also like to thank everyone in the Nathke laboratory for welcoming me to the lab and for helping me to carry out the experimental work within this thesis.

Lastly and most importantly I would like to thank my fiancée Iona, without whom this thesis would never have been completed. The long nights of helping me to draft and redraft the thesis from top to bottom, as well as providing vital emotional support during all of the ups and downs of my PhD paid off and I am eternally grateful for having such

a wonderful person to share my life with.

Declaration

I declare that the following thesis is my own composition and that it has not been submitted before in application for a higher degree.

John Watson Kelly

Certification

This is to certify that John Kelly has complied with all the requirements for the submission of this Doctor of Philosophy thesis to the University of Dundee.

Professor Mark A.J. Chaplain

Professor Inke Nathke

Abstract

This thesis has investigated some of the intricacies of the growth and development of a solid tumour. Mathematical models and biological experimentation were used to gain a better understanding of the dual roles that the proto-oncogenic protein β-catenin has in adhesion and transcription, as well as its involvement in the epithelial-mesenchymal transition. Emphasis was placed on the spatial location of β-catenin within cells to determine what function it is performing. A model was also created to explore the hypothesis that multiple forms of β-catenin exist within cells to perform separate functions. The cancer stem cell hypothesis was explored in solid tumour growth, without necrosis and angiogenesis, by the use of a discrete, cell-based model created with the software package CompuCell3D. This was compared to a novel continuum model, which can be used to perform *in silico* experiments of solid tumours with a stem-progenitor-mature cell structure for a biologically relevant number of cells. Lastly, a cell-based model of a solid, vascularised tumour was created in CompuCell3D to investigate how an age- and size-structured population of cells can affect the overall growth of the tumour. This model was also used to show how the age structure of cells in a solid tumour can affect the efficacy of chemotherapeutic treatments.

Chapter 1

Introduction

A tumour can be described as: an abnormal mass of tissue whose growth exceeds that of normal tissue, is uncoordinated with that of the normal tissue, and persists in the same excessive manner after cessation of the stimuli which evoke the change. [MacSween and Whaley (1992)]. Mathematical modelling is a useful tool to work in conjunction with biological and clinical experimentation to gain insight into the workings of cancer.

Tumour growth has several stages: avascular, angiogenesis and invasion and metastasis. Malignant growth occurs when the tumour invades the surrounding tissue in a destructive fashion. From here, cells can enter the blood or lymphatic systems and travel around the body before beginning a new tumour in a different part of the body. This process is known as metastasis and makes treatment extremely difficult. Therefore, the study of cancer invasion is necessary to prevent the deadly spread of the disease. In this thesis, several aspects of tumour growth are studied to examine how cancer can invade surrounding tissue with a view to better clinical treatments.

Chapters 2 and 3 provide background knowledge in the fields of biology and mathematical modelling, respectively. Chapter 4 examines the E-cadherin/β-catenin pathway, which governs cell-cell adhesion, and can lead to the epithelial-mesenchymal transition. This process is necessary for normal functions such as development and wound healing but it can be hi-jacked by cancer cells to increase their motility and invasiveness. Mathematical modelling and biological experimentation were used to gain insight into this pathway, which is implemented in Chapters 5 and 6. Chapter 5 examines the cancer stem cell hypothesis using continuum and discrete mathematical models of avascular tumours and has implications for the treatment of cancers. Chapter 6 develops a discrete multi-scale mathematical model of a vascularised tumour in order to examine how age and size structure effects growth and also includes a study of chemotherapy treatments. Finally, Chapter 7 discusses the findings of the thesis and explores future work which could be undertaken.

Chapter 2

Biological Background

2.1 The cell

Cells are the basic building block of all living matter on earth and due to this it is essential that the processes they perform and the systems they contribute to are studied and understood. The two major types of cells are prokaryotic and eukaryotic. Humans, as well as animals, plants, fungi and protozoans, are comprised of eukaryotic cells and are called eukaryotes. The defining factor of a eukaryotic cell is that it contains a nucleus which is enclosed by a membrane to separate it from the rest of the cell. Surrounding the nucleus is the cytoplasm, which itself is surrounded by a flexible phospholipid bilayer known as the plasma membrane. Along with the nucleus, cells also have other membrane-bound organelles that each perform separate functions. Figure 2.2 shows a detailed schematic of the eukaryotic cell.

The nucleus is the largest organelle and contains the DNA of the cell. DNA stores all

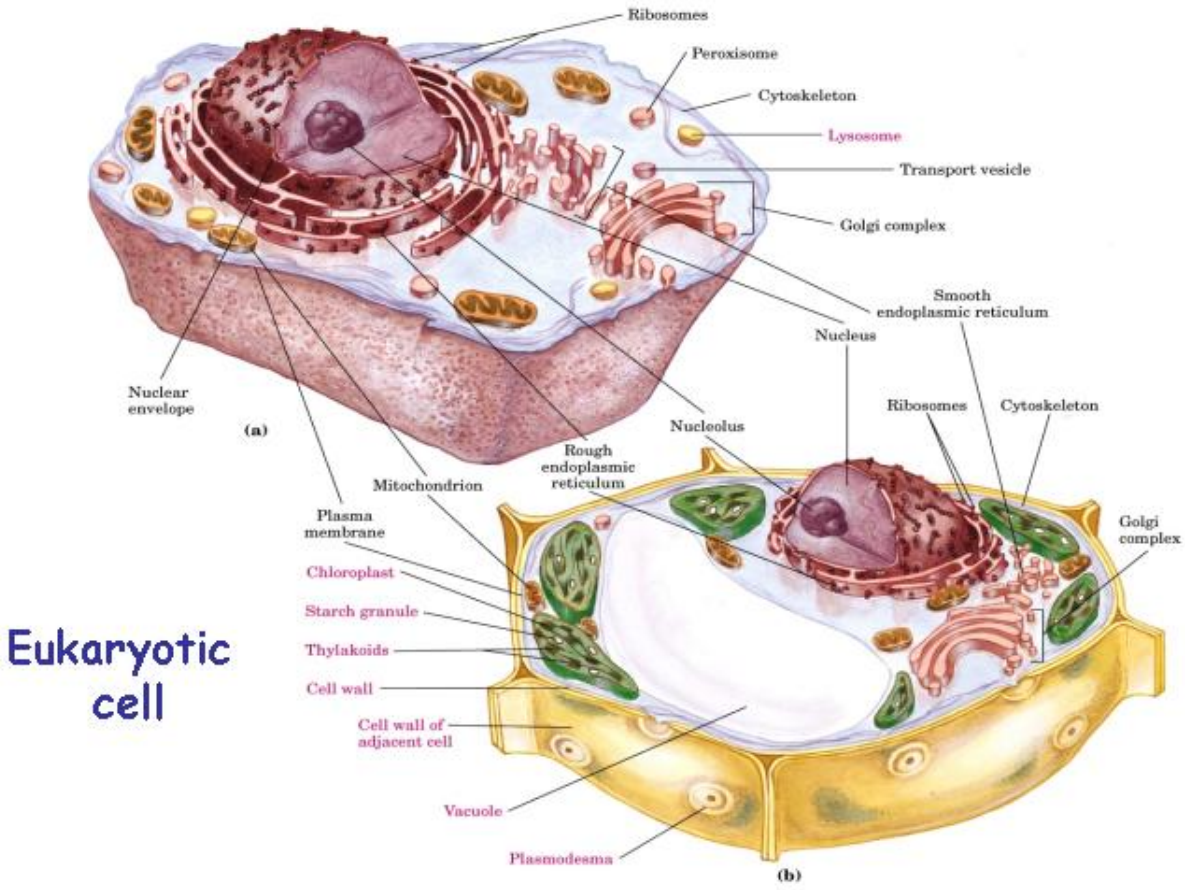

Figure 2.1: *A detailed schematic of the eukaryotic cell showing many of its components. Image taken from migration.wordpress.com/page/54/.*

of the genetic information that defines the entire organism as well as the cells functions. The main role or function of DNA is to produce proteins. The process begins with the transcription of the DNA into messenger RNA (mRNA) which is transported out of the nucleus into the cytoplasm. The mRNA is then translated into a protein by ribosomes at the endoplasmic reticulum. When the protein is completely built it is transported by vesicles to the Golgi apparatus where it is sorted before being sent to the location in which it will function.

The major success of the cell is the ability to replicate the DNA in a hereditary fashion by dividing into two daughter cells, which then can produce multicellular organisms. This process is known as mitosis and is tightly controlled by a number of proteins which respond to internal and external factors. This gives rise to the cell cycle, which is divided into four stages. A newly divided cell begins in the first gap phase, G1. During this time the cell grows and produces mRNA and proteins. The cell then begins the synthesis phase, S, in which the DNA is replicated. This is completed when every chromosome has been copied, effectively meaning that the amount of DNA within the cell has doubled. The cell then enters the second gap phase and continues to grow until the cell reaches its designated size. If it is the appropriate size and external and internal factors allow, the cell then enters the mitotic or M-phase and divides into two daughter cells. This is a relatively short phase and is further subdivided into the prophase, prometaphase, metaphase, anaphase, telophase and cytokinesis. A fifth phase called G0 is often considered as part of the cell cycle in which the cell stops preparing for cell division and is known to be resting. This happens in two ways: cells can become senescent (i.e. old), because there is irreparable cell damage or degradation caused by too many divisions; or a cell becomes quiescent, because external factors do not favour division. These include low levels of nutrient, low levels of growth factors and the presence of

anti-growth factors secreted by neighbouring cells.

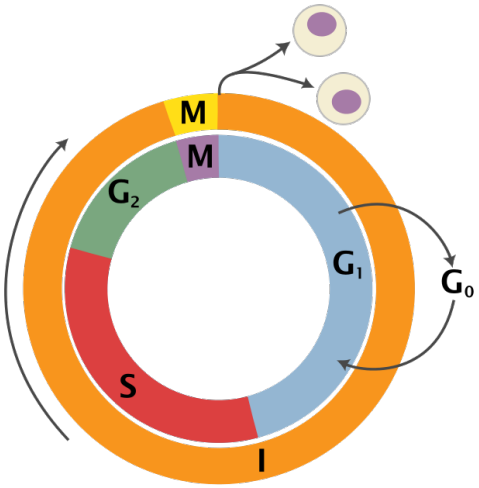

Figure 2.2: *Schematic of the cell cycle. On the outer circle, 'I' represents the interphase between cell division and 'M' shows where mitosis occurs. The inner circle shows that the interphase is broken up into the phases: G1, S and G2. The resting phase, G0, is also shown. Reproduced from http://upload.wikimedia.org/wikipedia/commons/d/d0/Cell_Cycle_2.svg in accordance with GNU Free Documentation license.*

.

2.2 The epithelial cell

Cells within the body are grouped together into five major classes of tissue: epithelial, connective, muscular, neural and blood [Lodish et al. (2012)]. The epithelial cells form the lining of the organs in the body such as the lungs, heart, blood vessels, bladder and digestive tract. This protects and separates the contents of the organs from other external objects and allows for the transport of nutrients and fluids. Epithelial cells are generally cuboidal or columnar in shape and have an apical-basal polarity. There are several types of junctions which connect each of the cells with their neighbours and the connective

tissue. These can be seen in Figure 2.3.

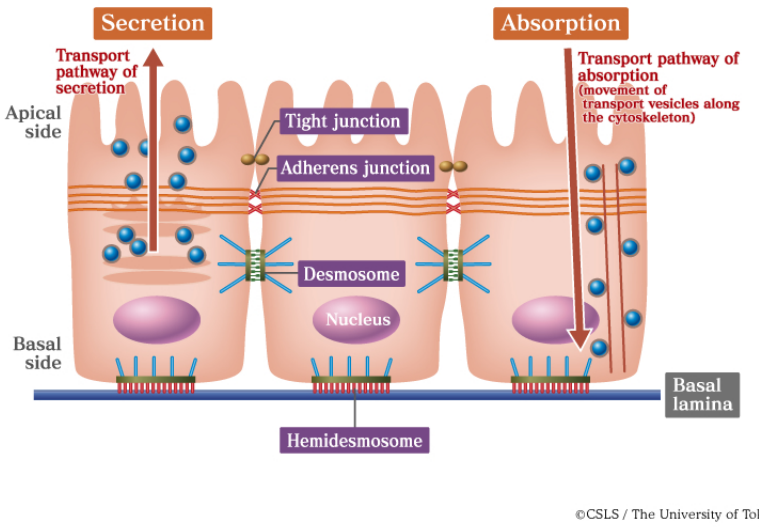

Figure 2.3: *Schematic of epithelial cells which shows apical-basal polarity and the junctions. Tight junctions seal the gaps between cells and adherens junctions bind the cytoskeletons to provide strength across the epithelial layer. Each cell is connected to the basal lamina by hemidesmosomes. Image taken from the University of Tokyo College of Life Sciences web textbook.*

Beneath the epithelial layer is the basal lamina (or basement membrane) upon which the cells form anchoring junctions. These provide strength by allowing the transmission of stresses. It also determines the polarity as it is situated at the basal side of the cells [Alberts (2008)].There are three main types of junctions for cell-cell interactions. These are channel forming, occluding and anchoring junctions. Channel forming junctions create passageways between the cytoplasm in neighbouring cells and allow for the transport of small molecules. Occluding junctions are known as tight junctions in animal tissues and are situated at the apical edge of the cell sealing the gap between cells to form a barrier. Anchoring junctions link the cytoskeletons of cells to transmit stress across the entire

epithelial layer. These include adherens junctions which connect to actin filaments and desmosomes which connect intermediate filaments. The most studied of these are adherens junctions, which are constructed by adhesion proteins called cadherins, named because they are calcium dependent adherins. There are hundreds of known cadherin proteins and each has a specific role depending on where they perform a task. Epithelial cadherin (E-cadherin) is the main cell-cell adhesion protein in adherens junctions and is a marker for epithelial cells. They are also a key factor in determining and maintaining the polarity of the cell.

2.2.1 E-cadherin and β-catenin

E-cadherin is a classical cadherin that is expressed in all epithelial tissues and, when engaged in adhesion, it is an inter-membrane protein. The extracellular region is formed by a unit of five cadherin repeats which are joined by hinges. Calcium ions bind to sites near each hinge to prevent it from flexing and the result is a rigid, slightly curved rod [Alberts (2008)]. The extracellular E-cadherin binds homophilically with that of the neighbouring cell in a 'velcro'-like fashion which uses many weak bonds to form strong adhesion between the cells. The intracellular tail of E-cadherin connects to the actin cytoskeleton of the cell through several proteins know as catenins. The most notable of the catenins that link E-cadherin to the actin cytoskelton is β-catenin. Figure 2.4 shows a schematic of the roles of E-cadherin and other proteins when engaged in adhesion.

β-catenin exists in the cytoplasm and functions at the membrane and in the nucleus of the cell. At the membrane β-catenin is bound to E-cadherin where it is important in cell-cell adhesion. When it is in the cytoplasm β-catenin is controlled by a destruction complex, which targets it for degradation. When in the nucleus it is associated with

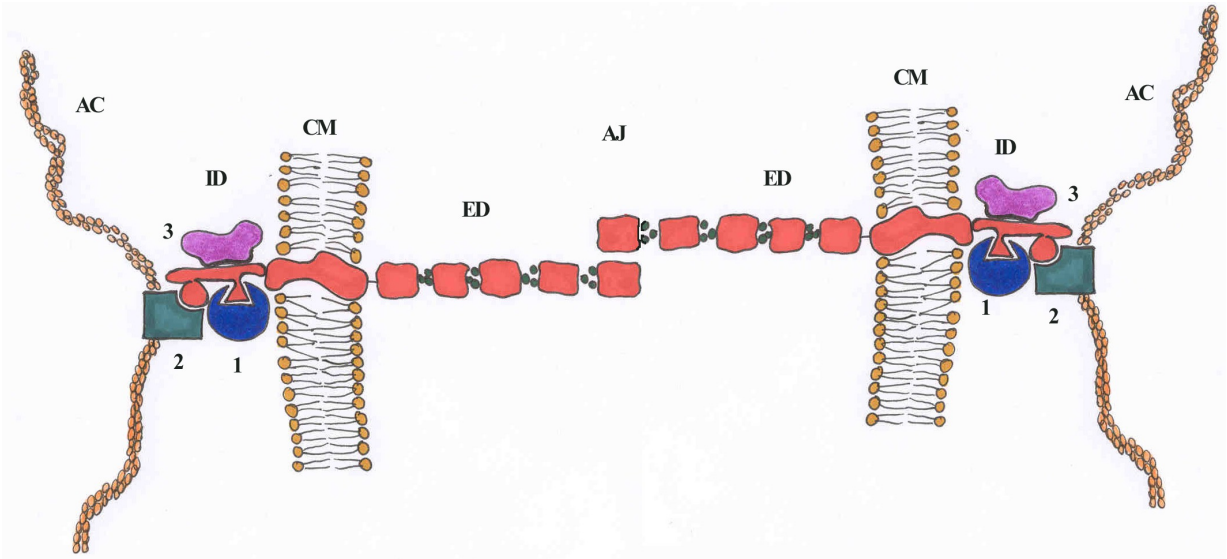

Figure 2.4: *Schematic of E-cadherin the other proteins involved cell-cell adhesion at adherens junctions. AJ = Adherens Junction, ED = Extracellular Domain, CM = Cell Membrane, ID = Intracellular Domain, AC = Actin Cytoskeleton, 1 = β-catenin, 2 = α-catenin and 3 = p120-catenin. Image reproduced from Pecina-Slaus (2003) in accordance with the Open Access licence.*

the LEF/TCF transcription factors which contributes to cell proliferation and motility [Weinberg (2007)]. The roles of E-cadherin and the destruction complex are to keep the levels of free β-catenin low to prevent it from entering the nucleus, in order to stop transcriptional activities. It is this control mechanism which has led to a great deal of interest in the E-cadherin-β-catenin pathway.

E-cadherin and β-catenin are known to bind to each other immediately after production in the endoplasmic reticulum [Hinck et al. (1994), Näthke et al. (1994)]. The complex is then trafficked to the membrane through vesicles where it is ready to take part in cell-cell adhesion. When cell-cell contact occurs, it can then bind to other proteins, such as α-catenin and p120-catenin, to form an adherens junction. Upon junction disassembly, the complex is broken by endocytosis. The proteins can then be recycled for use in cell-cell adhesion, they can degrade or they can remain free in the cytoplasm to perform other

tasks. As mentioned above, the free β-catenin is controlled by a destruction complex. This is comprised of axin, GSK3β and APC and it phosphorylates β-catenin to target it for ubiquination, thereby guaranteeing a rapid destruction. However, the destruction complex can be deactivated by the presence of proteins in the Wnt family. When Wnt proteins bind to the Frizzled receptors at the cell membrane, the Dishevelled protein works to suppress the activity of GSK3β which phosphorylates β-catenin. Therefore, β-catenin is saved from rapid destruction and a cytoplasmic pool is allowed to stabilise. If this pool reaches a critical threshold, some of the β-catenin molecules will be able to enter the nucleus to bind with LEF/TCF transcription factors, promoting the transcription of several genes. A schematic of these process can be seen in Figure 2.5. This is an important process as it can allow the cell to perform certain tasks, for example, division and migration.

2.2.2 The epithelial to mesenchymal transition

As described above, epithelial cells are extremely important in many functions within the human body because of their ability to form protective sheets of tissue. However, it is often necessary for epithelial cells to break their adhesive bonds and migrate away from the epithelial layer in which they originate. The process which governs this change is called the epithelial-mesenchymal transition (EMT).

Epithelial cells form strong bonds to neighbouring cells and the basement membrane. Undergoing EMT transforms the epithelial cells into cells of the mesenchymal phenotype, breaking these adhesive bonds. The mesenchymal cells are characterised by an increased resistance to apoptosis and an ability to migrate and invade other tissues. This

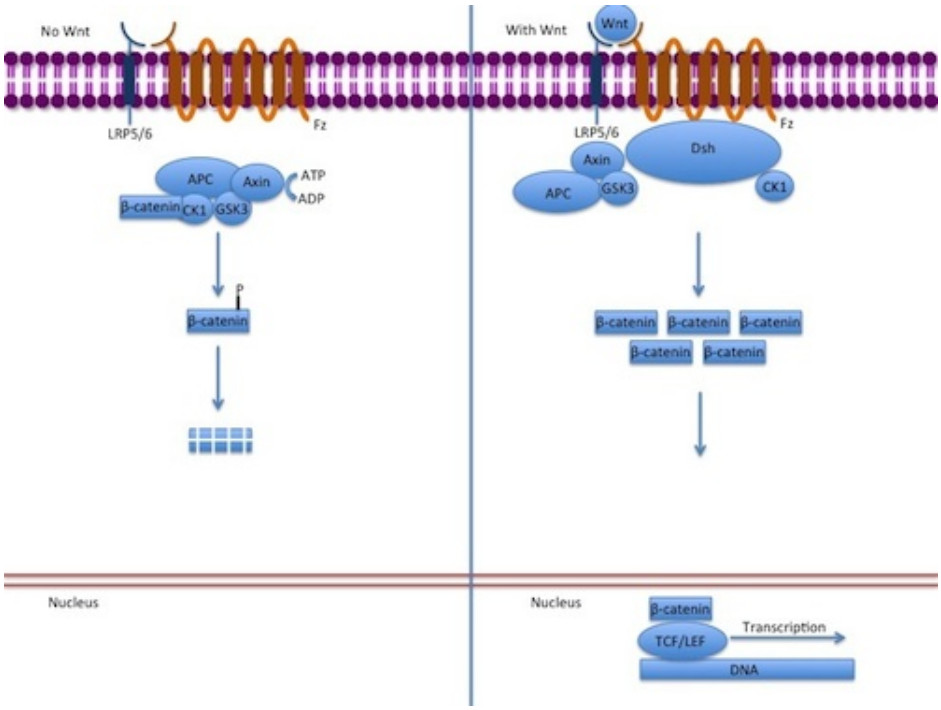

Figure 2.5: *Figure showing the effect of Wnt signalling on β-catenin in the cytoplasm. When Wnt is not present β-catenin is targeted for rapid destruction by a complex of APC, Axin and GSK3. However, when Wnt is present the destruction complex is interrupted and β-catenin is allowed to build up in the cytoplasm. From here it can translocate to the nucleus where it can bind to TCF/LEF to begin transcription. Image by Gpruett2 reproduced from http://commons.wikimedia.org/wiki/File:Canonical_Wnt_pathway_%3D375px).jpg in accordance with the Creative Commons Attribution License.*

occurs through several molecular processes such as the activation of transcription factors, reorganisation of cytoskeleton proteins and the production of extra cellular matrix degrading enzymes. The epithelial markers such as E-cadherin, ZO-1 and Type IV collagen are lost and replaced by mesenchymal markers such as N-cadherin, β-catenin and LEF-1. Due to this process the cuboidal shape of the cells is lost and altered into a form which is able to migrate through the connective tissue. Figure 2.6 shows a schematic of the epithelial-mesenchymal transition.

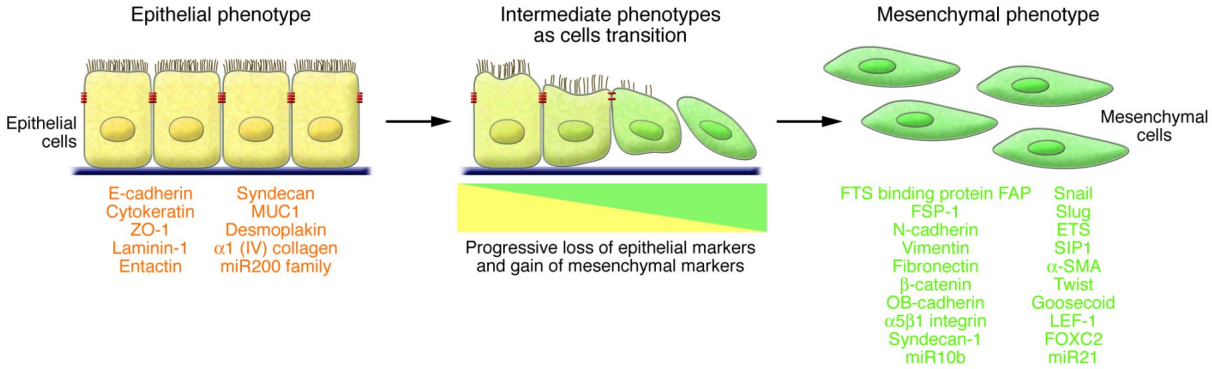

Figure 2.6: *Schematic of the changes that take place in the Epithelial-Mesenchymal Transition which shows protein markers for each phenotype. Reproduced with copyright permission from Kalluri and Weinberg (2009).*

EMT was first described through a model studying chick primitive streak formation in Hay (1995) and has since been classified into three different subtypes: type I, developmental; type II, fibrosis and tissue regeneration; and type III, cancer invasion and metastasis. Type I EMTs occur during implantation, embryo formation and organ development and are necessary to create a diversity of cell types. The important function of this type of EMT is the ability to migrate and generate a secondary epithelial layer through the reverse process called Mesenchymal to Epithelial transition (MET). Type II EMTs respond to tissue inflammation and damage and cease to proliferate once the inflammation has subsided. Due to this process, fibroblasts and other associated cells

are generated which can reconstruct the tissue from an injury. Type III EMTs occur in cancerous cells and can allow the cells to break through basal lamina and other protective membrane layers. For example, they can break through to the blood and lymphatic system, allowing for the creation of colonies in other parts of the body. This process is known as metastasis. Metastasis is the final stage of cancer development where the hosts defences are overwhelmed, eventually making the disease incurable.

Each subtype of the epithelial to mesenchymal transition is important to study and for an excellent review see Kalluri and Weinberg (2009). However, the type that is most important to this work is type III which can generate aggressive cancer cells [Wolf et al. (2007)]. For a review into the study of the Epithelial-Mesenchymal Transition in cancer invasion see Friedl and Wolf (2003) and Friedl and Wolf (2008).

2.3 Development of cancer

Cancer develops from a mutation of a single cell. This can be induced through a variety of factors including: disease, genetic predisposition and exposure to radiation or other carcinogens. This mutated cell then develops several traits which enables it and its progeny to become cancerous. Hanahan and Weinberg (2000) described six traits, known as the hallmarks of cancer, which are believed to be acquired by all cancer cells. These were described as: self-sufficiency in growth signals, insensitivity to anti-growth signals, evasion of apoptosis, limitless replicative potential, sustained angiogenesis, and invasion and metastasis of tissue.

Growth signals are important in the development and maintenance of normal tissue. Cells require the presence of growth signals to allow them to leave a quiescent state and

become proliferative. The presence of anti-growth signals is also important to maintain the number of cells required for the proper functioning of the organ or tissue in question. However, the first two hallmarks of cancer allow cells to provide their own growth signals and also ignore the anti-growth signals of the surrounding tissue. Therefore, cancer cells can be continuously proliferative and avoid a quiescent state as long as there are enough nutrients in the local environment.

Apoptosis, or programmed cell death, allows for cells that have been damaged irreparably to be disposed of in a manner which causes no harm to the surrounding tissue. A key protein that is part of the decision making process to begin apoptosis is p53, also known as the 'guardian of the genome' [Lane (1992)]. The loss of p53 functions in cancer cells is one of the main routes in which apoptosis can be avoided. Therefore, the tumour can continue to grow unimpeded by the body's attempts to destroy it.

The fourth hallmark, limitless replicative potential, works in conjunction with the trait of avoiding apoptosis to allow unbounded growth. After a number of cellular divisions, cells enter a phase known as replicative senescence [Alberts (2008)]. This occurs when too many cell divisions damage the DNA to the point where it is impossible to undergo mitosis once more. The number of divisions at which this happens is known as the Hayflick limit (Hayflick (1997)). However, cancer cells develop the ability to divide without limit which is increasingly seen to be caused by the protection of chromosomes by telomeres [Blasco (2005)]. With this ability a tumour cell is able to divide indefinitely, until the death of the host.

Sustained angiogenesis, the fifth hallmark, is important for the acquisition of nutrients to allow tumour cells to grow and divide. Oxygen and other nutrients are supplied to tumours by capillary blood vessels. Newly formed tumours are small and have enough

nutrient supply from nearby capillaries. However, when the tumour increases in size the nutrient levels at the centre will become critically low in that they will be unable to sustain cell proliferation and growth. These cells will become quiescent until the environment provides enough nutrients for them to re-enter the cell cycle. If the nutrient level drops to this critical level, in which the cell is no longer able to survive, then the cells die and become necrotic. However, to avoid death, cancer cells are able to encourage the growth of new blood vessels through angiogenesis, such that capillaries enter the tumour, providing vital extra nutrient. When the tumour is vascularised it is no longer limited by nutrient supply, allowing the invasion of the surrounding tissue, while still continuing its angiogenic activities.

The final hallmark, and also the final stage of cancer growth, recognises the ability of cancer cells to detach themselves from the primary tumour in order to invade further into surrounding tissue. This local invasion, combined with intravasation into blood and lymph vessels, enables the cancer cells to travel great distances around the body and form secondary tumours. One of the important sources of this hallmark is the epithelial to mesenchymal transition (EMT). This removes the E-cadherin to break cell-cell adhesion resulting in a motile and invasive cell. It can then enter the blood or lymphatic system to be transported around the body where it will recruit helper cells from the host to begin a new tumour in an area where nutrients and space are less limited. The previously discussed acquired traits will also aid the formation of the new tumour and will lead to the death of the host.

The six hallmarks of cancer have all provided exciting avenues for researchers to discover and explain the mechanisms that cancers use to grow and invade, with a view to finding effective methods for the treatment of patients. These traits were updated in Hanahan and Weinberg (2011) to discuss the advancements that have been made and

also to include two new emerging hallmarks of cancer. These are the abilities to avoid destruction by the immune system and to deregulate cellular energetics. Another important theory discussed by the authors is the possible existence of cancer stem cells, hypothesising that newly formed tumours are not comprised of a homogeneous set of cells but contain subpopulations of stem and progenitor cells. If this is correct it will be an important discovery and will further the understanding of cancer, helping to develop treatments to extend the host's life.

2.3.1 Stem cells

Stem cells are a key part to the development and maintenance of multicellular organisms. They are defined by their ability to produce daughter cells of a different type [Lanza (2009)]. This ability, known as pluripotency, means that a small number of unspecialised cells can give rise to all of the different cells that a living organism, such as the human body, require. A fully mature organism contains many types of stem cells that are used for the maintenance of cell populations throughout the body. The process of homeostasis allows for stem cells to give rise to progenitor cells which will, through further divisions, be able to replace mature and specialised cells that have died. Examples of this include skin repair, blood formation and the renewal of the gut lining. The offspring from the mitosis of stem cells can be: stem cells, as they are self renewing cells; progenitor cells; or a mixture of both. This process can happen in several different ways and can be seen in Figure 2.7. Symmetric division results in two cells of the same type and can be either two stem cells, thereby increasing the stem cell population, or two progenitor cells, which results in a lost stem cell. Asymmetric division describes mitosis in which the daughter cells are not of the same type. This is important because

it helps maintain the stem cell population while increasing the population of progenitor cells. The progenitor cells have a lower potency than stem cells and with successive divisions will become mature cells which are specialised to perform a specific function within the tissue. Two of the most important studies of stem cells in the body are that of the haematopoietic (blood forming) system and the renewal of the gut lining. The haematopoietic system contains many different cell types but all are the product of multipotent haematopoietic stem cells, called haemocytoblasts. These stems cells always self renew and produce a new progenitor cell through asymmetric division and for this reason are known as long term stem cells. The progenitor cells are then able to self renew for a small number of divisions before losing this ability and are known as short term stem cells. After several more divisions they differentiate into one of three lineages: erythroid cells, which are red blood cells responsible for carrying oxygen around the body; lymphocytes, which form the majority of the adaptive immune system; or myelocytes, which are a variety of cells that form part of the innate and adaptive immune systems as well as cells that are responsible for blood clotting. There is a large quantity of knowledge on the haematopoietic system as it has been studied greatly due to its associated cancer, leukaemia.

The lining of the small intestine is made up of many tiny protrusions knows as villi, which are able to absorb nutrients at a much higher capacity than a flat layer of epithelium. The cells on each villus are renewed every three days, with the new cells coming from crypt structures underneath the villus and the old cells extruding from the top. At the bottom of each crypt is a stem cell niche which drives the creation of new cells. The stem cells are slow cycling cells which divide asymmetrically to maintain the stem cell niche, producing progenitor cells. These divide at a higher rate and can specialise to become one of four cell types: absorptive, secretive, goblet or panath. The majority

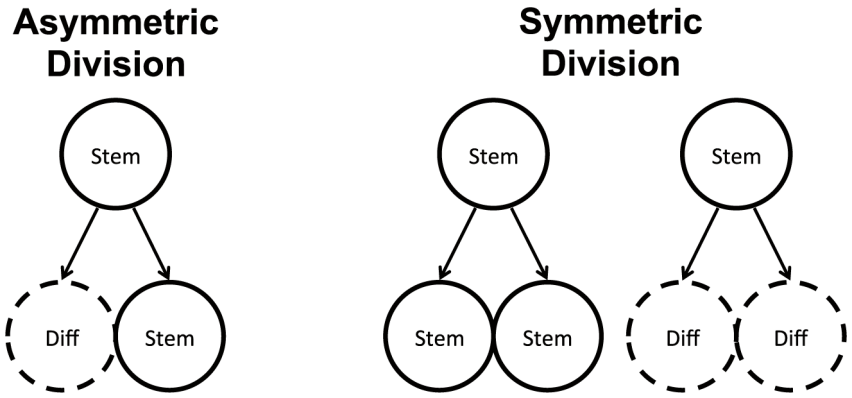

Figure 2.7: *Schematic of asymmetric and symmetric division of stem cells. A stem cell normally divides asymmetrically such that a differentiated progenitor cell is created while the stem cell population is maintained. However, it is also possible for a stem cell to divide symmetrically. As shown, symmetric division can result in two stem cells, which increases the stem cell population, or two differentiated cells, which reduces the stem cell population. Reproduced from Shahriyari and Komarova (2013) in accordance with the Creative Commons Attribution License.*

of cells on the villus are absorptive cells but secretive and goblet cells are dispersed at regular intervals. Also, panath cells sit below stem cells at the bottom of the crypt and act as guardians against bacteria. The Wnt signalling pathway has also been shown to be the cause for mitosis among the transient amplifying cells and may be responsible for the regular distribution of mature cell types [Korinek (1998)].

The pluripotent stem cell of the gut is able to effectively maintain the epithelium. However, cellular mutations can lead to the development of polyps, which are initially benign lumps but can become life threatening cancerous adenomas. The stem cell system associated with the gut has been extensively studied with regard to the development of cancer, but many questions are still to be answered.

The classical way to identify epithelial stem cells is to isolate and allow them to form a colony in *in vitro* experiments. However, more recently lineage analysis using genetic markers *in vivo* has been used to identify which cells are pluripotent Wright (2012). This

method can also be used to analyse the behaviour of stem cells. One genetic marker was found for stem cells of the crypt as it was shown that all of the epithelium in the gut was generated by Lgr5-positive cells in the crypts [Barker et al. (2007)]. Lgr5 is a gene associated with the Wnt signalling pathway.

2.3.2 The cancer stem cell hypothesis

The cancer stem cell hypothesis theorises that there exists a small subset of cells within a tumour which are able to self renew and create new tumour populations. These are known as cancer stem cells. This conflicts with other arguments where it is thought that any tumour cell can migrate and form a new cancer population, therefore growing indefinitely. However, evidence that this is not the case was found in Park et al. (1971) where only a small number of cancer cells in leukaemia were able to proliferate extensively to form new colonies. This created the idea that, just like normal cells within the body, tumours contained stem cells with progeny that could become fully mature cancer cells.

The hypothesis that only a subset of cancer cells is able to form tumours has vast implications for treatment of cancer patients. One of the most common treatments for cancer is chemotherapy, which attacks cells that have a high rate of mitosis. While the cancer is reduced to an undetectable size, it has been seen that it will often return within several years of remission and is likely to be much more aggressive. One possible explanation of this could be that the chemotherapy is able to kill the fast dividing mature cells but miss the slower dividing stem cells. However, if treatments could be found to eliminate cancer stem cells then tumours would gradually die as they are not able to divide indefinitely.

One of the major questions that the cancer stem cell hypothesis gives us is: how do cancer cells develop stem-like qualities? Several possible explanations are put forward in Reya et al. (2001). Cancer stem cells could be created by the mutation of normal stem cells. This idea seems one of the most likely as these cells are already pluripotent and have the ability to self renew. Another target could be progenitor cells which have a limited ability to self renew. Lastly, there is the possibility that mutations within mature cells can allow them to dedifferentiate to develop pluripotency. Unfortunately, the target cell of transforming mutations is unknown for most cancers and requires further research. More evidence that a small subset of cancer cells with pluiripotent qualities and the ability to self-renew is becoming available all the time. However, the implications of this for the development and treatment of cancer requires a great deal more exploration.

Chapter 3

Mathematical Background

3.1 The mathematical modelling of cancer

The use of mathematics to describe the growth of cancer has been a feature of mathematical biology research for a number of decades now and attempts to provide vital clues in the fight against cancer, complementary to experimental, biomedical and clinical research. Classical mathematical tools for the modelling of cancer have been systems of ordinary differential equations (ODEs) and partial differential equations (PDEs).

Ordinary Differential Equations are used to represent the rate of change in system variables over time and allow for reaction-kinetic-based interactions between different variables to be modelled. The precise variables being modelled may vary across different spatial and temporal scales such as cells, substrates, molecules, enzymes, ions and tissues, but it is assumed that they all exist in a well-mixed reactor, such that the dynamics are governed by various reaction rates between the species and the whole system may

be derived using the Law of Mass Action.

Within cancer modelling, systems of ODEs have been very successful at describing, qualitatively and quantitatively, events that occur within the body. For example, a system of ODEs has been used to accurately model the lineage structure of the hematopoietic system within the body [Stiehl and Marciniak-Czochra (2010)]. The model split the blood population into separate compartments: stem cells, progenitor cells and mature cells. The results showed that it was possible to find a steady state that accurately reflected the number of each type of blood cell within the human body. This model was later extended to include a stem cell based model of cancer alongside the normal blood cell population to investigate the development and progression of leukaemia. Through parameter variation, it was found that several steady states were possible: an invasive state, in which the cancer overtakes the normal population; a healthy state, in which the cancer cells are eliminated; and a coexistence state whereby both the cancer and normal cells exist together. This ODE model was able to accurately describe the dynamics of the system as the blood cells within the body are regarded as well mixed. However, ODE models are not able to describe reactions which either occur in different spatial locations or where cells are moving. For example, an avascular tumour which contains a proliferating rim, a quiescent region and a necrotic core is spatially structured and it would be very difficult for an ODE model to capture this feature in a biologically relevant way.

Therefore, to include more biologically relevant features it is necessary to use Partial Differential Equations (PDEs). This type of model allows for additional independent variables, such as space and age. For example, a spatially structured model can represent the change in concentration of a variable in time and space to represent movement. One of the most influential early mathematical models of tumour growth was

in Greenspan (1972). In this paper, the growth of a tumour spheroid in the avascular stage of development was modelled by the diffusion of a nutrient and an internal pressure. After a certain period of time the model predicts that the tumour will have three different zones: necrotic, appearing at the centre of the tumour; quiescent forming a ring around the necrotic core; and proliferative, a thin layer of cells that appear around the quiescent zone. If the nutrient concentration dropped below a critical value, cells died and became necrotic. Where the nutrient level was moderate, the cells entered a quiescent state in which they consumed nutrients but were unable to divide. When the nutrient levels were high at the rim, the cells were able to divide, thereby increasing the size of the tumour. The geometry of the tumour was always radially symmetric so it was possible to describe the size of each section of the tumour by its radius. The internal pressure in the model is used to describe the adhesion between cells which produces an inward pressure to maintain a compact tumour mass. The results in this paper showed that degradation of necrotic cells results in the inward motion of cells because of the internal pressure. This, combined with the creation of new cells at the proliferating rim, could explain why avascular tumours have a maximum size.

Greenspan (1976) extended this work to examine the stabilities to perturbations of the spherical shape of a tumour in dynamic equilibrium. This work featured a proliferating rim, a quiescent region and a large necrotic core which were governed by nutrient levels and the internal pressure to represent cell-cell adhesion and surface tension of the tumour. Perturbations to symmetric, spherical growth gave results that showed the tumour shape became less stable as the size increases. The stability was determined by a function that described whether or not the instability to perturbations occurred before the tumour reached a steady state size. The idea of perturbations in the tumour shape gives an avenue to explore how a tumour can become invasive.

Greenspan's work was extended to examine how a benign growth, which is radially symmetric, can change to become a malignant and invasive tumour at the avascular stage through the loss of cell-cell adhesion in Byrne and Chaplain (1996). This paper described the growth of an avascular tumour before the onset of quiescence or a necrotic core with the growth rate determined by a nutrient. It also included an explicit representation of cell-cell adhesion. The Gibbs-Thomson relation was implemented to relate the nutrient concentration across the boundary of the tumour to the local curvature, which is the energy used for cell-cell adhesion. Through perturbation analysis it was found that cell-cell adhesion acted as a stabilizing force against cell proliferation to prevent asymmetric growth. Therefore, it was suggested that cell-cell adhesion is clinically important to estimate the invasion ability of a tumour.

The models discussed above were able to describe the growth of multicellular spheroids *in vitro* with cell-cell adhesion. However, they did not include the interactions that cells have with the extracellular matrix. Macklin and Lowengrub (2007) used a reformulation of Greenspan (1976) and Byrne and Chaplain (1996) to include the interactions that the cancer cell population has with the surrounding tissue. This consisted of PDEs and was solved using the level set method, allowing for the deformation of boundaries in order to accurately describe cancer invasion. This model was able to simulate avascular solid tumours in two and three dimensions which are not radially symmetric, but include regions of necrosis. With different combinations of parameter values, the model was able to give rise to three types of tumour growth: fragmenting, when the tumour broke into separate pieces; invasive, in which the tumour had a fingering pattern; and hollow growth, which saw the tumour encapsulating ECM tissue. It was confirmed that increasing the cell-cell adhesion within the tumour could lead to the stabilization of growth. However, amongst other results, it was discovered that the invasive, fingering

morphology became apparent when the surrounding ECM was rich in nutrients and the movement of cells was restricted. This occurred, for example, when increasing cell-cell or cell-matrix adhesion or by increasing the rigidity of the matrix. This has implications for clinical therapies as the results of the model give indications that the onset of invasion will be more aggressive rather than preventative in certain situations.

Previously, discrete approaches had been considered to portray the adhesion between cells by representing the formation and breaking of cadherin bonds, such as Glazier and Graner (1993). This model was able to replicate experimental findings of cell sorting through the differential adhesion between cell populations. However, this had not been modelled using a continuum approach. Therefore, Armstrong et al. (2006) sought to explicitly model the adhesive bonds between cells through a dependence on the force exhibited by the cell density. It was assumed that cells were less motile in areas of high density, which was implemented using non-local terms through an integro-differential equation. This approach was able to yield aggregations in a single cell population in one dimension. The model was then extended to examine the interactions of two cell populations with different adhesion strengths and across-adhesion strength, in one and two dimensions. The results were able to replicate the aggregations found in cell sorting experiments. Therefore, a representation of cell-cell adhesion through cadherin bonds had been successfully created in a continuum model and it was possible to include this in models of cancer invasion. This model, however, was not applied to cancer.

Using Armstrong et al. (2006) as a basis, Gerisch and Chaplain (2008) developed a model of cancer invasion. The paper included two models: a local and non local description of cell-cell and cell-matrix adhesion within a non-motile ECM. Also, there is differential adhesion in these models which account for cadherin mediated cell-cell adhesion and integrin mediated cell-matrix adhesion. The two models were compared

against one another and it was found that results were similar for most parameter sets. However, the non-local model was able to produce spatially heterogeneous steady state solutions in the case that there was a balance between cell-cell and cell-matrix adhesion. A further extension of Armstrong et al. (2006) for cancer invasion included a heterogeneous ECM, which better represents a collagen matrix *in vitro*. It was found that the variations in the ECM density can greatly affect the shape of the tumour growth and that cell-cell and cell-matrix adhesion parameters can also determine how the tumour reacts to it. A very recent extension of Gerisch and Chaplain (2008) in Domschke et al. (2014) also included two subpopulations of cancer cells with different cell-cell and cell-matrix adhesion strength. Here, it was found that a mutated, more aggressive subpopulation with a higher cell-matrix adhesion strength was able to invade further into the ECM, thus increasing the malignancy of the tumour.

These PDE models of tumour growth have examined the effect of adhesion in spatio-temporal dynamics of cancer cell populations. However, they do not consider aspects such as cell size or independent cell ageing which are important when considering how cells react to external factors such as cancer therapies. An age-structured cancer population model was created in Basse et al. (2003), Basse et al. (2004) and Basse et al. (2005) to study tumour growth with applications to therapy. The papers create a multi-compartment model of a tumour population, separated by stages in the cell cycle. The passage from one stage to the next was governed by the DNA size content variable. The cell cycle is studied as chemotherapy drugs affect cells differently depending on what stage they are in. The model compared well with experimental data from flow cytometric analysis of human tumour cell lines and was used to explore how the anticancer drug paclitaxel affects tumour cells.

Attempts have been made to create a multi-scale, spatio-temporal model of tumour

growth that explicitly includes cell age and cell size structure. Ayati et al. (2006) created an extremely complicated PDE model of tumour invasion. It contained a tumour cell population, which was separated into proliferating, quiescent and necrotic zones, dependant on nutrient concentration, surrounded by the extracellular matrix. Cells within the proliferative zone aged and grew; cells in the quiescent zone had the same age and size as when they became quiescent; and cells in the necrotic zone were homogeneous. Invasion progressed through the degradation of the ECM by a matrix degrading enzyme, with the cells moving by random motion or haptotaxis. The complexity of the model required simplification by way of removing the size structure in cells so that it could be solved numerically. While this model does not include direct cell-cell or cell-matrix adhesion, it does present methods to model different aspects of tumour growth through the use of PDEs.

There have been many ODE and PDE models that have allowed insight into many aspects of cancer. However, as the complexity of models increases, in an attempt to represent aspects such as detailed cell behaviours and interactions, PDE models become overstretched. This creates models that are impossible to solve analytically and difficult to solve numerically. When this happens there is a danger that the emphasis of modelling shifts from biological relevance to mathematical analysis. This has led to the rise of individual-based modelling to represent biological phenomena.

3.2 Individual based modelling

In order to gain more insight into biological mechanisms, it is necessary to accurately replicate how cancer behaves across a range of scales. However, it is instinctive to

presume that the interactions that are conducted on a cellular scale are the most important in terms of cancer development as the replication and invasion of cancer cells are the main driving force behind the disease. In order to model cellular features such as growth, division, movement and interactions with other cells they must be represented individually. However, cellular behaviour can also be affected by events which happen at the tissue scale. These include nutrients, oxygen, growth factors, drug therapies and chemotaxis and they are typically modelled using partial differential equations. Cell behaviours can also be studied on the sub-cellular level in which protein interactions play a key role. Some sub-cellular features that have been studied are the cell cycle, cell metabolism, the Wnt signalling pathway and the Delta-Notch signalling pathway. These typically take the form of reaction kinetics, which are translated into ordinary differential equations. Several computational methods have been created which explicitly model each cell as a discrete entity and also include features across a range of scales. These can be subdivided into two categories: lattice-based and lattice-free.

Lattice-free models are noted by a free geometry meaning that cells are unrestricted by a regular grid. The techniques are typically computationally expensive but they do allow for the accurate modelling of biological phenomena, especially cell mechanics.

A popular lattice-free modelling technique is implemented in the software CHASTE (Cancer Heart and Soft Tissue Environment) [Pitt-Francis et al. (2009)]. Cells are described by the position of their centre and they are connected to neighbouring cells by linear, over-damped springs in an effort to maintain cells at an equal distance from one another. A Voronoi tessellation of the domain is used to define the shape of each cell. Migration is achieved by mitosis of cells, which upsets the balance in cell distances. This technique has been used to model many biological features. A multiscale model of the renewal of the epithelial lining in the gut was created in van Leeuwen et al. (2009)

and it was later used to explore the early stages of colorectal carcinogenesis [Mirams et al. (2012)].

Another lattice-free modelling method is known as the particle centre-based or force-based technique. This describes cells as spheres and uses Newton's second law of motion as a basis for migration and adhesion of cells. This is more flexible than the technique used in CHASTE but it does not allow the shape of each cell to change. This technique has been utilised to model many aspects of cancer. Drasdo and Hohme (2005) created models of tumours in two forms: two-dimensional monolayers and three-dimensional spheroids. Ramis-Conde et al. (2008b) extended this model to include sub-cellular E-cadherin/β-catenin dynamics as a direct biological representation of cell-cell adhesion. This model was further extended to explore the metastasis of cancer cells through the blood system in Ramis-Conde et al. (2009), which studied how the dynamics of cadherins can play a major role in intravasation. A highly detailed model of breast cancer, or ductal carcinoma in situ, was developed in Macklin et al. (2012) with a view to help patient specific modelling and treatment.

Lattice-based, or on-lattice, models are defined by a geometry that is underpinned by a regular grid. These grids can be either square or hexagonal in nature. In the simplest form of on-lattice models each lattice space can hold one cell and are referred to as cellular automaton models. Cellular features such as movement and division are governed by individual rules. It is also possible to include sub-cellular dynamics within each cell and tissue level features using partial differential equations. However, the geometry of these models creates an artificial scenario which does not completely reflect the biological environment. Also, the results generated from these models may be caused purely by the rules imposed on each cell. Despite this, cellular automaton models have been used in cancer modelling primarily because they are computationally inexpensive.

Anderson (2005) developed a discrete-continuum hybrid model to explore the effects of cell-cell adhesion and cell-matrix interactions in the invasion of solid tumours. The model is comprised of four variables: tumour cells, the extracellular matrix, matrix-degrading enzymes and oxygen. The tumour cells are represented as cellular automata and the other three variables are represented by continuous fields. The simulation results were able to recreate 'finger-like' protrusions of tumour growth into the surrounding extracellular matrix. This was thought to be driven by cell-matrix interactions and random mutations of tumour cells into more aggressive phenotypes. This paper was later extended in Ramis-Conde et al. (2008a) in which cell-cell adhesion was modelled using a potential function. Enderling et al. (2009) created a cellular automaton model to explore the cancer stem cell hypothesis and how tumour dormancy can be created and lost because of the presence of cancer stem cells. Powathil et al. (2012) used a cellular automaton model to describe how cell cycle heterogeneity among cells can affect how a tumour responds to chemotherapeutic treatments. In this model, the cell cycle was represented on the sub-cellular scale by ordinary differential equations created by Tyson and Novak (2001). This was complemented by a sub-cellular model of oxygen consumption, linked with tissue level consumption, represented by a continuous field. The tumour was allowed to grow to produce regions of proliferative and quiescent cells around randomly distributed blood vessels. When the oxygen level dropped below a critical level, the cell cycle arrested and cells entered a hypoxic quiescent state. Chemotherapy drugs were represented by a continuous field which was secreted from the blood vessels and allowed to diffuse throughout the domain. This complex model showed that the heterogeneity of cell-cycle status within the tumour could impair the efficacy of chemotherapy.

An extended version of the cellular automaton modelling technique has been created in

the form of the cellular Potts model. The cellular Potts model has a regular lattice comprised of pixels with each cell, or cellular compartment, made up of several connecting pixels. Therefore, cells are no longer regarded as single points but are spatial objects that allow for a change in shape and size. The simulation progresses through a series of Monte Carlo steps (MCS) which attempt to minimise the overall effective energy in the system. At each MCS, attempts are made to transform the neighbouring pixels at the boundary of each cell to increase its volume. If the pixel transformation, known as a 'flip', reduces the overall effective energy then the pixel in question will be changed. However, if the flip increases the effective energy then it will not be performed. Turner and Sherratt (2002) implemented the cellular Potts model to study the effects that cell-cell and cell-matrix adhesion have on cancer invasion, which yielded two main results. Firstly, cell-matrix adhesion was found to have a stronger effect on the invasiveness of the tumour than cell-cell adhesion. Also, when proliferation was included in the model this was seen to allow the tumour to grow further into the tissue but reduced the ability to produce 'finger-like' structures. The cellular Potts model is used extensively in this thesis in the form of the open source software package, CompuCell3D. This package attempts to unify the functions of other cellular Potts models into a user friendly modelling environment.

3.3 The CompuCell3D modelling platform

CompuCell3D provides a user friendly programming environment in order to develop models using the cellular Potts technique, also known as the Glazier-Graner-Hogeweg model. It was developed in the programming language C, but allows the user to create models using XML and Python which are simpler programming languages. All

CompuCell3D simulations have a list of objects, such as generalised cells or fields, a description of interactions and initial conditions.

Each generalised cell is made up of lattice sites, which are referred to as pixels, and can represent biological cells, compartments of cells or other biological objects such as the extra cellular matrix. Each lattice site is represented by a vector of integers $\mathbf{i}$. When a pixel is part of a generalised cell, the cell index is referred to by $\sigma(\mathbf{i})$ and the cell type is called $\tau(\sigma(\mathbf{i}))$. The description of interactions between generalised cells is implemented using the effective energy. This determines many characteristics such as cell size, shape, motility, adhesion strength and the reaction to gradients of chemotactic fields.

A simulation progresses by attempts of generalised cells to extend their boundaries in an effort to minimise the effective energy. These are called index-copy attempts because they try to change the cell index of a neighbouring pixel to that of its own cell type. The success of the index copy attempt is dependent upon a Boltzmann acceptance function which takes into account the change in energy. A Monte Carlo Step (MCS) is completed when every lattice site has made an index-copy attempt.

Fields can be used to model tissue scale objects such as nutrient dynamics, the extracellular matrix or chemical gradients. These are governed by partial differential equations and the dynamics can include secretion, diffusion, absorption, reaction, and decay. Each generalised cell also has auxiliary equations to describe their interactions with fields, such as absorption and secretion. The reactions are described by ordinary differential equations within each cell. Simple forward Euler methods are used to solve the PDEs. Therefore, great care must be taken when choosing parameter values to ensure that the solution is stable.

3.3.1 Effective energy

The effective energy is the basis for operation of all Cellular Potts Models, including CompuCell3D, because it determines the behavior of the interactions between cells. The energy is described in two ways: boundary energy or constraints.

One of the most important boundary energy components of the effective energy equations governs the adhesion of cells. This is defined by the boundary energy which is calculated using $J(\tau(\sigma),\tau(\sigma'))$, the boundary energy per unit area between the two cells (σ,σ') of types $(\tau(\sigma),\tau(\sigma'))$. This is calculated by the sum over all neighbouring pixels that form the boundary between two cells:

$$H_{boundary} = \sum_{\mathbf{i},\mathbf{j}\ \text{neighbors}} J\Big(\tau(\sigma(\mathbf{i}),\tau(\sigma(\mathbf{j}))\Big)\Big(\mathbf{1}-\delta_{\mathbf{ij}}(\sigma(\mathbf{i}),\sigma(\mathbf{j}))\Big). \tag{3.1}$$

The effective energy represents other types of cellular behaviours using constraints, which are in a general elastic form:

$$H_{constraint} = \lambda(value - target\ value)^2. \tag{3.2}$$

Therefore, if $value = target\ value$ the energy is zero because the constraint has been satisfied. This is known as the equilibrium condition. Since CompuCell3D tries to minimise the effective energy in a simulation the constraint will be driven to the equilibrium condition. However, the stochastic nature of the simulations means that the condition does not always have to be met and it is possible that two or more constraints conflict with each other so that they are only able to be partially met. The value λ, also known as the spring constant, determines how far the value can deviate from the target. A large

value of λ multiplies any deviation to create a larger effective energy which will prevent a flip from occurring. Therefore, smaller values of λ allow for greater deviations.

The most common use for constraint energies for biological cells in CompuCell3D is to restrict the size of cells to given target values. This is done through two constraints: the volume and the surface area. The volume constraint energy for each cell σ is calculated by:

$$H_{vol} = \sum_{\sigma} \lambda_{vol}(\sigma)\Big(v(\sigma) - V_t(\sigma)\Big)^2, \tag{3.3}$$

where $\lambda_{vol}(\sigma)$ is the inverse compressibility of the cell, $v(\sigma)$ is the number of pixels in the cell and $V_t(\sigma)$ is the cell's target volume in pixels. The constraint is able to define the pressure within the cell as $P \equiv -2\lambda_{vol}(v(\sigma) - V_t(\sigma))^2$. When $v < V_t$ the cell has positive internal pressure, which encourages it to expand, and when $v > V_t$ the cell has negative internal pressure, which encourages it to shrink. The surface area constraint has the form:

$$H_{surf} = \sum_{\sigma} \lambda_{surf}(\sigma)(s(\sigma) - S_t(\sigma))^2, \tag{3.4}$$

where $s(\sigma)$ is the surface area of the cell σ in pixels, S_t is the target surface area in pixels and λ_{surf} is the inverse membrane compressibility. It should be noted that the surface area is not equal to the amount of cell membrane, as this value always stays roughly the same for biological cells. If the boundary energy in Equation (3.1) and the

volume constraint in Equation (3.3) are combined the result is the basic Glazier-Graner-Hogeweg effective energy used in CompuCell3D:

$$H_{GGH} = \sum_{\mathbf{i},\mathbf{j}\ \text{neighbors}} J\Big(\tau(\sigma(\mathbf{i}),\tau(\sigma(\mathbf{j}))\Big)\Big(\mathbf{1}-\delta(\sigma(\mathbf{i}),\sigma(\mathbf{j}))\Big) + \sum_{\sigma}\lambda_{vol}(\sigma)\Big(\ v(\sigma)-V_t(\sigma)\Big)^2 \tag{3.5}$$

3.3.2 A Monte-Carlo step

The dynamics of CompuCell3D simulations are controlled by index-copy attempts and a Monte-Carlo step is complete when every pixel on the lattice has made an index-copy attempt to a neighbouring pixel.

To begin an index-copy attempt, a lattice site is randomly chosen to be a target pixel, $\mathbf{i}$, and then a neighbouring lattice site is chosen to be a source pixel $\mathbf{i}'$. An attempt will then be made to change the target pixel to the same generalised cell as the source pixel, thereby increasing the volume of the source cell and decreasing the volume of the target cell. If the source and target pixels belong to the same cell ($\sigma(\mathbf{i}) = \sigma(\mathbf{i}')$) then no calculations are necessary.

To determine whether or not an index copy attempt is successful the following acceptance probability is used:

$$P\Big(\sigma(\mathbf{i}) \rightarrow \sigma(\mathbf{i}')\Big) = \begin{cases} exp(-\Delta H/T_m), & \Delta H > 0, \\ 1, & \Delta H \leq 0, \end{cases} \tag{3.6}$$

where ΔH is the change in effective energy and T_m is a parameter defined to be the effective cell motility, or can be called the amplitude of cell-membrane fluctuations.

This Boltzmann acceptance function tells the simulation that if the change in effective energy is less than or equal to zero for an index-copy attempt then the attempt will be successful. However, if the resulting change in effective energy is greater than zero the attempt may still be successful with the probability $exp(-\Delta H/T_m)$. The parameters ΔH and T_m allow for a conversion between the number of MCS and time for an experiment. The conversion depends on the average values of $\Delta H/T_m$. In biologically relevant simulations, experimental time and MCS are proportional.

3.3.3 Subcellular dynamics

CompuCell3D has the ability to link sub-cellular scale dynamics to cellular behaviours through the use of BionetSolver. This has the ability to solve ordinary differential equation models of signaling, regulatory or metabolic pathways for each cell at each MCS. It can then link the parameter values to steer events at the cellular level such as adhesion, growth and/or division. Also, it can take into account information from tissue level fields such as nutrients, oxygen or chemicals and use this in the intracellular pathways.

3.3.4 Models created in CompuCell3D

CompuCell3D allows for the creation of complicated simulations of biological phenomena in a much simpler fashion than using custom code. It also allows users to develop new features to the software using the C programming language. There are many examples of CompuCell3D successfully replicating biological phenomena, as well as models of cancer.

One of the most complex models created in CompuCell3D studied the process called

somitogensis [Hester et al. (2011)]. This can be observed in all vertebrate embryo development and results in the creation of a segmented structure. The entire process requires a great deal of coordination among biological mechanisms on several scales. This model began with a layer of presomitic mesoderm (PSM), which consisted of cells which have the ability to break off and form somites. The cellular scale dynamics were supplemented with three gradients within the PSM: Fibroblast growth factor 8, FGF8; the wingless homolog, Wnt3a; and Raldh2, which synthesizes retinoid acid to promote differentiation. Each cell also contained three linked intracellular protein pathway oscillators to create a segmentation clock: the ERK pathway, which responds to the FGF8 signal in the local environment; the canonical Wnt pathway, which includes β-catenin and responds to the local Wnt signal strength; and the Delta-Notch pathway, which reacts to the concentration of the Delta signal from neighbouring cells. This multi-scale model was able to generate spatially and temporally regular somites with the ability to change the size and rate of formation through parameter variations to represent different species.

CompuCell3D has been used to create several models of cancer growth. Avascular tumour growth was modelled in two dimensions in Poplawski et al. (2009) for highly motile cells, such as those found in glioma. This included: tumour cells; the tissue matrix, represented by a non-diffusing field; a nutrient field to govern the growth of the cells; and a field to represent matrix-degrading enzymes. It was shown that this model can capture many of the features of tumour growth similar to models which use other techniques, but CompuCell3D is able to include more features such as cell shape. The results showed that the type of growth that the tumour exhibits, smooth (non-invasive) versus fingered (invasive), was dependant on the rate of the tumour's nutrient consumption, diffusion-limitation of nutrients, and surface tension between the tumour

and the surrounding matrix. It agreed with several other models that the competition for nutrients led to irregular, invasive tumours. Later, this model was expanded into three dimensions and it was shown to mimic the results from the 2-D model[Poplawski et al. (2010)].

Vascular tumour growth has been also been modelled extensively [Merks and Glazier (2006); Merks et al. (2008); Bauer et al. (2007, 2009); Shirinifard et al. (2009)]. In Shirinifard et al. (2009) a three dimensional model of tumour growth with a vascular network and angiogenetic properties was created. The simulations have an initial condition of a regular vascular network and a single tumour cell. The blood vessels secrete oxygen, which is allowed to diffuse throughout the domain to oxygenate the cancer cells. Other features included hypoxia and necrosis, in areas of low oxygen concentration, and angiogenesis, induced through VEGF signalling. This model was able to simulate 75 days of tumour growth which reached a size of approximately 10^4 cells. It was able to show that cell motility has an effect on the shape of the tumour, with finger like structures appearing at lower rates of motility. Despite the exclusion of some biological features, such as the explicit flow of blood in vessels or metabolic pathway for oxygen consumption in cells, the model was able to create an accurate description of tumour growth with angiogensis.

The invasion of tumours was modelled in Andasari et al. (2012) in an effort to compare the Graner-Glazier-Hogeweg modelling technique against the particle centre-based model in Ramis-Conde et al. (2008b). This employed the intracellular dynamics for adhesion that were described by Ramis-Conde et al. (2008b) to explore the level of invasiveness of a three dimensional tumour *in vitro*. The results showed that the two modelling techniques were qualitatively the same and that they both agreed qualitatively with experimental data. However, the results were shown to be quantitatively

different because of the fundamental differences in the modelling approaches.

The large number of features that CompuCell3D contains plus its relative ease of use make it an ideal platform for the mathematical modelling of biological phenomena, including cancer. A more extensive description of the software may be found in Swat et al. (2012).

Chapter 4

Modelling β-catenin and E-cadherin Dynamics

The E-cadherin/β-catenin pathway is crucial to understanding many key processes in developmental biology and carcinogenesis. β-catenin is the key protein in this process due to its ability to regulate adhesion and transcription within cells, as well as its involvement in the canonical Wnt pathway. Several attempts to study it mathematically have been made through the use of systems of ordinary differential equations.

Lee et al. (2003) created the first model of the canonical Wnt pathway in the form of kinetic reactions. This incorporated many of the major interactions that β-catenin has with other proteins in this pathway including: Dishevelled, Axin, GSK3β, APC and TCF. The parameters used in it were derived through biological experimentation and the model was able to quantitatively replicate data from several experimental scenarios, which included Wnt "on" and "off". The model also made some interesting predictions. One of these was the importance of axin within the Wnt pathway. Axin was shown

to increase the strength of the Wnt signal by being able to reduce the degradation of β-catenin. This allows the promotion of transcriptional activity, while at the same time maintaining the concentrations of APC and GSK3β , preventing a disturbance in other signalling pathways. The model was later extended to explore different aspects of the Wnt pathway.

Cho et al. (2006) extended the model of Lee et al. (2003) to study the effect of APC mutations in colorectal tumourigenesis, while the Wnt signalling pathway was turned off. The concentration of free β-catenin was shown to increase for mutations in APC, axin and β-catenin. However, the most preferred APC mutations for tumourigenesis did not result in the highest levels of β-catenin. This led to the theory that there is an ideal level of β-catenin to promote transcription. Wawra et al. (2007) used the model in the context of embryogenesis by extending it to include time-delay differential equations for the examination of vertebrate somitogenesis. Kim et al. (2007) added reactions of the ERK pathway to show that crosstalk between ERK and Wnt signalling pathways results in sustained transcriptional activities in the form of a positive feedback loop. Sun (2009) examined GSK3β-dependant and independent phosphorylation of β-catenin and found that it may be necessary to include a kinetic reaction for the dephosphorylation of β-catenin.

The model of Lee et al. (2003) was groundbreaking in its approach because it was one of the first models to extend techniques from metabolic control theory for the purposes of protein signalling pathways and it has been able to generate predictive results. While the canonical Wnt pathway is described very well by this model, it only takes into account the transcriptional activities of β-catenin and excludes its role in adhesion. Also, this model assumes that the cytoplasm of the cell is a ‘well-mixed vat’, neglecting reactions that take place in separate areas of the cell.

A mathematical model to examine how a cell will dictate the adhesive and transcriptional activities of β-catenin was created in van Leeuwen et al. (2007). This was a multi-compartment model which examined two hypotheses: a single form of β-catenin and two forms of β-catenin. The simulations with a single form of β-catenin are used to examine the competition between adhesion and transcription. The first hypothesis includes a form of β-catenin which has been altered by Wnt signalling and is unable to bind to E-cadherin therefore, it can only participate in transcriptional activities. The second hypothesis, with two conformations of β-catenin, includes a reduction of E-cadherin while Wnt signalling is "on". The distinction between the two hypotheses can be found in one of the experimental scenarios performed. Under the first assumption, cell-cell adhesion would not decrease during Wnt signalling, but under the second assumption the opposite is true. Overall this system of differential equations was a major step in the modelling of this pathway and was used in a multi-scale model of an intestinal crypt [van Leeuwen et al. (2009)].

Concurrently with van Leeuwen et al. (2007), a model of the E-cadherin/β-catenin pathway that also included the effects of the Epithelial-Mesenchymal transition was developed in Ramis-Conde et al. (2008b). This model is described in Section 4.1.1. In Section 4.1.2, a novel extension of Ramis-Conde et al. (2008b) will be created and studied. Using a system of partial differential equations, the model will attempt to accurately describe the interactions of β-catenin, E-cadherin, the adhesion complex of E-cadherin/β-catenin, and the phosphorylation complex of β-catenin and the proteasome. The movement of the proteins will be described by passive diffusion and active transport. The resulting system of partial differential equations will be solved using the finite element technique as implemented by COMSOL Multiphysics 3.5 [COMSOL (2005)].

In Section 4.2, a novel ordinary differential equation model of the Wnt pathway with E-cadherin was investigated. It uses the models described above [Lee et al. (2003); van Leeuwen et al. (2007)] to further examine the adhesive and transcriptional activities of β-catenin.

Section 4.3 describes biological experiments carried out in the Nathke laboratory at the University of Dundee. Madin-Darby canine kidney cells were used to measure the concentrations of β-catenin in the cytoplasm, nucleus and at the membrane. The cells were grown at different confluences and immunostained for proteins such that their concentrations were able to be measured by immunofluorescence.

4.1 The movement of β-catenin in cells

Several ordinary differential equation models have been developed to model the levels of β-catenin, E-cadherin and other Wnt pathway proteins. However, none of these explicitly describe the location of the proteins within the cell in a spatial context. The use of partial differential equations to model spatio-temporal dynamics has previously been studied. Sturrock et al. (2010) examined the Hes1 and p53-Mdm2 intracellular pathways and Terry et al. (2011) considered the notch signalling pathway. These models focused on explaining the oscillatory dynamics exhibited in each of these pathways. This section will develop a system of partial differential equations to describe the spatio-temporal dynamics of the E-cadherin/β-catenin pathway. However, the ODE model of Ramis-Conde et al. (2008b) will be described in detail as it will be used as a basis for the PDE system.

4.1.1 A basic model of E-cadherin/β-catenin dynamics

The proteins taken into consideration in this model describe a simplified version of the canonical Wnt signalling pathway with E-cadherin/β-catenin dynamics and the Epithelial-Mesenchymal transition. There are three forms of E-cadherin: $[E_c]$, E-cadherin in the cytoplasm; $[E_m]$, E-cadherin at the membrane but not engaged in adhesion; and $[E/\beta]$, a complex of E-cadherin and β-catenin that is engaged in cell-cell adhesion. Free β-catenin in the cytoplasm is called $[\beta]$ and the destruction complex is simplified to a generic proteasome $[P]$, which forms a complex with $[\beta]$ called $[C]$, targeting the β-catenin for destruction. The reactions of the system, presented in Figure 4.1, are described as

$$[E_c] \rightarrow_{\{contact\}} [E_m], \tag{4.1}$$

$$[\beta] + [E_m] \xrightarrow{\nu} [E/\beta], \tag{4.2}$$

$$[E/\beta] \rightarrow_{\{detachment\}} [E_c] + [\beta], \tag{4.3}$$

$$[\beta] + [P] \underset{k^-}{\overset{k^+}{\rightleftharpoons}} [C] \xrightarrow{k_2} [P] + [\omega]. \tag{4.4}$$

Reaction (4.1) describes the movement of E-cadherin from the cytoplasm to the membrane upon cell-cell contact, where it awaits β-catenin to be able to engage in cell-cell adhesion. The formation of the adhesion complex, which happens at the rate ν, is described in (4.2). When the adhesive bonds break and contact is lost, the complex $[E/\beta]$ is broken and the constituent parts are returned to the cytoplasm by endocytosis. Lastly, (4.4) describes the formation of the complex $[C]$ which actively degrades the free β-catenin in the cell. This can be used to take into account the Wnt pathway by the alteration of the reaction rate k^+. The variable $[\omega]$ describes the final product of the degradation process.

The focus of this model is on the concentration of free β-catenin within the cell. To allow for this, it was assumed that the total concentrations of E-cadherin and the proteasome complex remain constant within the cell and described as

$$E_T = [E_c] + [E_m] + [E/\beta], \tag{4.5}$$

$$P_T = [C] + [P]. \tag{4.6}$$

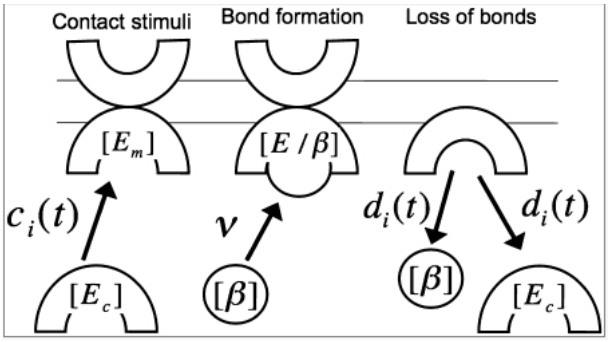

Figure 4.1: *The three states of E-cadherin considered in the model are: free in the cytoplasm, at the membrane and in a multiprotein complex with β-catenin. When two cells come into contact, the cadherin travels to the membrane determined by the function $c_i(t)$. When at the membrane it binds to β-catenin and forms a bond with the neighbouring cell. When detachment occurs the complex β-catenin-E-cadherin is broken at a rate governed by the function $d_i(t)$ and E-cadherin and β-catenin are returned to the cytosol in their free state. Reproduced with copyright permission from Ramis-Conde et al. (2008b).*

From the reactions (4.1) - (4.6), the following system of ordinary differential equations

for a cell, i, can be created [Ramis-Conde et al. (2008b)]:

$$\frac{d[E_c]}{dt} = -c_i(t)[E_c] + d_i(t)[E/\beta], \tag{4.7}$$

$$\frac{d[E/\beta]}{dt} = \nu(E_T - [E_c] - [E/\beta])[\beta] - d_i(t)[E/\beta], \tag{4.8}$$

$$\begin{aligned}\frac{d[\beta]}{dt} &= -\nu(E_T - [E_c] - [E/\beta])[\beta] + d_i(t)[E/\beta] \\ &\quad - k^+[\beta](P_T - [C]) + k^-[C] + k_m,\end{aligned} \tag{4.9}$$

$$\frac{d[C]}{dt} = k^+[\beta](P_T - [C]) - k^-[C] - k_2[C], \tag{4.10}$$

where, ν, k^+, k^-, k_m and k_2 are all positive constants. The function $c_i(t)$ is used to describe the increase of the area of physical cell-cell contact and the corresponding level of E-cadherin, from the cytoplasm, needed to be transported to the membrane to engage in adhesion. The function $d_i(t)$ describes the area of contact lost and the dissociation of the $[E/\beta]$ that results from it. These are described by:

$$c_i(t) = \sum_{\text{new contacts}} a_{c,j}(t)\rho_c,$$

$$d_i(t) = \sum_{\text{new detachments}} a_{d,j}(t)\rho_d.$$

The equations (4.8) and (4.9) are only assumed to govern cells of an epithelial phenotype that have a free β-catenin concentration below a threshold value c_T. However, if the cytosolic β-catenin levels increase to above c_T it is assumed that the levels are high enough such that it is free to enter the nucleus and engage in transcriptional activities. This causes the cell to undergo the Epithlial-Mesenchymal transition (EMT) resulting in higher motility and loss of cell-cell contacts. When this transition occurs it is assumed

that

$$\frac{d[E/\beta]}{dt} = -(\alpha + d_i(t))[E/\beta], \tag{4.11}$$

$$\frac{d[\beta]}{dt} = (\alpha + d_i(t))[E/\beta] - k^+[\beta](P_T - [C]) + k^-[C] + k_m \tag{4.12}$$

replace the equations (4.8) and (4.9), respectively. The parameter α represents the rate of dissociation of $[E/\beta]$ when the cell is transformed to the mesenchymal phenotype. For a full description of this model see Ramis-Conde et al. (2008b).

4.1.1.1 Results and discussion

The equations (4.7) to (4.12) were solved in several scenarios using the ode45 solver in Matlab. Figure 4.2 shows an initial condition that represents no cell-cell attachment and at $t = 0.4$ an attachment was simulated. When this happens, the levels of $[E_c]$ and $[\beta]$ drop at the same rate and reach a new steady state. This happens as the level of $[E/\beta]$ rises from zero to a new steady state, which represents the levels of these proteins during a stable cell-cell attachment.

Figure 4.3 has an initial condition of the attached steady state and detachment is simulated at $t = 0.4$. The results show that during the breaking of the bonds of E-cadherin and subsequent detachment of the cells, the levels of free β-catenin and E-cadherin climb steeply. The increase of β-catenin will lead to it being translocated to the nucleus where it can promote cell proliferation.

Ramis-Conde et al. (2008b) showed that this stripped down ODE model was able to qualitatively replicate the adhesive and transcriptional activities of β-catenin in discrete cell based models. This paper focused on the migration of tumour cells and the

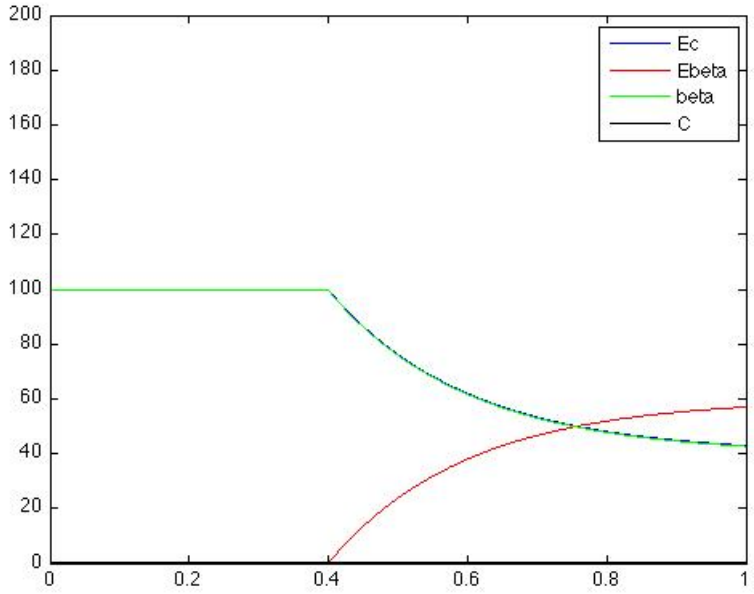

Figure 4.2: *This plot shows the concentrations of the variables over time. Cell-cell attachment occurs at time $t = 0.4$ minutes. When this happens, E-cadherin and β-catenin rapidly bond to create adherins junctions at the cell surface.*

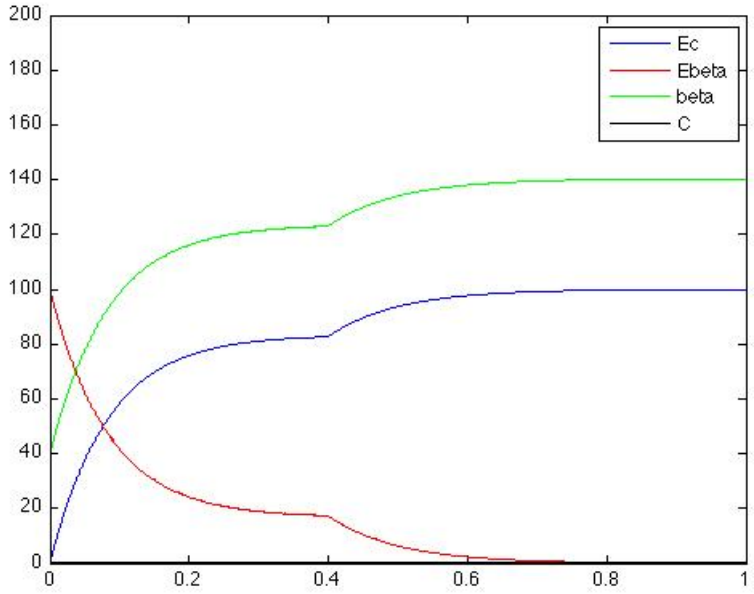

Figure 4.3: *Plot showing the concentrations of the variables over time. At time* $t = 0.4$ *minutes the cell loses all of its contacts with the neighbouring cells. The* β*-catenin concentration increases which may allow a cancerous cell to begin invasion.*

importance of EMT in cancer cell invasion. This was later expanded upon to study transendothelial migration of cancer cells for the purposes of metastasis [Ramis-Conde et al. (2009)] and it was also shown to be applicable in cellular Potts models [Andasari et al. (2012)].

4.1.2 Single cell model

To better understand the process of cell-cell adhesion, the spatial dynamics as well as the temporal dynamics are important. The model of Ramis-Conde shows the temporal dynamics but here it is suggested that the spatial dynamics of the proteins can be modelled using a system of partial differential equations. This involves compartmentalizing the different parts of the cell. The diagram of the cell, Figure 4.4, shows that it splits into several different regions: the nucleus, nuclear membrane, cytoplasm and cell membrane. There is no explicit cell membrane shown here as only one cell in an epithelial sheet is being shown. The membrane will be added when more than one cell is simulated. It is hoped that similar dynamics shown in Figure 4.2 can be replicated in this two dimensional model, but with an understanding of where the proteins are in the cell.

4.1.2.1 In the cytoplasm

E-cadherin and β-catenin are usually found in the cytoplasm of the cell. Therefore, this part of the cell is where most of the reactions will take place in the model.

Like many proteins, E-cadherin is created in the rough endoplasmic reticulum by ribosomes. It is then passed onto the Golgi apparatus before being transported to the cell

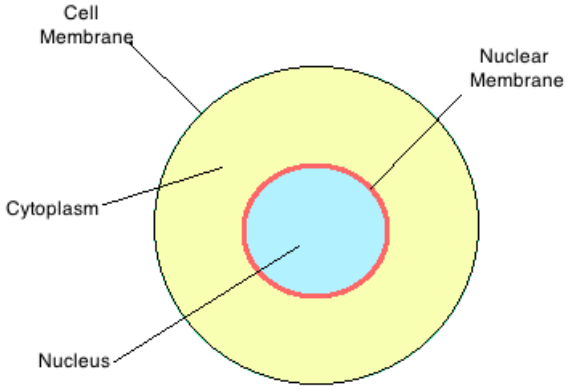

Figure 4.4: *Schematic of single cell model. The areas of the cell taken into account in the model are: the nucleus, nuclear membrane, cytoplasm and cell membrane. To engage in cell-adhesion β-catenin must be at the cell membrane and bind to E-cadherin. In the absence of Wnt signalling, β-catenin in the cytoplasm is degraded by a proteasome. However, when the Wnt signalling is active, degradation is stopped and the β-catenin population will build up in the domain. When this happens, it is able to transport in to the nucleus by passing through the nuclear membrane, which is represented by a thin boundary layer.*

membrane where is performs its function in cell-cell adhesion [Alberts (2008)]. Mathematically, the transportation of the newly created E-cadherin to the cell membrane may be represented by the use of an advection field, used in similar intracellular simulations [Sturrock et al. (2010); Terry et al. (2011)].

While at the cell membrane, the cytoplasmic tail of E-cadherin binds with p120-, α- and β-catenins, which binds it to the cytoskeleton of the cell. The rest of E-cadherin extends through the cell membrane to bind with E-cadherin from another cell in *trans* and *cis* configurations [Leckband and Sivasankar (2000)]. It is fixed at the membrane until the E-cadherin bonds are broken.

When the bonds between E-cadherins across extracellular space are broken by mechanical stress or intracellular signalling, the bonds between E-cadherin and the catenins are also lost. The E-cadherin enters the cell by the process of endocytosis. This movement of E-cadherin into the cytoplasm may be represented by a diffusion term. Therefore, the spatial terms for E-cadherin are

$$\frac{\partial [E]}{\partial t} = \overbrace{\nabla \cdot (D_{Ecyto} \nabla [E])}^{Diffusion} + \overbrace{\mathbf{a}[E]}^{Advection}),$$

where

$$\mathbf{a} = A \left(\frac{x}{\sqrt{x^2+y^2}}, \frac{y}{\sqrt{x^2+y^2}} \right).$$

Another consequence of the loss of E-cadherin-mediated cell-cell adhesion is that β-catenin is released in a phosphorylated state, which means it can move freely within the cytoplasm. Usually, soluble β-catenin levels in the cytoplasm are regulated by a complex of Axin, APC and active GSK-3β, which bind to β-catenin and target it for destuction by proteolysis [Weinberg (2007)]. However, when the levels of soluble β-catenin

reach a threshold concentration β-catenin is transported to the nucleus, where it promotes cell proliferation [Huber et al. (1996); Kemler et al. (2004)]. In this model only simple diffusion has been used to describe the movement of β-catenin in the cytoplasm. However, a more complicated term, which takes into account a direct transportation to the nucleus, may be used. The spatial term for β-catenin in the cytoplasm is:

$$\frac{\partial[\beta]}{\partial t} = \overbrace{D_{\beta cyto}\nabla^2[\beta]}^{Diffusion}.$$

As said above, E-cadherin and several catenins bind near the membrane, however, in this simulation this complex has been simplified to E-cadherin-β-catenin, ignoring α-catenin and p120-catenin. Like E-cadherin, the spatial terms include an advection field and diffusion. The advection field keeps the E-cadherin-β-catenin at the edge of the cell and a very small diffusion coefficient is used to represent the lack of movement when E-cadherin is participating in homophilic, extracellular binding. Therefore, the spatial terms for E-cadherin-β-catenin are

$$\frac{\partial[E/\beta]}{\partial t} = \overbrace{\nabla\cdot(D_{E/\beta cyto}\nabla[E/\beta]}^{Diffusion} + \overbrace{\mathbf{a}[E/\beta]}^{Advection}).$$

Lastly, the complex that degrades the soluble β-catenin in the cytoplasm is represented by the simplified proteasome complex. The kinetics from [Ramis-Conde et al. (2008b)] are used, which means that the proteasome $[P]$ can be represented by the complex of the proteasome and β-catenin, given as $[C]$. The only spatial term used for this is

$$\frac{\partial[C]}{\partial t} = \overbrace{D_{Ccyto}\nabla^2[C]}^{Diffusion}.$$

These spatial terms along with the kinetics terms from [Ramis-Conde et al. (2008b)] give the complete system of equations in this section of the cell:

$$\frac{\partial [E]}{\partial t} = \nabla \cdot (D_{Ecyto} \nabla [E] + \mathbf{a}[E]) - c_i(t) + d_i(t)[E/\beta], \tag{4.13}$$

$$\frac{\partial [E/\beta]}{\partial t} = \nabla \cdot (D_{E/\beta cyto} \nabla [E/\beta] + \mathbf{a}[E/\beta]) + \nu(E_T - [E] - [E/\beta])[\beta] - d_i(t)[E/\beta], \tag{4.14}$$

$$\frac{\partial [\beta]}{\partial t} = D_{\beta cyto} \nabla^2 [\beta] - \nu(E_T - [E] - [E/\beta]) + d_i(t)[E/\beta] - k^+[\beta](P_T - [C]) + k^-[C] + k_m, \tag{4.15}$$

$$\frac{\partial [C]}{\partial t} = D_{Ccyto} \nabla^2 [C] + k^+[\beta](P_T - [C]) - k^-[C] - k_2[C]. \tag{4.16}$$

4.1.2.2 The nuclear membrane

This nuclear membrane is used to represent the difficulty that β-catenin can have being transported from the cytoplasm to the nucleus. Numerically, this has been represented in Comsol by a thin boundary layer where it has simple diffusion. However, a more complicated term can be used that makes it easier for the β-catenin to move into the nucleus when a high enough concentration has been reached in the cytoplasm.

The only equation in this compartment is:

$$\frac{\partial [\beta]}{\partial t} = D_{\beta nucmem} \nabla^2 [\beta]. \tag{4.17}$$

4.1.2.3 In the nucleus

In this model the only protein that can enter the nucleus is β-catenin. The binding of β-catenin with TCF and LEF, which promotes cell proliferation, has not been included. Therefore the only equation in this compartment is:

$$\frac{\partial[\beta]}{\partial t} = D_{\beta nuc}\nabla^2[\beta]. \tag{4.18}$$

4.1.2.4 Initial conditions

For the simulations, the entire concentration of E-cadherin molecules is assumed to be created in the ribosome area with no E-cadherin anywhere else in the cell. The free β-catenin is initially distributed throughout the cell in both the nucleus and the cytoplasm. There is originally no E-cadherin-β-catenin or proteasome-β-catenin complex. This yields:

$$E(\mathbf{x},0) = \begin{cases} 100, & \text{in Golgi apparatus area,} \\ 0, & \text{everywhere else,} \end{cases} \tag{4.19}$$

$$\beta(\mathbf{x},0) = \begin{cases} 10, & \text{in nucleus,} \\ 5, & \text{in cytoplasm,} \end{cases} \tag{4.20}$$

$$E/\beta(\mathbf{x},0) = 0, \quad \text{everywhere,} \tag{4.21}$$

$$C(\mathbf{x},0) = 0, \quad \text{everywhere.} \tag{4.22}$$

4.1.2.5 Boundary conditions

For the exterior edge of the cell, which represents the membrane, zero flux boundary conditions are imposed. This is represented by:

$$\mathbf{n} \cdot \mathbf{N} = 0 \tag{4.23}$$

$$\text{where } \mathbf{N} = -D\nabla u_i + u_i \mathbf{u}$$

$$\text{and } \mathbf{u} = \begin{pmatrix} [E] \\ [E/\beta] \\ [\beta] \\ [C] \end{pmatrix}$$

Across the thin boundary layer, there is a flux of β-catenin. This is represented by:

$$\mathbf{n}_1 \cdot \mathbf{N}_1 = \frac{D_{\beta nucmem}(c_1 - c_2)}{d} \tag{4.24}$$

$$\mathbf{n}_2 \cdot \mathbf{N}_2 = \frac{D_{\beta nucmem}(c_2 - c_1)}{d} \tag{4.25}$$

where d is the thickness of the thin boundary layer.

4.1.2.6 Parameter values

All of the parameters used in this simulation are shown in Table 4.1. The parameters for the kinetics of the system are taken from [Ramis-Conde et al. (2008b)] and the additional advection and diffusion coefficients have been estimated.

Table 4.1: *Parameter Values for Single Cell model*

Parameter	Definition	Value
ν	E-cadherin-β-catenin binding rate	100 min^{-1}
k^+	β-catenin-proteasome binding rate	100 min^{-1}
k^-	β-catenin-proteasome dissociation rate	19 min^{-1}
k_2	β-catenin degradation rate in proteasome	0.03 min^{-1}
k_m	β-catenin production rate	0.01 nM/min^{-1}
P_t	Proteasome total concentration	0.33514 nM
E_t	E-caherin total concentration	100 nM
c_T	β-catenin threshold value	50nM
α	E-cadherin-β-catenin dissociation rate	2 min^{-1}
A	Advection field coefficient	20 μm min^{-1}
D_{Ecyto}	Diffusion coefficient for $[E]$ in cytoplasm	1 μm min^{-1}
$D_{\beta cyto}$	Diffusion coefficient for $[\beta]$ in cytoplasm	2 μm min^{-1}
$D_{E/\beta cyto}$	Diffusion coefficient for $[E/\beta]$ in cytoplasm	1 μm min^{-1}
D_{Ccyto}	Diffusion coefficient for $[C]$ in cytoplasm	1 μm min^{-1}
$D_{\beta nucmem}$	Diffusion coefficient for $[\beta]$ in nuclear membrane	0.01 μm min^{-1}
$D_{\beta nuc}$	Diffusion coefficient for $[\beta]$ in nucleus	1 μm min^{-1}
d	Thickness of thin boundary layer	0.03 μm

4.1.2.7 Results

Equations (4.13)–(4.18) along with the Initial conditions (4.19)–(4.22) and Boundary conditions (4.23)–(4.25) were solved on the domain using COMSOL. The equations and parameters describe cells becoming attached to each other.

Figure 4.5 shows the progression of the concentration of E-cadherin within the cell over time. The total concentration begins in the ribosome area, just outside the nucleus and is transported to the edge of the cell very quickly. The interactions between E-cadherin and β-catenin result in a dynamic steady state, which shows most of the free E-cadherin near the edge of the cell. This is a result of constant breaking up and getting back together of E-cadherin-β-catenin bonds during adhesion.

Figure 4.6 shows the initial condition of no E-cadherin-β-catenin complexes. As the simulation progresses, these bonds are formed in the cytoplasm and then transported to the edge of the cell. This models the fact that E-cadherin binds to β-catenin immediately after synthesis [Hinck et al. (1994); Näthke et al. (1994)] and not just when both proteins have reached the membrane. A dynamic steady state is reached because of a constant turnover in the creation and destruction of E-cadherin-β-catenin bonds.

Figure 4.7 shows the concentration of free (soluble) β-catenin within the cell. Most of the free β-catenin goes to the edge of the cell because of the turnover of E-cadherin-β-catenin complexes. The rest of the cytoplasm has a very small concentration of β-catenin because this is where the proteasome is degrading it. There is also a population of β-catenin in the nucleus, which has decreased.

Lastly, figure 4.8 shows the concentration of the proteasome-β-catenin complex. This also reaches a steady state.

The levels of each protein in Figures 4.5 - 4.8 are similar to the levels shown in Figure 4.2. However, the position of the proteins within the cell can be seen. Therefore, the spatial model may now be expanded by examining a domain of two cells undergoing cell-cell adhesion.

4.1.3 Two cell model

Using the Single Cell Model above, which looks at one cell in an epithelial sheet, a model to look at the interactions between two cells is the next logical step. Therefore, this section is concerned with the geometry shown in Figure 4.9. Two hexagons are used to represent the cells and each has a central circle representing the nucleus. To adjoin the two hexagons, there is a thin rectangle representing an adherins junction and there are also two thin boundary layers in between the hexagons and the rectangle to represent the cell membranes.

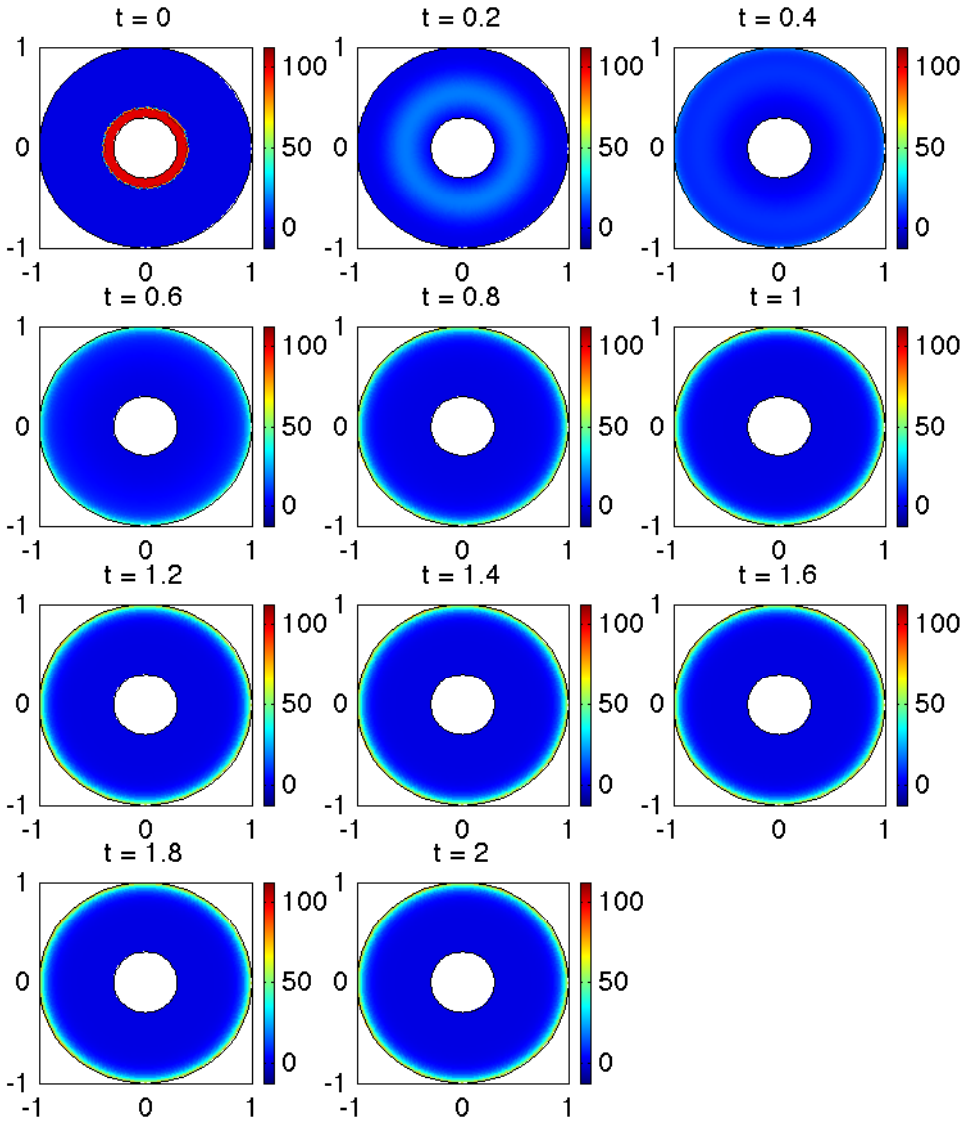

Figure 4.5: *These figures show the concentration of E-cadherin within the cell's cytoplasm from a time of 0 to 2 minutes as the cell makes contact with other cells (not shown). Initially the E-cadherin is located in the cytoplasm near the nucleus, which represents the Golgi apparatus. Upon cell-cell contact, the E-cadherin is transported to the membrane where it can engage in cell-cell adhesion by binding with β-catenin. A dynamic equilibrium is achieved at t=1 minute.*

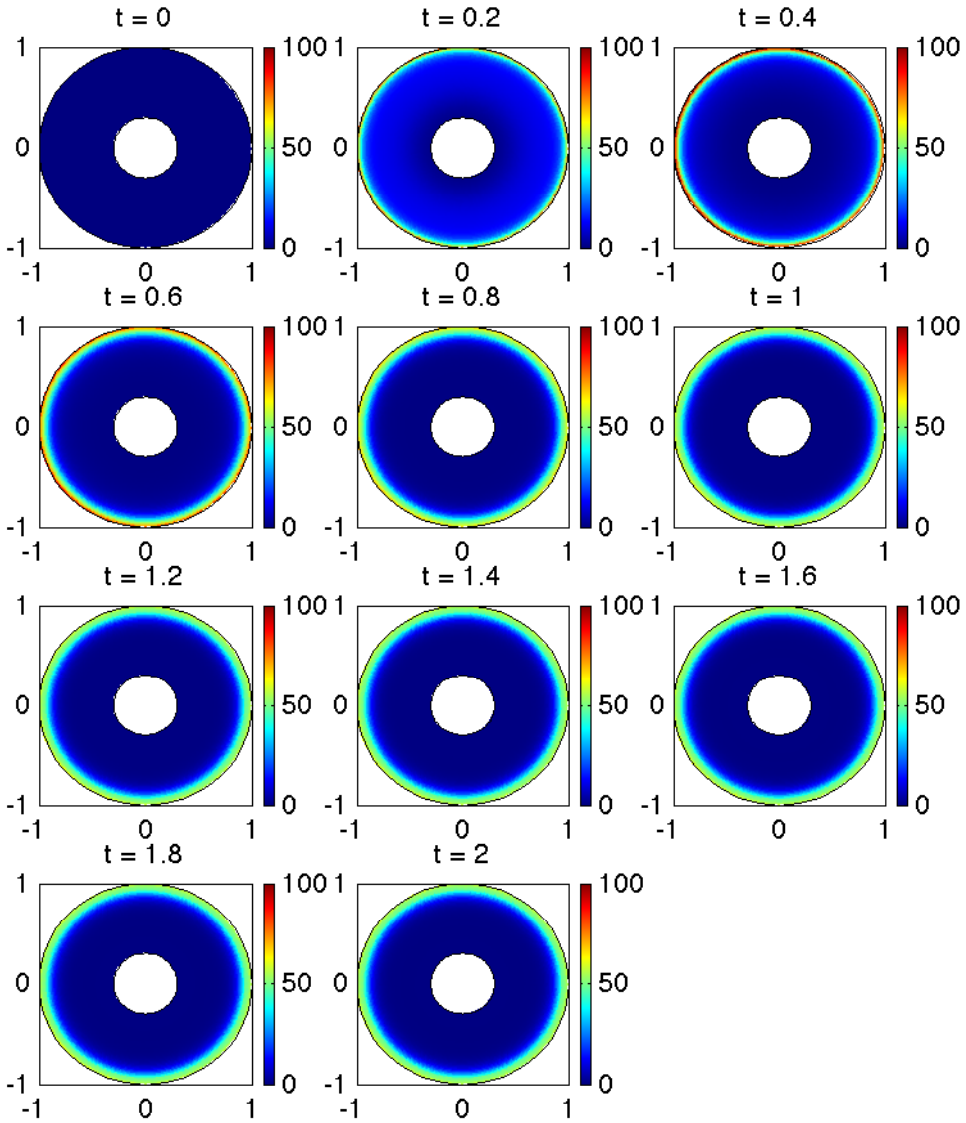

Figure 4.6: *These figures show the concentration of the E-cadherin/β-catenin complex within the cell's cytoplasm from a time of 0 to 2 minutes as the cell makes contact with other cells (not shown). Initially there are no complexes because the cell is not engaged in cell-cell adhesion. However, as time progresses the complex is formed near the membrane to form adherens junctions. A dynamic equilibrium is achieved at t=1 minute.*

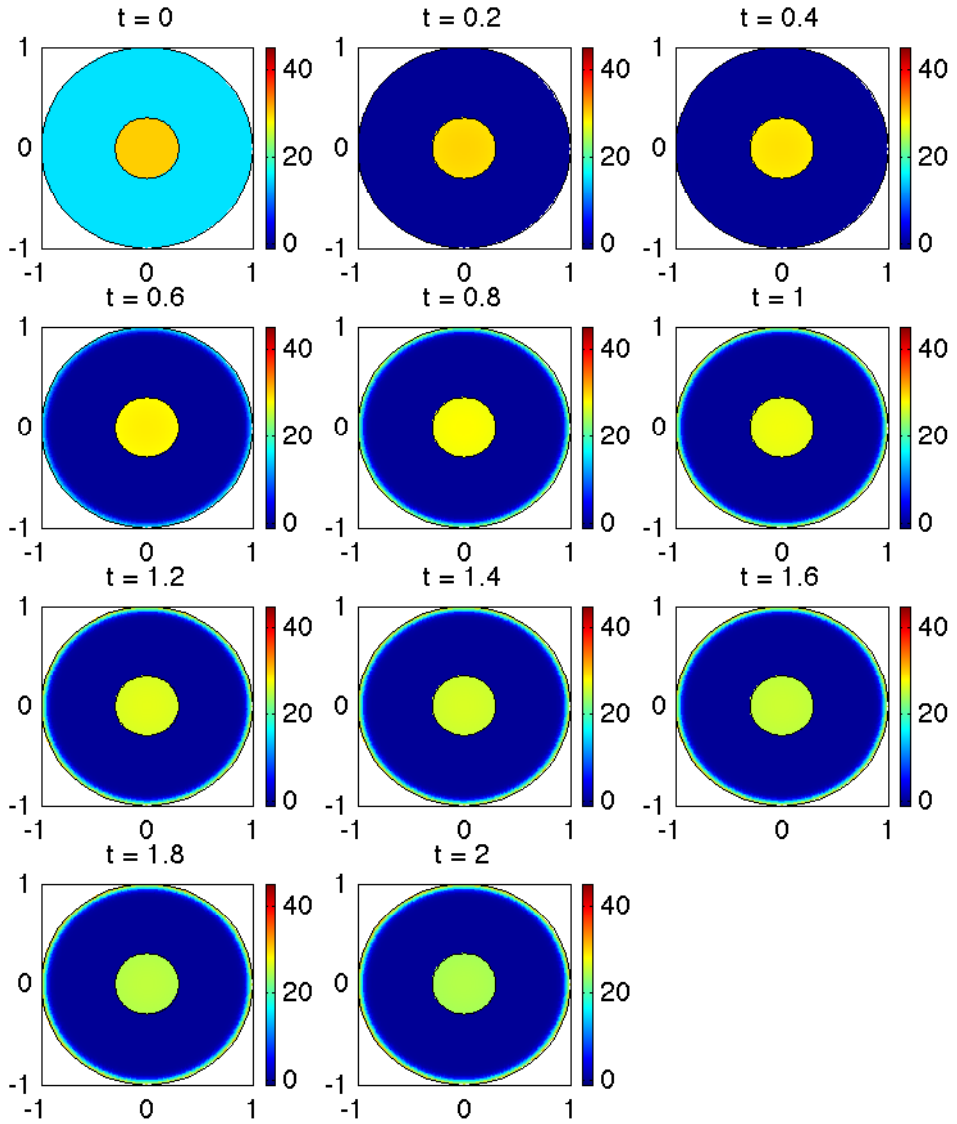

Figure 4.7: *These figures show the concentration of free β-catenin within the cell's cytoplasm and nucleus from a time of 0 to 2 minutes as the cell makes contact with other cells (not shown). Initially, there is a high concentration of β-catenin in the nucleus and a moderate concentration distributed evenly in the cytoplasm. This describes a mesenchymal cell, in which the destruction complex of Axin, Apc and GSK-3β is not working to target β-catenin for destruction. Therefore, β-catenin is allowed to build up in the cytoplasm and nucleus. When the cell makes contact with other cells, it undergoes the Mesenchymal-Epithelial transition. This causes a reduction in the nuclear concentration of β-catenin and the β-catenin in the cytoplasm is transported to the membrane, where it can bind to E-cadherin to form adherens junctions. A dynamic equilibrium is reached in the cytoplasm at t=1 minute but nuclear concentration continues to reduce after this time.*

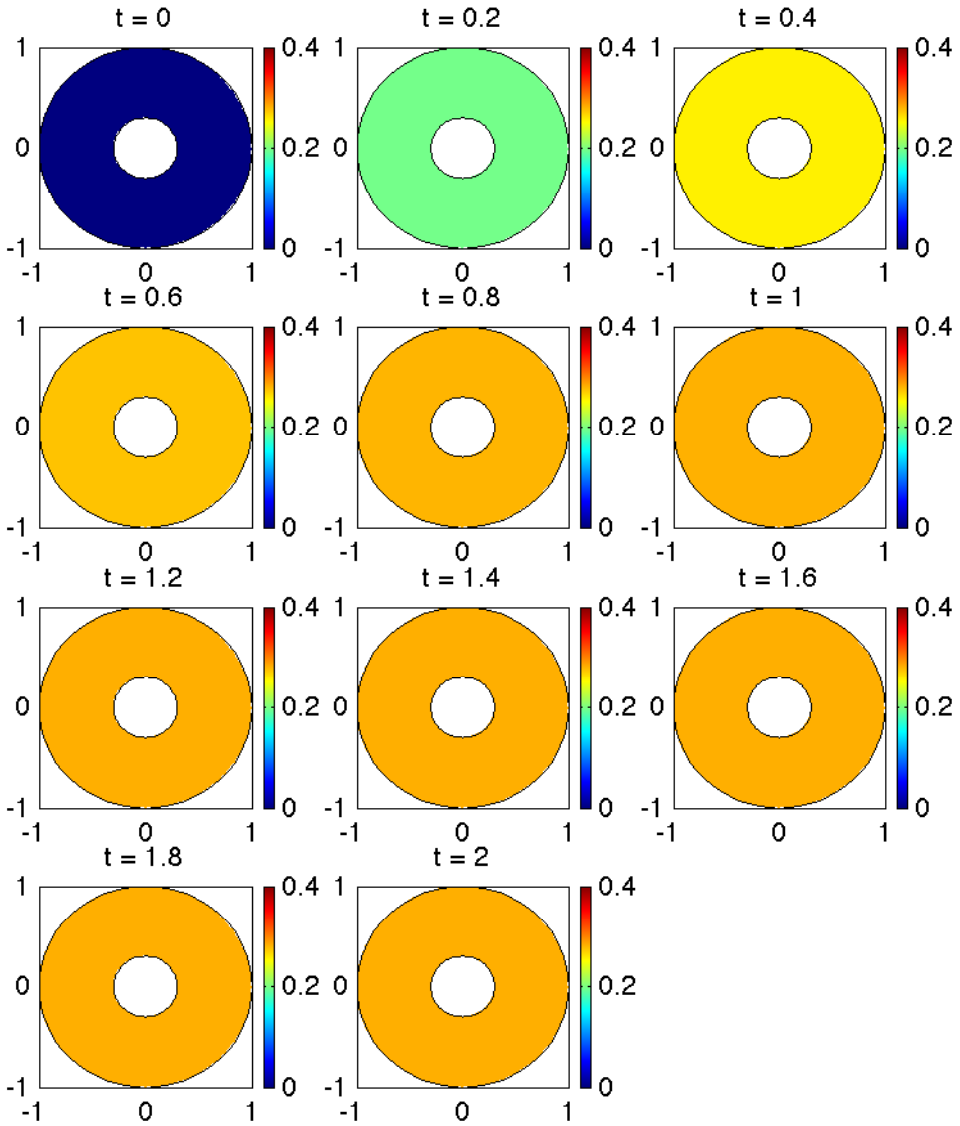

Figure 4.8: *These figures show the concentration of the β-catenin/proteasome complex within the cell's cytoplasm from a time of 0 to 2 minutes as the cell makes contact with other cells (not shown). Initially there are no β-catenin/proteasome complexes because the destruction complex is not functioning as the cell is of the mesenchymal phenotype. As cell-cell contact is made, the complex is formed and β-catenin is destroyed. A dynamic equilibrium is reached at t=1 minute.*

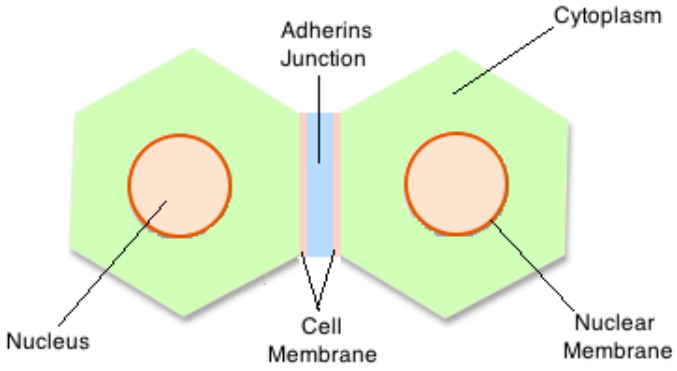

Figure 4.9: *Schematic of two cells in contact, represented by hexagons. Each cell contains a nucleus with a nuclear membrane which separates it from the cytoplasm, represented by a thin boundary layer. At the point of cell-cell contact, the cell membrane is depicted by a thin boundary layer. A thin adherens junction zone is used to represent the extracellular space in which E-cadherin proteins from both cells bind to each other to form adhesive bonds.*

4.1.3.1 In the cytoplasms

Using the single cell model as a basis for this model, we use the following equations in the cytoplasm of both cells:

$$\frac{\partial[E]}{\partial t} = \nabla \cdot (D_{Ecyto}\nabla[E] + \mathbf{a}[E]) - c_i(t) + d_i(t)[E/\beta], \tag{4.26}$$

$$\frac{\partial[E/\beta]}{\partial t} = \nabla \cdot (D_{E/\beta cyto}\nabla[E/\beta] + \mathbf{a}[E/\beta]) + \nu(E_T - [E] - [E/\beta])[\beta] - d_i(t)[E/\beta], \tag{4.27}$$

$$\frac{\partial[\beta]}{\partial t} = D_{\beta cyto}\nabla^2[\beta] - \nu(E_T - [E] - [E/\beta]) + d_i(t)[E/\beta] - k^+[\beta](P_T - [C]) + k^-[C] + k_m, \tag{4.28}$$

$$\frac{\partial[C]}{\partial t} = D_{Ccyto}\nabla^2[C] + k^+[\beta](P_T - [C]) - k^-[C] - k_2[C], \tag{4.29}$$

where

$$\mathbf{a} = A\left(\frac{x}{\sqrt{x^2+y^2}}, \frac{y}{\sqrt{x^2+y^2}}\right).$$

4.1.3.2 In the nuclei

The nuclei of both the cells have exactly the same properties as in the single cell model. Therefore,

$$\frac{d[\beta]}{dt} = D_{\beta nuc}\nabla^2[\beta] \tag{4.30}$$

will used to describe both of the nuclei.

4.1.3.3 In the nuclear membranes

The nuclear membrane of both cells has the same properties of the single cell model. Therefore, the equation for this section of the model is

$$\frac{\partial[\beta]}{\partial t} = D_{\beta nucmem}\nabla^2[\beta], \tag{4.31}$$

where $D_{E/\beta nucmem}$ will be small.

4.1.3.4 In the cellular membranes

There is a thin boundary layer, which is used to represent the membrane of the two cells. This represents the membrane of the cell, which the main part of E-cadherin must pass through to get to extracellular space so that it can bind with E-cadherin from another cell. This is modeled by making it difficult for the E-cadherin to cross into the *adherins junction zone*. This gives the following equation:

$$\frac{\partial[E/\beta]}{\partial t} = D_{E/\beta mem}\nabla^2[E/\beta] \tag{4.32}$$

where $D_{E/\beta nucmem}$ will be small.

4.1.3.5 In the adherens junction zone

This section is used to model the adherins junction between two cells and, as a consequence of this, only the complex E-cadherin-β-catenin is allowed to enter this part. This is the section that would incorporate the homophilic binding of E-cadherin molecules

in extracellular space. As there is no free E-cadherin or β-catenin in this section, there are no kinetics. Therefore, the diffusion of E-cadherin-β-catenin is the only term here. This gives the equation

$$\frac{\partial [E/\beta]}{\partial t} = D_{E/\beta AJ} \nabla^2 \cdot [E/\beta], \tag{4.33}$$

where the diffusion coefficient $D_{E/\beta AJ}$ will be very small.

4.1.3.6 Initial conditions

The initial conditions are similar to the single cell model and are as follows:

$$E(\mathbf{x},0) = \begin{cases} 100, & \text{in each Golgi apparatus area,} \\ 0, & \text{everywhere else,} \end{cases} \tag{4.34}$$

$$\beta(\mathbf{x},0) = \begin{cases} 10, & \text{in each nucleus,} \\ 5, & \text{in each cytoplasm,} \\ 0, & \text{in adherins junction,} \end{cases} \tag{4.35}$$

$$E/\beta(\mathbf{x},0) = \begin{cases} 1, & \text{in adherins junction,} \\ 0, & \text{everywhere else,} \end{cases} \tag{4.36}$$

$$C(\mathbf{x},0) = 0, \quad \text{everywhere.} \tag{4.37}$$

4.1.3.7 Boundary conditions

For the exterior edge of the cell away from the adherins junction zero flux boundary conditions are imposed. This is represented by

$$\mathbf{n} \cdot \mathbf{N} = 0, \tag{4.38}$$

$$\text{where } \mathbf{N} = -D\nabla u_i + u_i \mathbf{u},$$

$$\text{and } \mathbf{u} = \begin{pmatrix} [E] \\ [E/\beta] \\ [\beta] \\ [C] \end{pmatrix}.$$

Across the thin boundary layers at the adherins junction, there is a flux of E-cadherin-β-catenin. This is represented by

$$\mathbf{n}_1 \cdot \mathbf{N}_1 = \frac{D_{E/\beta aj}(c_1 - c_2)}{d1}, \tag{4.39}$$

$$\mathbf{n}_2 \cdot \mathbf{N}_2 = \frac{D_{E/\beta aj}(c_2 - c_1)}{d1}, \tag{4.40}$$

where $d1$ represents the thickness of the thin boundary layers at the adherins junction Across the thin boundary layers that represent the nuclear membranes, there is a flux of β-catenin. This is represented by

$$\mathbf{n}_1 \cdot \mathbf{N}_1 = \frac{D_{\beta nucmem}(c_1 - c_2)}{d2}, \tag{4.41}$$

$$\mathbf{n}_2 \cdot \mathbf{N}_2 = \frac{D_{\beta nucmem}(c_2 - c_1)}{d2}, \tag{4.42}$$

where $d2$ is the thickness of the thin boundary layers that represent the nuclear membranes.

4.1.3.8 Parameter values

Most of the parameters are the same as the Single Cell model shown in Table 4.1. However, some of the parameter values have been changed for this model, shown in Table 4.2. Table 4.2 also contains some of the additional parameters that are required.

Table 4.2: *Parameter Values for Two Cell Model*

Parameter	Definition	Value
A	Advection field coefficient	1 μm min^{-1}
$D_{E/\beta cyto}$	Diffusion coefficient for $[E/\beta]$ in cytoplasm	0.2 μm min^{-1}
$D_{E/\beta aj}$	Diffusion coefficient for $[E/\beta]$ at the adherins junction	0.2 μm min^{-1}
D_{Ccyto}	Diffusion coefficient for $[C]$ in cytoplasm	0.5 μm min^{-1}
$D_{\beta cyto}$	Diffusion coefficient for $[\beta]$ in cytoplasm	1 μm min^{-1}
$D_{\beta nucmem}$	Diffusion coefficient for $[\beta]$ in nuclear membrane	0.9 μm min^{-1}
$D_{\beta nuc}$	Diffusion coefficient for $[\beta]$ in nucleus	0.5 μm min^{-1}
D_{Ccyto}	Diffusion coefficient for $[C]$ in cytoplasm	0.5μm min^{-1}
$d1$	Thickness of thin boundary layer at adherins junctions	0.001 μm
$d2$	Thickness of thin boundary layer at nuclear membrane	0.001 μm

4.1.3.9 Results

The equations (4.26) - (4.33) along with initial conditions (4.34) - (4.37) and boundary conditions (4.38) - (4.42) were solved in COMSOL multiphysics. The simulations describe the attachment of two cells.

Figure 4.10 shows the progression of the concentration of E-cadherin in the two cell

model. The initial condition is shown at time $t = 0$ where all of the E-cadherin is contained in the ribosome area. As time progresses, the E-cadherin is quickly transported to the cell surface before collecting at the point of contact with the second cell. A steady state is reached, which describes a strong adhesion between the two cells. This can be compared with Figure 4.11 where the E-cadherin has been bound to a green fluorescent protein so that it can be identified. The cells in the epithelial sheet are attached to one another and the E-cadherin is located in between the cells, just as it is in the simulation.

Figure 4.12 shows the progression of the concentration of the complex E-cadherin-β-catenin in space and time. When the cells are not engaging in adhesion there is no E-cadherin-β-catenin, as shown at $t = 0$. As time passes, the complex collects near the cellular membrane until a steady state is reached. This describes a stable adherins junction connecting the two cells.

Figure 4.13 shows the progression of β-catenin within the two cells. At $t = 0$ the initial condition shows a constant level in the nucleus and a different constant level in the cytoplasm. Initially, β-catenin is represented mathematically as being evenly distributed within the cell. As time moves forward the β-catenin moves towards the site of cell-cell adhesion. Here, it helps to bind the trans-membrane E-cadherin connections to the cytoskeleton of the cell. A steady state is reached as with the other proteins.

Figure 4.14 shows the spatial and temporal progression of the multi-protein complex of β-catenin and the proteasome complex. Initially there is none of this complex in the cell. As time moves on, the complex follows the same placement as the β-catenin and therefore has a similar figure. A steady state is reached just as the other proteins do.

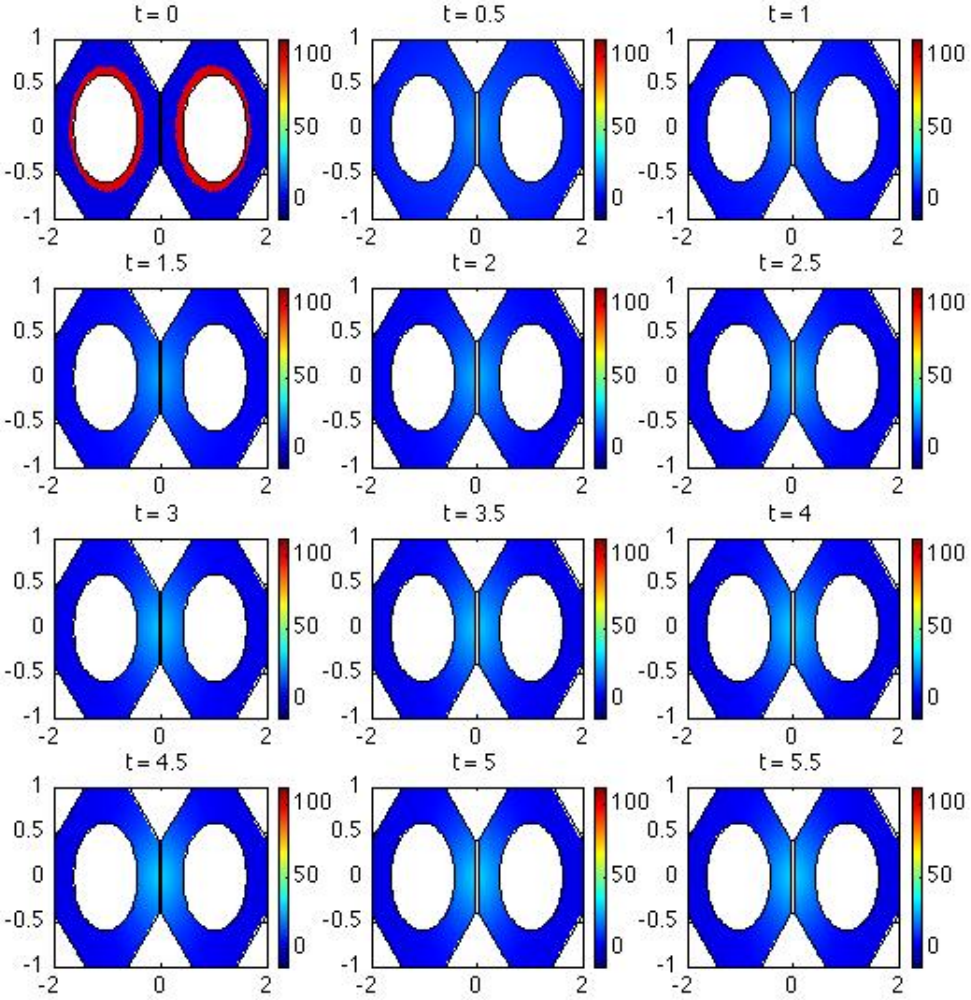

Figure 4.10: *These figures show the concentration of E-cadherin within the cytoplasm of two cells as they come into contact to form an adherens junction from time 0 to 5.5 minutes. Initially the E-cadherin is located around the nucleus of each cell, the Golgi apparatus zone. As time progresses, the E-cadherin is transported to the membrane at the point of cell-cell contact where it can engage in cell-cell adhesion by binding to* β*-catenin. Dynamic equilibrium is achieved at t=4 minutes.*

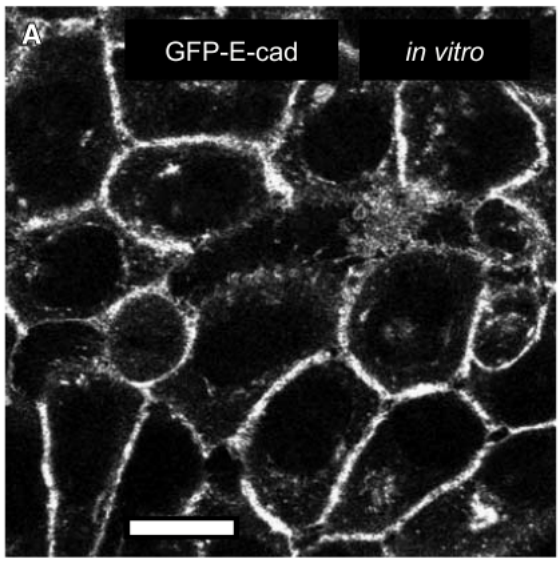

Figure 4.11: *Location of GFP-E-cadherin shown in an in vitro experiment of a cell monolayer. Reproduced with copyright permission from Serrels et al. (2009).*

4.1.4 Discussion

While the E-cadherin-β-catenin pathway and its importance in the development of cancer has been researched in great depth, a mathematical model to investigate the spatial activity of the proteins in question has not previously been formulated. This chapter has developed a two cell model to examine the spatial positioning of the proteins within the cells. This was based on the work of Ramis-Conde et al. (2008b) which led to an initial model of a single cell within an epithelial sheet. The information from the single cell model was then used to aid the development of the two cell model.

The results of the two cell model show that the E-cadherin and E-cadherin-β-catenin are mainly located at the membrane where the cells are in contact. This compares well with the cells *in vitro* in Figure 4.11. Also, low levels of β-catenin have been shown in the cell. This means that the proteasome that represents GSK-3β and other proteins are

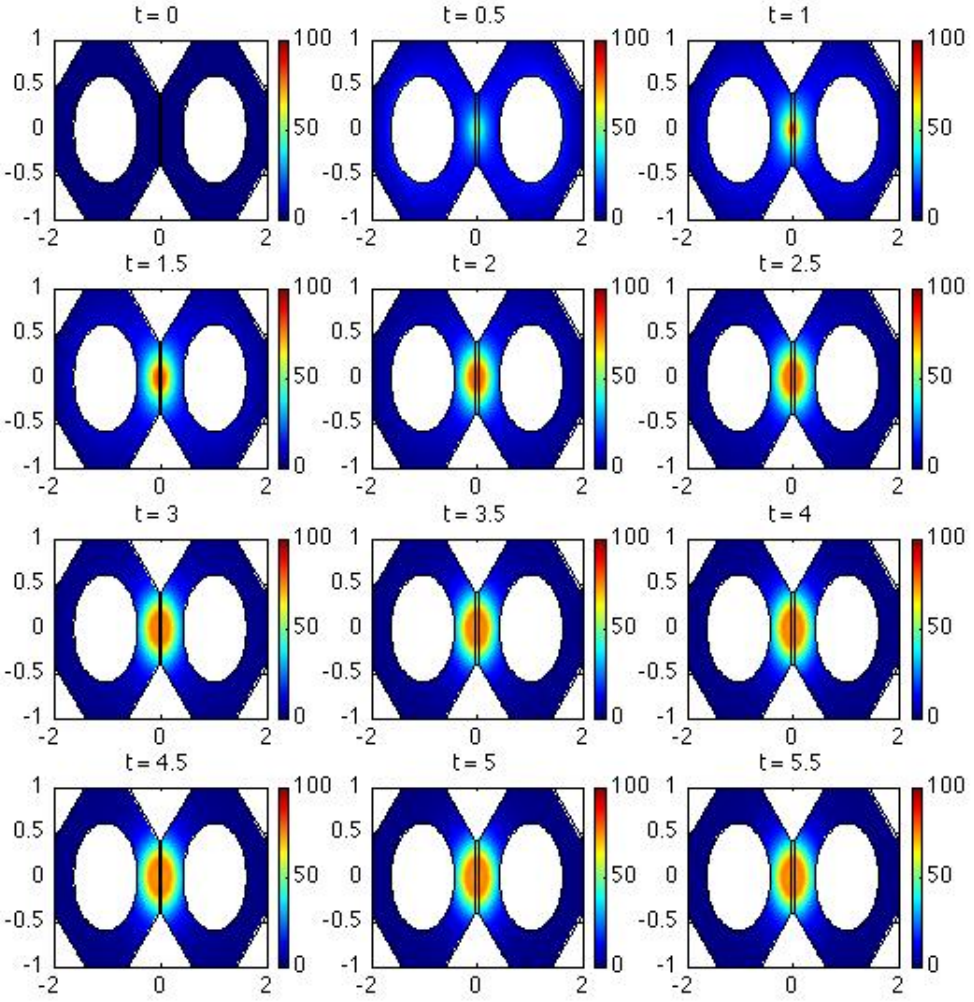

Figure 4.12: *These figures show the concentration of the E-cadherin/β-catenin complex within the cytoplasm of two cells and the extracellular domain between them as they come into contact to form an adherens junction from time 0 to 5.5 minutes. Initially there are no E-cadherin/β-catenin complexes because the cells are not in contact. As contact is made, E-cadherin and β-catenin bind together at the membrane and the complex enters the extracellular domain to form an adherens junction. Dynamic equilibrium is achieved at t=4 minutes.*

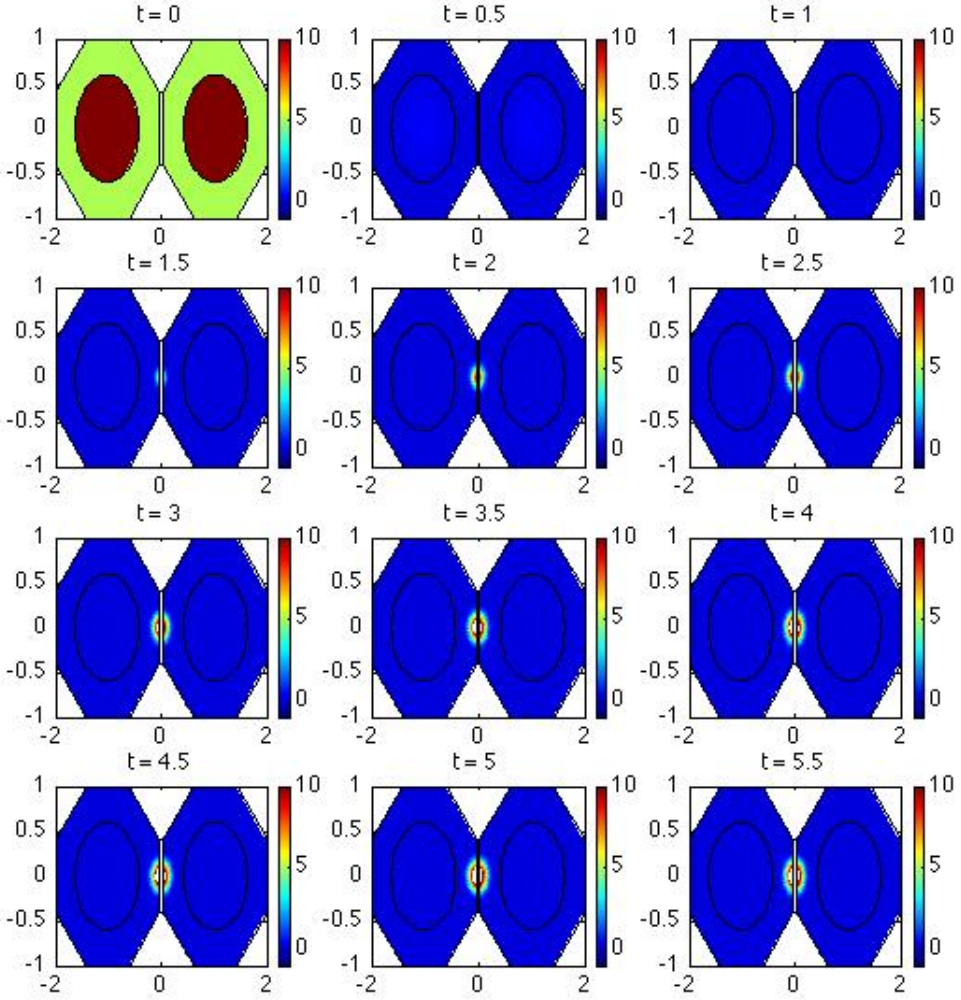

Figure 4.13: *These figures show the concentration of β-catenin within the cytoplasm and nucleus of two cells as they come into contact to form an adherens junction from time 0 to 5.5 minutes. Initially there is a high concentration of β-catenin in the nucleus and a moderate concentration in the cytoplasm of both cells as they are of the mesenchymal phenotype. As cell-cell contact is made, the β-catenin is transported to the membrane at the point of contact where it can bind to E-cadherin to engage in adhesion. Also, β-catenin in the cytoplasm is degraded by the proteasome. A dynamic equilibrium is achieved at t=4 minutes.*

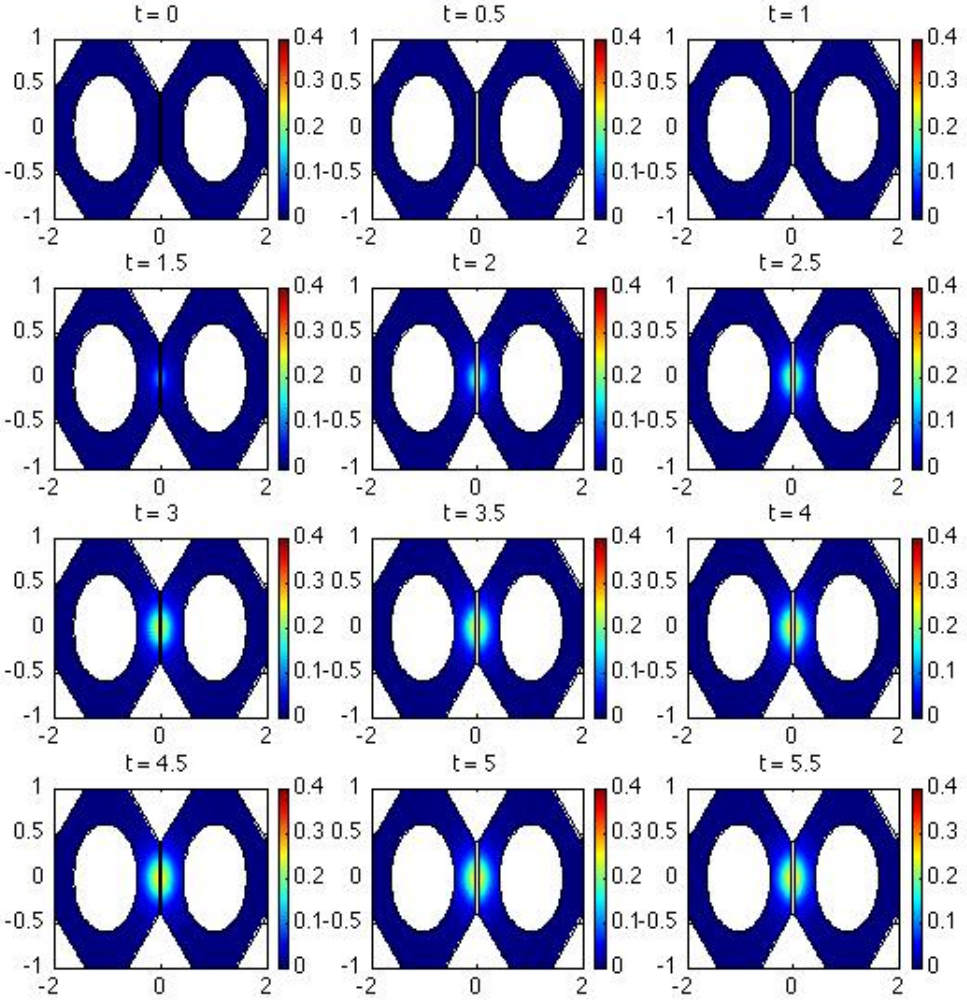

Figure 4.14: *These figures show the concentration of the β-catenin/proteasome complex within the cytoplasm of two cells and the extracellular domain between them as they come into contact to form an adherens junction from time 0 to 5.5 minutes. Initially the proteasome is not active because the cell is of the mesenchymal phenotype and therefore the concentration is zero. As contact is made, the proteasome is able to form complexes with β-catenin in order to degrade it. A dynamic equilibrium is achieved at t=4 minutes.*

performing the job of destroying the β-catenin at the right levels. Therefore, the model has created a stable adhesion between two cells in an epithelial sheet.

The next step that will be carried out is to perturb this stable model. From an initial condition of stable adhesion between the cells, detachment will be simulated. This will be done by altering the equations, which happened in [Ramis-Conde et al. (2008b)]. Breaking of the E-cadherin bonds in intercellular space may be caused by mechanical stress or by signalling from within the cell. The broken E-cadherin-β-catenin bonds will result in free E-cadherin and β-catenin in the cytoplasm. The soluble β-catenin levels may grow high enough to be translocated to the nucleus and promote proliferation. This alteration to the model may be a good indication of what happens to a cancerous cell and may give an insight into why they try to break their adhesive bonds.

A way to improve the model would be to use more accurate parameter values, as most of the parameters have been estimated. It is hoped that this will be accomplished by performing experiments on cells *in vitro*. This would use MDCK cells that lack calcium, which means the E-cadherin would be unable to perform its adhesive function. Therefore, the cells would sit beside each other but not engage in adhesion. The E-cadherin and β-catenin would then be bound to proteins that are visible under immunofluorescence, for example green fluorescent protein (GFP). Then by adding calcium to the dish, adhesion would begin. By the use of immunofluorescence, some parameter values will be able to be calculated. The inclusion of the recorded parameter values would greatly improve the accuracy and viability of the model and allowing better predictions.

Another modelling technique to consider in the future is to use an element of randomness. Within a cell many random actions take place and the best way to model this is to use stochastic processes. Adding stochasticity would enhance the current model and

bring it closer to real life observations of intra/extra-celluar activities.

4.2 Different forms of β-catenin within the cell

In order for β-catenin to perform different functions within the cell it has been shown that it can take several forms. Gottardi and Gumbiner (2004a) described five conformations of β-catenin within the cell which governs how it can interact with other proteins. The five forms of β-catenin described by Gottardi and Gumbiner (2004a) can be seen in Figure 4.15 and are phosphorylated, closed, open, a dimer with α-catenin and inactive.

It is well known that cytoplasmic β-catenin is targeted by the destruction complex for degradation by the process of phosphorylation. When targeted, the phosphorylated form of β-catenin is quickly degraded by a proteasome. However, the destruction complex is disrupted if Wnt is present and leads to a build up of β-catenin within the cytoplasm. For a review of this in the context of cancer see Polakis (1999).

The closed conformation, which selectively binds to TCF, was shown to exist and is controlled by Wnt proteins. However, the precise mechanism by which this change happens is not known. This form is of particular interest because it could be the key to understanding β-catenin's oncogenic properties.

The open conformation is capable of both adhesion and transcription and was observed under certain conditions in Gottardi and Gumbiner (2004a). Therefore, it is postulated that this form exists under normal conditions and it would explain why E-cadherin is able to inhibit the transcriptional activity that was seen above in Ramis-Conde et al. (2008b).

The dimer of β-catenin and α-catenin is important in adhesion because α-catenin is necessary to connect the adherens junction to the actin cytoskeleton of the cell. However, there is also evidence to suggest that it is actively able to inhibit the transcriptional activities of β-catenin [Giannini et al. (2000); Daugherty et al. (2014)]. Therefore, it is regarded as only able to participate in adhesion activities. It should be noted that α-catenin does not transform the β-catenin so if the bond is broken then it would be able to engage in transcription.

The final conformation is an inactive form of β-catenin which is unable to bind with E-cadherin or TCF making it unable to participate in adhesion or transcription. This was found in Gottardi et al. (2001) and it could be caused by ICAT, a polypeptide that binds to β-catenin. [Gottardi and Gumbiner (2004b), Tago et al. (2000)].

In this section, a new ordinary differential equation model is developed of the E-cadherin and β-catenin pathway. While several models of this pathway have been created [Lee et al. (2003), Ramis-Conde et al. (2008b), Mirams et al. (2010)], this approach is novel because it examines the different conformations of β-catenin described above.

4.2.1 Description of variables

In the system of differential equations presented in this section there are twelve variables and these are shown in Table 4.3. They exist in three separate regions of the cell: in the cytoplasm, in the nucleus and at the membrane.

In the cytoplasm, there exists five conformations of β-catenin that that were described in Gottardi and Gumbiner (2004a): β_O, β_C β_D β_P β_I. It should be noted that D is the destruction complex made up of Axin, Apc and GSK-3β. This is active when Wnt is not

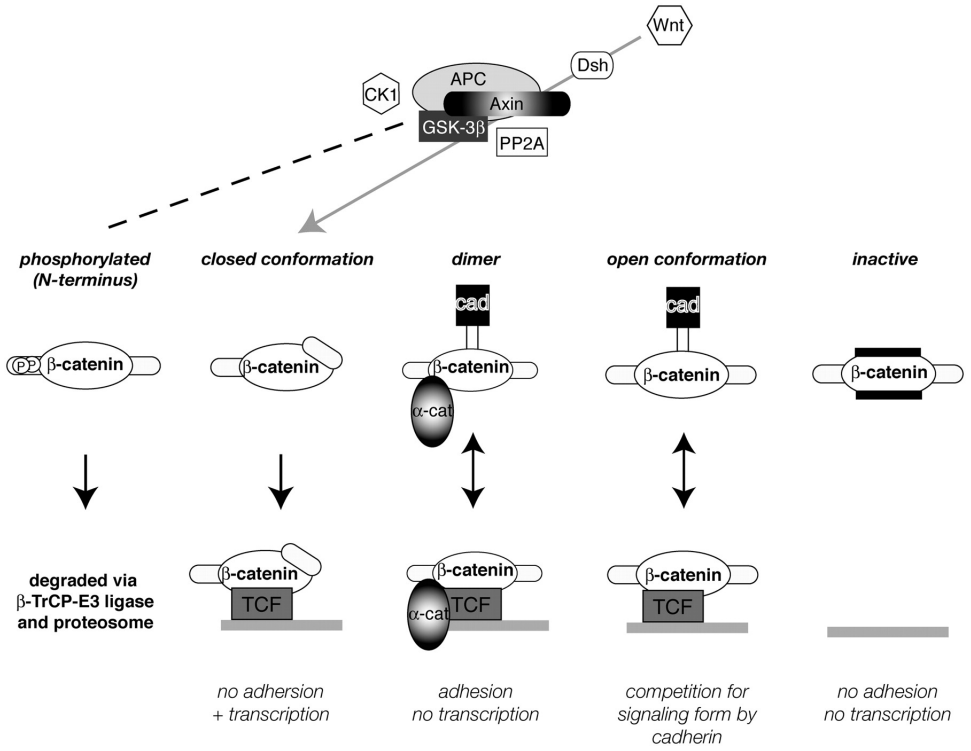

Figure 4.15: *The types of β-catenin as described by Gottardi and Gumbiner (2004a). When Wnt is not present, β-catenin in the cytoplasm is targeted by the destruction complex of APC, Axin, GSK-3β by phosphorylation and will be degraded by proteasomes. When Wnt is present, the β-catenin in the cytoplasm is transformed into a closed form which prevents it from binding to E-cadherin and stops it from participating in adhesion. When β-catenin is bound to α-catenin, it is prevented from binding to TCF and cannot take part in transcriptional activities. In this paper it was found that there exists an open conformation of β-catenin which can participate in both adhesion and transcription. It could be the case that this is also generated by Wnt signalling. An inactive form of β-catenin was also found, which is unable to participate in adhesion or transaction and may caused by an inhibiting protein. Reproduced from Gottardi and Gumbiner (2004a) in accordance with with Rockefellar University Press Copyright Policy.*

present in the cell's environment. This is disrupted by the presence of Wnt and therefore it will be unable to bind to the various forms of β-catenin. C is the complex of β-catenin with the destruction complex, D. It will produce β_P which is targeted for degradation. E represents the E-cadherin which is not engaged in adhesion. It is located near the cytoplasm where it is waiting for the cell to come into contact with a neighbouring cell so that it can form an adhesive bond in the intercellular space. E_β is when E-cadherin and β-catenin are bound together and taking part in adhesion. There are three variables which are present in the nucleus of the cell. These are: β_N, β-catenin that has been transported to the nucleus; T, a transcription factor; and the complex of the two, T_β.

Table 4.3: *Description of variables in the system of ODEs.*

Variable	Description
β_O	Open conformation capable of both adhesion and transcription.
β_C	Closed conformation only capable of transcription.
β_D	Dimer of β-catenin and α-catenin only capable of transcription.
β_P	Phosphorylated β-catenin which has been targeted for destruction.
β_I	The inactive form of β-catenin which is not capable of adhesion or transcription.
D	Desctruction Complex made up of Axin, Apc and GSK-3β.
C	Descruction complex bound to β-catenin.
E	E-cadherin which is not engaged in adhesion.
E_β	E-cadherin engaged in adhesion with β-catenin.
β_N	β-catenin that is present in the nucleus.
T	Transcription factor.
T_β	Complex of the Transcription factor with β-catenin.

4.2.2 Kinetic reactions

This novel E-cadherin/β-catenin pathway is described by a series of Michaelis-Menten reactions.

The form of β-catenin created by the cell is the open conformation, β_O as it is the natural form of the protein. It is able to participate in adhesion by binding to alpha-catenin and E-cadherin, by being phosphorylated by the destruction complex, by being transformed by Wnt signalling into the closed conformation, by being 'inactivated' by ICAT and being transported to the nucleus where it can interact with TCF.

$$\stackrel{k1}{\rightarrow} [\beta_O] \tag{4.43}$$

The destruction complex, D, is able to interact with β_O, β_C,β_D and β_I by forming a complex, C. After the complex is formed it can result in the phosphorylation of β-catenin to create β_P, which is subsequently destroyed. It is also possible that the complex C may break up into the destruction complex and β-catenin.

$$[\beta_i] + [D] \underset{k2^-}{\overset{k2^+}{\rightleftharpoons}} [C] \stackrel{k3}{\rightarrow} [\beta_P] + D \tag{4.44}$$

$$\text{where } i = O, C, D, I,$$

$$[\beta_P] \stackrel{k4}{\rightarrow} \tag{4.45}$$

The reactions that take place at the membrane involve the E-cadherin, β_O and β_D. As in Ramis-Conde et al. (2008b), when the cell is not engaged in cell-cell adhesion, the E-cadherin, E, waits near the membrane for cell contact. Once this happens the E-cadherin binds to β-catenin, β_O or β_D, to form E_β which binds to E-cadherin from the neighbouring cell in intercellular space. When the cell-cell contact is broken, the E_β

complex is brought into the cytoplasm by endocytosis.

$$[E] + [\beta_j] \underset{k5^-}{\overset{k5^+}{\rightleftharpoons}} [E_\beta], \quad \text{where } j = O, D. \tag{4.46}$$

When the β-catenin reaches critical levels within the cytoplasm it may be transported into the nucleus. These reactions describe the transportation of β_O and β_C, the two forms of β-catenin which are capable of transcriptional activities, to the nucleus where it is called N.

$$[\beta_O] \underset{k6^-}{\overset{k6^+}{\rightleftharpoons}} [N] \tag{4.47}$$

$$[\beta_C] \underset{k6^-}{\overset{k6^+}{\rightleftharpoons}} [N] \tag{4.48}$$

The following reactions describe how β-catenin in the nucleus and N can engage in transcriptional activities by forming a complex called T_β.

$$[T] + [N] \underset{k7^-}{\overset{k7^+}{\rightleftharpoons}} [T_\beta] \tag{4.49}$$

β-catenin is targeted for degradation by the destruction complex. However, small amounts of β-catenin can be degraded independently of this mechanism. This is described as follows:

$$\beta_{ALL} \overset{k8}{\rightarrow} \tag{4.50}$$

$$N \overset{k8}{\rightarrow} \tag{4.51}$$

TCF and the destruction complex are created and destroyed in a simple manner in this model because the main focus is on the amount and location of the different forms of β-catenin. The creation and destruction of T and D is shown below.

$$\overset{k9}{\rightarrow} [T] \overset{k10}{\rightarrow} \tag{4.52}$$

$$\overset{k11}{\rightarrow} [D] \overset{k12}{\rightarrow} \tag{4.53}$$

4.2.3 Differential equations

The Michaelis-Menten reactions are converted using the Law of Mass Action into the following system of differential equations:

$$\frac{d[\beta_O]}{dt} = k1 - k2^+[\beta_O][D] + k2^-[C] - k5^+[\beta_O][E] + k5^-[E_\beta] \tag{4.54}$$
$$- k6^+[\beta_O] + k6^-[N] - k8[\beta_O],$$
$$\frac{d[\beta_C]}{dt} = k2^-[C] - k2^+[\beta_C][D] - k6^+[\beta_C] + k6^-[N] - k8[\beta_C], \tag{4.55}$$
$$\frac{d[\beta_D]}{dt} = k2^-[C] - k2^+[\beta_D][D] - k5^+[\beta_D][E] + k5^-[E_\beta] - k8[\beta_D], \tag{4.56}$$
$$\frac{d[\beta_I]}{dt} = k2^-[C] - k2^+[\beta_I][D] - k8[\beta_I], \tag{4.57}$$
$$\frac{d[\beta_P]}{dt} = k3[C] - k4, \tag{4.58}$$
$$\frac{d[E]}{dt} = k5^-[E_\beta] - k5^+[E]([\beta_O] + [\beta_D], \tag{4.59}$$
$$\frac{d[E_\beta]}{dt} = k5^+[E]([\beta_O] + [\beta_D]) - k5^-[E_\beta], \tag{4.60}$$
$$\frac{d[N]}{dt} = k6^+([\beta_O] + [\beta_C]) - k6^-[N] - k8[N], \tag{4.61}$$
$$\frac{d[T]}{dt} = k9 + k7^-[T_\beta] - k7^+[N][T] - k10[T], \tag{4.62}$$
$$\frac{d[T_\beta]}{dt} = k7^+[N][T] - k7^-[T_\beta], \tag{4.63}$$
$$\frac{d[D]}{dt} = k11 + k2^-[C] - k2^+([\beta_O] + [\beta_C] + [\beta_D] + [\beta_I])[D] - k12[D], \tag{4.64}$$
$$\frac{d[C]}{dt} = k2^+([\beta_O] + [\beta_C] + [\beta_D] + [\beta_I])[D] - k2^-[C]. \tag{4.65}$$

The set of equations (4.54)-(4.65) are solved numerically and the results are shown in the next section.

4.2.4 Results

Figure 4.16 shows the results of an epithelial cell that has contact with other cells. It does not have any mutations in Apc or β-catenin and Wnt is 'off'. The E-cadherin and most of the β-catenin is being used in adhesion. This can be deduced from the increasing level of $[E_\beta]$, shown in Figures 4.16(a) and 4.16(b), and due to the large percentage of β-catenin at the membrane, depicted in Figure 4.16(c) .

Figure 4.17 shows the results of an active Wnt signal. As can be seen in 4.17(c), the concentration of $[E_\beta]$ is reduced because of the breakage of cell-cell contacts. This, in turn, leads to more β-catenin that is free in the cytoplasm, giving it the ability to transport to the nucleus. The open configuration of β-catenin is released from the E-cadherin and is shuttled to the nucleus. However, the β-catenin dimer cannot move to the nucleus and it degrades independently of APC. Moreover, the closed conformation β-catenin moves into the nucleus, caused by a lack of destruction complexes $[D]$ that control it. At the final time, most of the β-catenin within the cell is in the nucleus, as seen in Figure 4.17(c) .

The ODE model presented here can be used to investigate possible mechanisms by which cells can regulate the adhesive and transcriptional functions of β-catenin. This can prove to be an important factor as this protein can induce the epithelial-mesenchymal transition, which has implications in developmental biology and cancer invasion.

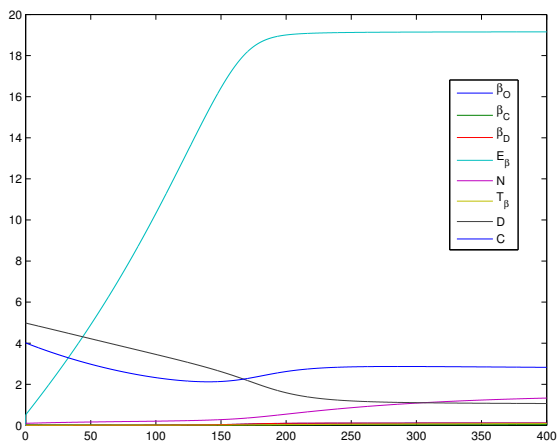

(a)

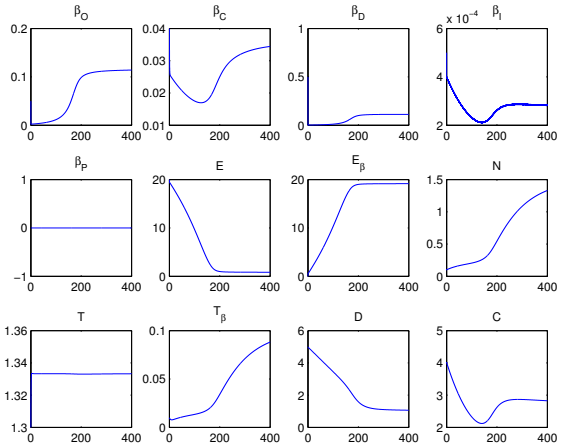

(b)

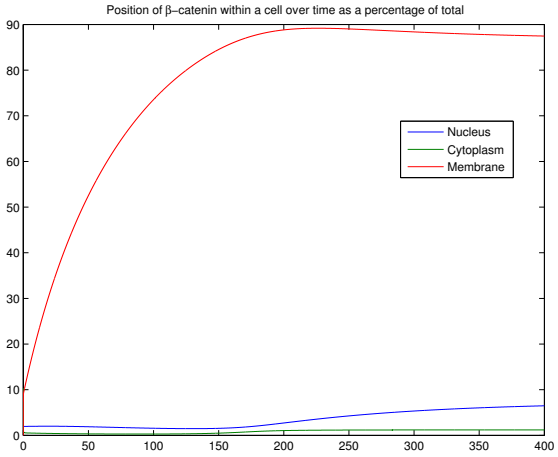

(c)

Figure 4.16: *The protein concentrations resulting from cell-cell contact with Wnt signalling off. Figure (a) displays each the change in the concentration of each protein over time. Figure (b) gives a clearer view of each protein concentration individually over time. Figure (c) shows the percentage of β-catenin that is present in each section of the cell over time. As cell-cell contact is made, it can been seen in (a) and (b) that there is an increase in the concentration of the E-cadherin/β-catenin complexes. Figure (c) shows that as this happens, the majority of the β-catenin within the cell is present at the membrane.*

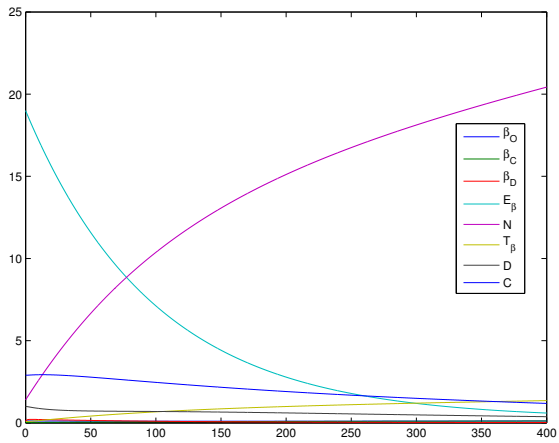

(a)

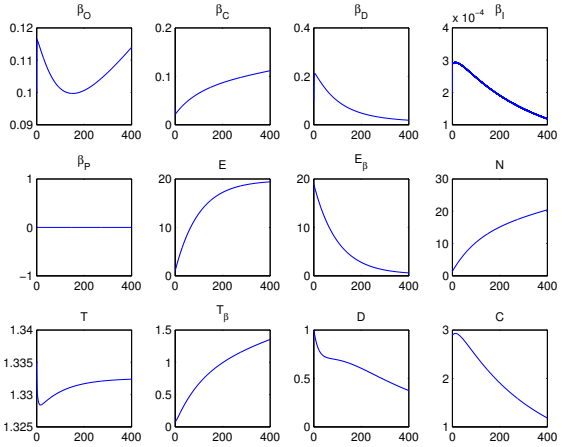

(b)

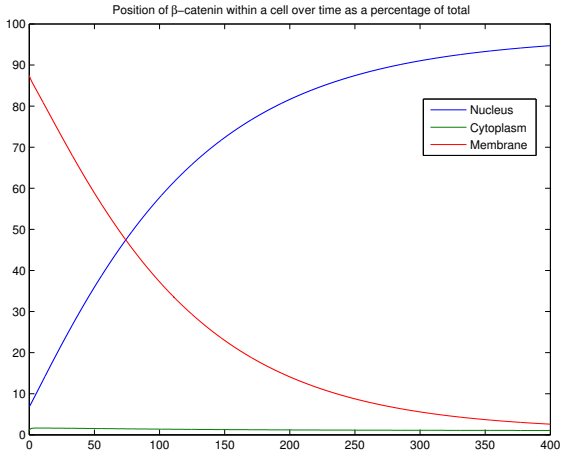

(c)

Figure 4.17: *Concentrations of proteins within an epithelial cell, which become mesenchymal because of the presence of Wnt signalling. Figures (a) and (b) show the concentrations of the proteins over time and (c) shows the percentage of total β-catenin that is present in the nucleus, cytoplasm and at the membrane. The figures show that as soon as Wnt signalling is active and the cell-cell contacts are broken, the E-cadherin/β-catenin bonds are broken rapidly as the complex is endocytolysised. The Wnt signal also causes the destruction complex to break which allows the open and closed conformations of β-catenin to build in the cytoplasm and transport to the nucleus. This overall result of an active Wnt signal can be seen in figure (c), which shows the β-catenin population moving from the membrane to the cytoplasm.*

4.3 Biological experiments

4.3.1 Introduction

The combination of mathematical modelling and biological experimentation is an essential partnership that strives to improve model results. Mathematicians can use biological results to make their models more representative of the biological system and allow model predictions to be more biologically valid. Equally biologists can make use of mathematical models to test predicted results and also to perform experiments *in silico*, which are not possible to do in a wet lab. The E-cadherin/β-catenin pathway has been a prime case for interdisciplinary research because of the interest from both biologists and mathematicians. One of the first such cases of this was in Lee et al. (2003) which develops an ordinary differential equation model for the canonical Wnt signalling pathway and uses experimentation to identify some of the parameter values and find a best fit for the others. This model examines how β-catenin engages in transcriptional activities and how this is affected by the destruction complex with the Wnt signal active and inactive. However, it does not take into account how β-catenin can play a role in adhesion with E-cadherin.

In Lee et al. (2003), a mathematical description of the canonical Wnt pathway was created using the core proteins: β-catenin, Wnt, Dsh, APC, axin, GSK3β, protein phosphate 2A (PP2A) and TCF. The description was in the form of kinetic reactions which included protein creation and destruction, protein phosphorylation and dephosphorylation and the forming and breaking of complexes. These reactions were then translated into a system of fifteen ordinary differential equations which were then condensed into seven ordinary differential equations coupled with four conservation equations. With

this model fully developed, it was then possible to attempt to calculate the parameter values using biological experimentation with Xenopus egg cells.

The calculation of parameters was performed while cells were in a reference state when Wnt signalling was not active. This ensured that Dsh was inactive and β-catenin levels were low because of continuous phosphorylation by the destruction complex and its subsequent degradation. This reference state was defined by the reaction rates, steady state levels of proteins and conservation qualities it exhibited. Therefore, if these constants could be directly calculated then the model would be able to fully replicate the behaviour of the cells in this state. The researchers were able to make measurements of many of the parameters within the model or use existing measurements from literature. However, some of the parameters had to be estimated such that the steady states and flux values of the model agreed with data. For a full explanation of the model and methods used see Lee et al. (2003).

With the combination of theoretical analysis and experimentation, the model created in this paper was able to quantitatively reproduce the experimental data from the reference state and also several perturbations which were created by varying the concentrations of axin, GSK3β and TCF. The model was also extended to reproduce the experimental results of the system when Wnt signalling was active. The authors were then able to show that the model could reproduce a wide variety of experiments and began to use it in a predictive manner.

Predictions were made on a number of aspects of the Wnt signalling pathway which were confirmed using experimentation. An interesting result was the importance of axin within the system. It was shown that the axin concentration amplifies the Wnt signal in the reduction of degradation of β-catenin, promoting transcriptional activity

and oncogenicity, however, it keeps APC and GSK3β at the same concentrations to prevent them from disturbing other signalling pathways. This paper was one of the first to show that metabolic control theory can be effectively extended to model signal transduction and that a joint mathematical and experimental approach was possible to make discoveries in this field.

A new mathematical model to investigate the dual nature of β-catenin was created in van Leeuwen et al. (2007). This used a multicompartment model of the Wnt signalling pathway and E-cadherin/β-catenin pathway in normal and cancerous cells. However, this was not refined by experimental data. In response to this paper, Tan et al. (2011) realised the need for quantitative data on the location of β-catenin within mammalian cells; whether it was in the nucleus, cytoplasm or at the membrane. Therefore, the first experiments carried out in this paper were to quantify the size of each of the three parts of the cell. A technique was developed using fluorescent markers for each of the three cellular compartments: Calcein AM fluorescent dye for the cytoplasm, Hoeschst 33342 nucleic acid stain for the nucleus and Vybrant Dil cell labelling solution for the membrane. When these markers were applied to the cells it was possible to use confocal imaging to measure the volume of each part. These results showed that about half of the volume of a cell is made up of its cytoplasm while the nucleus and the membrane each make up about a quarter of the cell's volume. The development of this technique is important in modelling cellular signalling pathways because it can be used to give quantitative data on where the proteins are situated within the cell and how they translocated from one part to another.

Tan et al. (2011) went on to recalibrate the model of Lee et al. (2003) with the incorporation of E-cadherin for mammalian cells rather than Xenopus egg cells. It also provides

data on the location of β-catenin within the cell using a sub cellular fractionation technique. In order to take the measurements, this technique requires a level of estimation. In an attempt to improve upon this, it is possible to use fluorescence microscopy to measure β-catenin concentrations within sub compartments of the cell.

This section describes the experimental work carried out in the Nathke lab to improve the current knowledge of β-catenin location within the cell under different confluence conditions. The measurements were taken using immunofluorescence imaging and an analysis of the finding is reviewed in the next section.

4.3.2 Materials and methods

4.3.2.1 Cell cultures and treatments

The types of cells used for all of the experiments were from the Madin-Darby Canine Kidney (MDCK) cell line. These cells are an ideal candidate for the study of epithelia because they have the certain attributes. Firstly, they have a rapid growth rate which makes it easy to build up a large colony of cells to be used for experiments. They form well defined junctions such as adherens and tight junctions, which is where β-catenin will bind to E-cadherin for adhesion purposes. The cells will develop apical-basal polarity because of their epithelial nature and are perfect for imaging using confocal microscopy. MDCK cells have been used in many wide ranging experiments and are representative of human cells. For a review of the different MDCK cell lines and their uses please see Dukes et al. (2011).

The MDCK cells were grown in T-75 flasks with Dulbecco's modified Eagle's medium (DMEM), which was supplemented with antibiotics and 10% fetal calf serum, a growth

factor. The cells were passaged upon reaching 80% confluency and then were split into different flasks to increase the viable cell population. This was achieved by aspirating the medium in the flask followed by rinsing the cells with phosphate buffered saline (PBS) to eliminate any remaining medium. To break the adhesive bonds, pure trypsin was added to the flask and left for five minutes in the incubator. When all of the cells were detached from the flask, the trypsin was diluted with 6ml of medium and the whole solution, containing the cells, was pipetted into a tube to be placed in a centrifuge. Centrifuging the tube causes the cells to form a pellet at the base which allows for the removal of the trypsin/medium solution. The cells were then re-suspended in 8ml of medium. Four new flasks were each supplied with 10ml of fresh medium and 2ml of the cell/medium solution. These were then placed in the incubator allow for the growth and division of cells.

When the colony of cells had reached a large enough size the cells were available for experimentation. The first step was to place the cells on to coverslips so that they could be fixed, immunostained and imaged. Square coverslips measuring 22mm by 22mm were used in conjunction with a 6 well plate. To help the cells attach, the coverslips were coated with Type I collagen which mimics the extra cellular matrix and promotes adhesion between cells. To prepare this, each coverslip was sterilised by dipping it into 70% ethanol solution before being placed into a well of a plate and washed three times with PBS solution. The collagen solution was placed directly onto the coverslip and allowed to air dry before being washed again with PBS. The cells were then able to be placed on to the collagen coated coverslip.

Testing took place to determine how many cells should be seeded to give specific confluence. It was found that 0.4×10^6 cells gave a 40% confluence and 1.0×10^6 cells gave a 100% confluence if the cells were allowed to settle in the well with 2ml each of

fresh medium for 24 hours in the incubator. The next step was to fix the cells.

Fixing the cells preserves them in their current state and retains their cellular and sub cellular structure. To do this the medium was removed from the wells, they were then washed three times with PBS and the cells were then covered with 4% paraformaldehyde for 10 minutes at room temperature. They were again washed with PBS three times to remove any residual paraformaldehyde. At this stage, the cells are preserved and can be stored in a fridge before being immunostained and imaged.

4.3.2.2 Antibodies, fluorescent markers and reagents

To carry out the actions in this section, the coverslips are moved from the dish to a humidified chamber. The first stage in immunostaining cells is to permeabilise the membranes of the cell to allow antibodies access to the compartments within the cell to detect proteins. This was done by adding the detergent NP-40 diluted to 0.1% in PBS to the cells for 10 minutes. The small concentration and short exposure time is necessary because NP-40 is a harsh chemical and may disrupt the proteins within the cells. It was removed by washing the cells with PBS five times.

Before adding the primary antibodies to the cells, it is necessary to block nonspecific antibody binding sites to prevent false positive results and incorrect higher concentrations of the protein in question. The blocking solution consisted of PBS with 1% BSA (bovine serum albumin), 3% normal goat serum and 0.2% Triton X-100. It was added to the cells and allowed to incubate for 45 minutes then the cells were washed five times with PBS.

The primary antibodies were diluted in a working buffer of PBS, 0.1% BSA, 0.3%

normal goat serum and 0.2% Triton X-100. A mouse monoclonal β-catenin antigen from BD Biosciences was diluted at 1:300. A polyclonal rabbit ZO-1 antigen from ABCam was diluted at 1:1000 and used to detect the location of tight junctions, which are useful indicators for the apical side of the cell. These antigens were added to the cells and incubated at room temperature for 60 minutes. After this time, the cells were washed five times with PBS.

The secondary antibodies were diluted in the same working buffer as the primary antibodies. Alexa Fluor 594 dog/anti-mouse was diluted at 1:500 and used to detect β-catenin. It has a red output under fluorescent microscopy. Alexa Fluor 647 dog/anti-rabbit was diluted at 1:500 and used to detect ZO-1. It has a far-red (infrared) output under fluorescent microscopy and is shown in images as white. Alexa Fluor 488 phalloidin diluted at 1:500 was also added to the secondary antibodies. This is able to detect the filamentous actin within the cell which shows, among other things, the membrane of the cell. It is green under microscopy. The three antibodies were added together and placed on the cells for 60 minutes. The cells were then washed five times with PBS.

One more fluorescent marker was added to the cells to stain for the nucleus. 4',6-diamidino-2-phenylindole (DAPI) was added to the cells at a dilution rate of 1:10000 and incubated for 30 seconds. The cells were then washed five times. DAPI works by binding to DNA, which is only found in the nucleus, and has an output wavelength of 461nm to give off a blue colour in fluorescent microscopy.

The final step, to prepare the coverslips for microscopy, was to place them on an imaging slide which measured 25mm by 75mm. A small drop of mounting media (10 μl) was placed on a slide. This is used to avoid bubbles in the slide. A coverslip was then placed with the cells facing downwards on top of the mounting media. It was then secured in

place onto the slide with clear nail polish.

Two types of microscope were used to image the slides. A DeltaVision widefield microscope and a Zeiss 710 confocal microscope. The images were Z stacks of each slide taken at 1 μm steps and the data was imported into Volocity (Perkin Elmer) for analysis.

4.3.2.3 Measuring protein concentrations

The Volocity software package uses the data generated by the fluorescence microscopy to measure intensity of fluorescent markers. Figure 4.18 shows an example of an image that was used for measurements. To measure the intensity, and therefore concentration, of β-catenin it was necessary to set up a strict regime to ensure that the output data was consistent for each cell. This is described as follows:

1. Identify cells which are able to be used
2. Select which slice from the Z stack to be measured
3. Find the nucleus by thresholding on DAPI
4. Find the membrane by thresholding on Phalloidin
5. Define the cytoplasm as the area engulfed by the membrane and outside of the nucleus
6. Take intensity readings in each part of the cell for total intensity of β-catenin and calculate intensity per square micron.

The cells to be used to take measurements need to be undamaged and in contact with neighbouring cells on all sides. Cells may become damaged during the preparation of

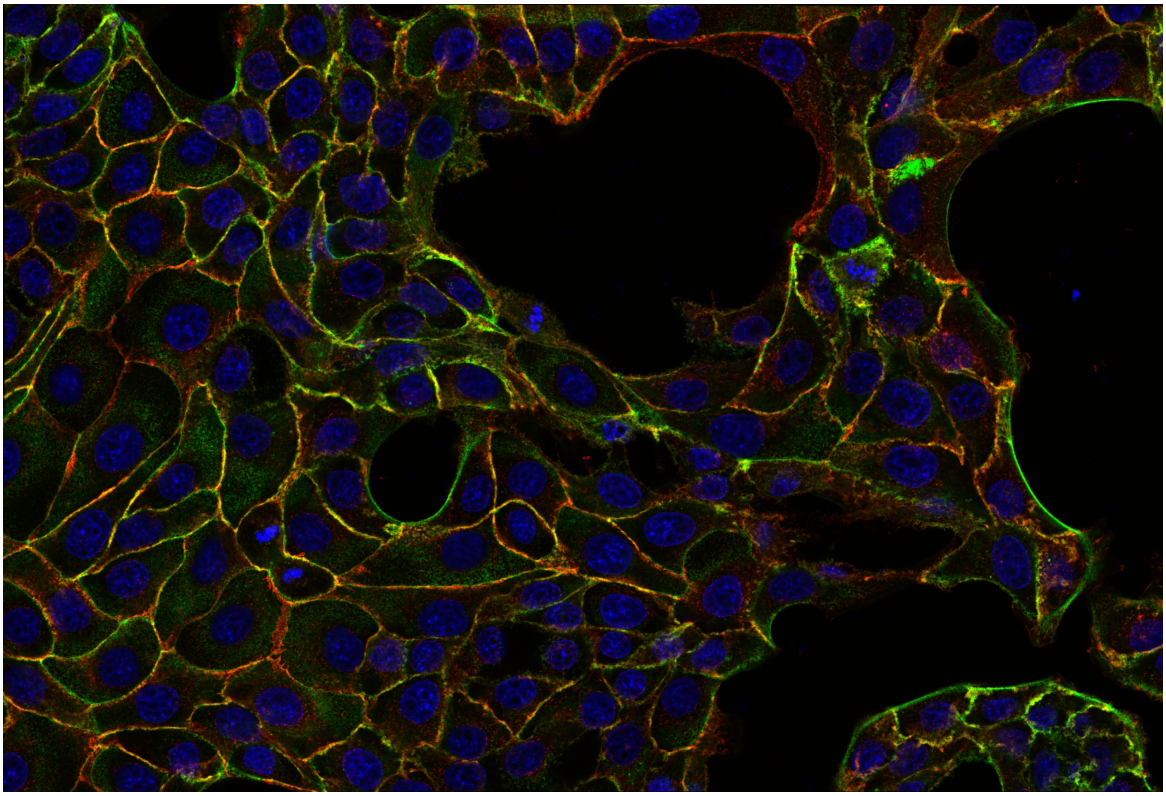

Figure 4.18: *Image taken by fluorescent imaging. This is a two dimensional Z-stack of cells taken from an experiment with cells at 40% confluence. Phalloidin (green), DAPI (blue), ZO-1 (white) and β-catenin (red). The membranes of the cells are represented by intense green strands which identifies F-actin. The F-actin can also be seen at a lesser intensity within the cell. The nuclei are clearly marked by blue DAPI. The brightest nuclei are in the process of mitosis and are ignored in the imaging. The tight junctions of the cells, which represent the apical side, are shown in white as they are marked with the ZO-1 antigen. β-catenin is represented by red and is the protein concentration that will be measured. The black patches in the image are present because this sample had a confluence of 40% and represents areas with no cells.*

the slides. For example, cells at the edge of the coverslip may be damaged by tweezers as it is moved from a dish to a humidified chamber or onto a slide. If cells are not surrounded then they will be very flat and may be migrating. This would mean that they lose apical-basal polarity and have forward-back polarity instead. Also, cells which are in the process of mitosis were excluded.

The selection of which Z stack to measure on a cell is the most important part of this process. A slice which included the adherens junction zone was chosen because of this area's importance in cell-cell adhesion. The highest concentrations of β-catenin along the membrane are always in this zone because of the bonds with E-cadherin. Therefore, this is the logical place to measure. Also, β-catenin in the cytoplasm and nucleus were found to be evenly distributed in the z-axis. To help with the standardisation of selection, the Z stack was chosen based on the location of the top and bottom of the cell. The ZO-1 marker, which marks the tight junctions of the cell, was used to identify the top. The bottom was found by looking for a pattern of actin as it interacted with the substrate. The slice in the middle of the top and bottom slices was chosen to be measured.

The nucleus is easily located because of the DAPI staining. Volocity is able to threshold on the intensity of the DAPI signal and find the area of the nucleus. The strength of the DAPI signal means that this process is able to be automated.

Locating the membrane for each cell is much more difficult. The Phalloidin staining is used to find the F-actin which is in the highest concentrations at the membrane of the cell. However, the intensity of the signal is not consistent along the membrane and there is also a weaker signal in the cytoplasm because F-actin is part of the cytoskeleton. Therefore, the membrane has to be found by the user with the guidance of a threshold on the phalloidin signal by the software. Another problem with this technique is that

the F-actin signal is from the membranes of two cells which are in contact. Therefore, when the area of the membrane is found it must be divided by two to account for this.

The location of the cytoplasm is simple because it is the area left in the cell. The simple equation gives the area of the cytoplasm:

$$Area_{Cytoplasm} = Total\ Area - (Area_{Membrane} + Area_{Nucleus}).$$

The measurements for the intensity of β-catenin were taken in each area of the cell. Total intensity was given by the sum of the intensity in the area. To account for possible background intensity of β-catenin, a small, empty sample of the domain was measured and this reading was used to adjust all other β-catenin measurements. The total intensity was divided by the size of the area in which it was taken to give intensity per square micron. This allows for an easy comparison of β-catenin concentrations across cellular compartments and different cells.

4.3.3 Results

Figure 4.19 shows the average level of total β-catenin intensity across cells at confluence levels of 40% and 100%. As can be seen, the total β-catenin intensity per square micron across the entire cell is higher in the lower confluence sample. It is possible to explain this by the shape of the cells. A cell population with high confluence *in vitro* is able to mimic a layer of epithelium very well. In these experiments, the cells are pressed together, rectangular in shape, have strong apical-basal polarity and are roughly 40 microns tall. Therefore, strong adhesion junctions are formed that result in β-catenin being degraded at a high rate in the cytoplasm. However, the cells at low confluence are

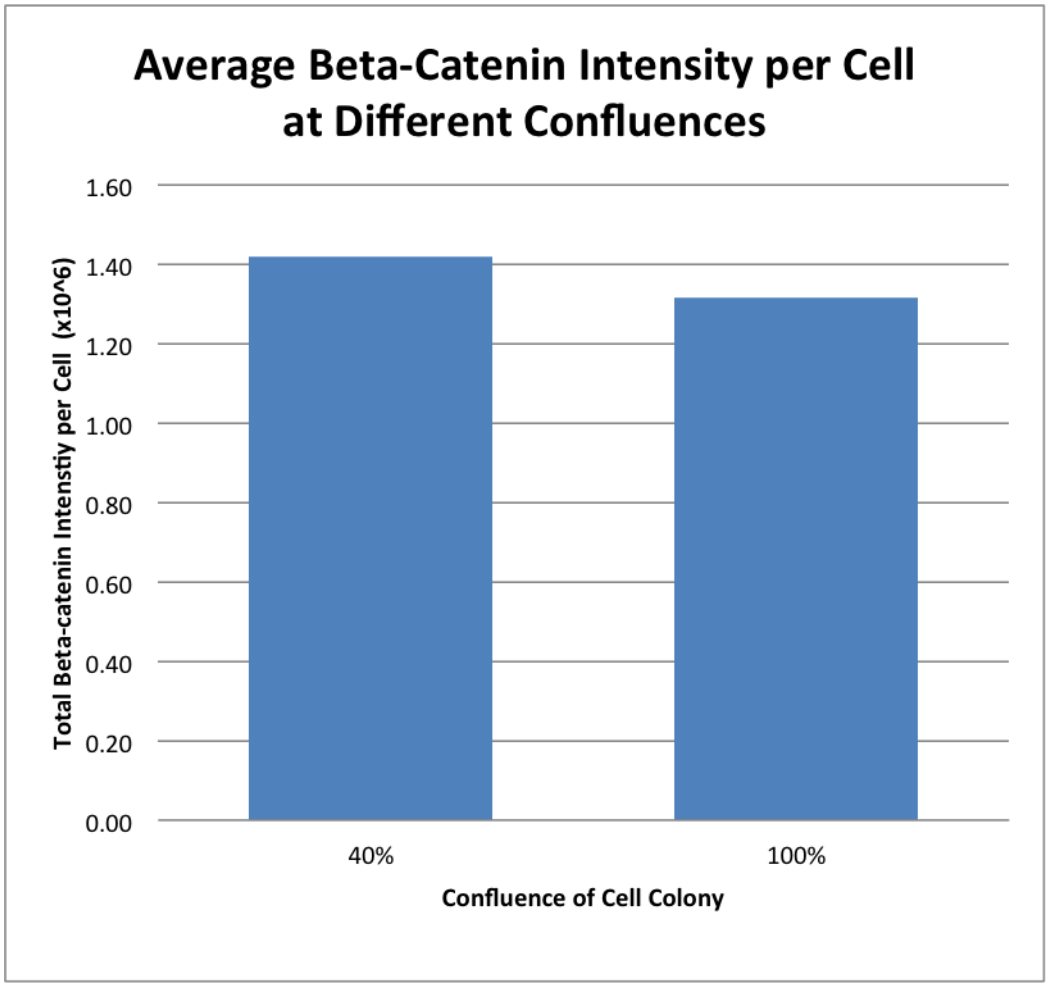

Figure 4.19: *Measurements of β-catenin intensity of cells at 40% and 100% confluence. This shows that the total β-catenin in a cell is higher if the confluence of the is lower than 100%. Cells at a high confluence are densely packed together and form strong adhesive bonds to hold the epithelial layer together. They are also more cuboidal in shape and are taller in the apical-basal axis. Cells at 40% confluence were not densely packed and were not cuboidal. Instead, they were much flatter and shorter in the apical-basal axis. These physical differences could be the reason for the difference in β-catenin levels.*

not pressed together. The shape is flat and uneven, typically with a bulge at the nucleus, and the height is only 20 microns. Therefore, the cells have a higher desire to divide in order to fill in the space, forming an epithelial sheet. For this to happen the β-catenin in the cell must be higher so that it can engage in transcriptional activities. The next figure confirms this by showing the intensity of β-catenin in the cytoplasm, in the nucleus and at the membrane of cells.

Figure 4.20 shows the relative distribution of β-catenin in the nucleus, cytoplasm and membrane for cells at 40% and 100%. In the high confluence cell population, the percentage of β-catenin at the membrane is higher than the low confluence population. This is because the cell has strong adhesion links with its neighbours, known to encourage β-catenin degradation in the cytoplasm, preventing it entering the nucleus. However, the population of cells at a lower confluence have a higher percentage of β-catenin in the nucleus so it can take part in transcriptional activities such as division. This is significant because even though the cells are completely surrounded by neighbours and in contact with them, just as in the high confluence case, there is a difference in the location of β-catenin. This is a factor which can be explored by mathematical modelling.

4.3.4 Discussion

The *in vitro* experiments have shown that in an epithelial monolayer the overall confluence of the population can have an effect on the levels and location of β-catenin within the cell. If cells are highly confluent, which replicates the situation in epithelial tissue, then the pressure of the cells being squeezed and held together by adhesion may be the key factor in preventing β-catenin from rising to high levels in the cytoplasm

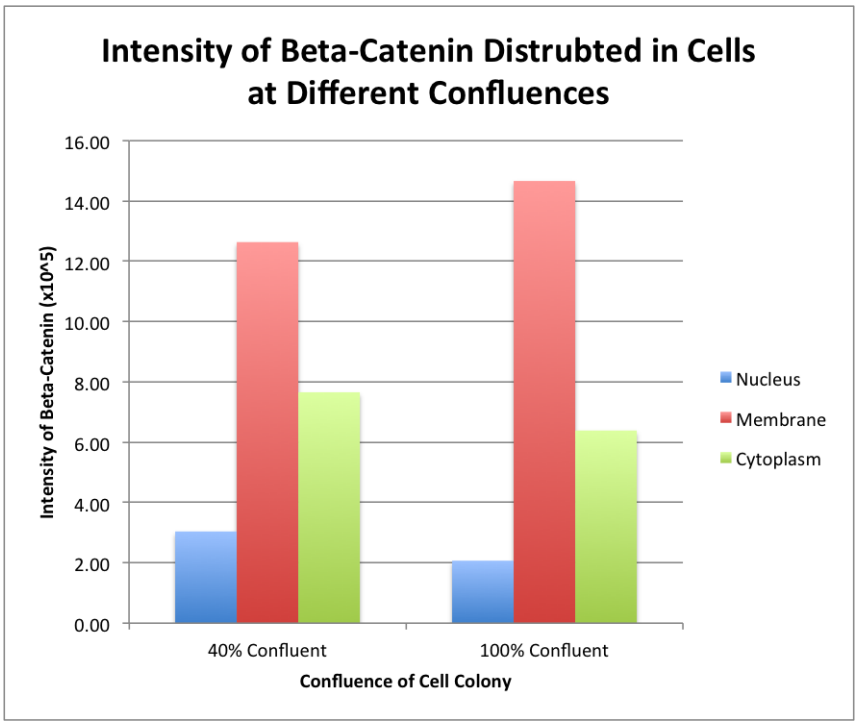

(a)

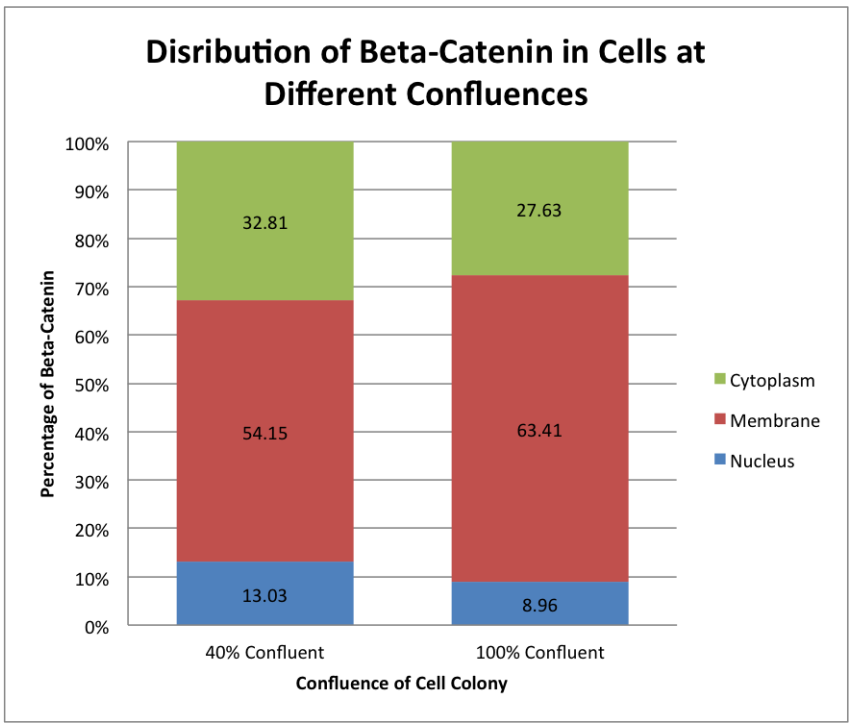

(b)

Figure 4.20: *Measurements of β-catenin intensity in sub-compartments of cells at different confluences. (a) shows the intensity of β-catenin in the nucleus, in the cytoplasm and at the membrane of cells at 40% confluency and 100% confluency. (b) shows the distribution of β-catenin as a percentage of the total β-catenin intensity in the cell. The figures show that cells at a higher confluency have more β-catenin at the membrane of the cell because they will form more adhesive bonds with their neighbours. Lower confluency cells, on the other hand, have more a higher percentage of β-catenin in the cytoplasm and the nucleus which means the cell is more likely to migrate, divide or go through the epithalial-mesenchymal transition.*

and nucleus. When the layer becomes looser and the cells are allowed to relax, the β-catenin will rise and encourage the cells to migrate, divide and perhaps go through the epithelial-mesenchymal transition. It is a well known in developmental biology that external pressure, as well as Wnt signalling, has an effect on tissue formation. It is also a key concept in cancer and may explain why the most aggressive tumour cells are found on a leading edge where the external pressure on the cells is the least. This is important for mathematical modelling because previous models such as [Ramis-Conde et al. (2008b)] have used changes in cell contact, but not considered changes in pressure. The sub-cellular model of Ramis-Conde et al. (2008b) has a threshold value of β-catenin to trigger the Epithelial-Mesenchymal Transition and the cell breaks all of its adhesive bonds in order to migrate and divide. These experiments indicate that the modelling should also consider the effect of external pressure on a cell's level of β-catenin.

Attempts to mathematically model external pressure upon cell migration and adhesion in the CHASTE software in the context of the colonic crypt have been made in [Dunn et al. (2012a,b)]. However, no models have been created to investigate the effect of cell shape and external pressure on E-cadherin/β-catenin dynamics. This link is a concept that needs further exploration.

4.4 Conclusion

The study of the E-cadherin/β-catenin pathway is fundamentally important because of its relevance in the development and progression of cancer. In this chapter, the pathway has been explored further by adding improvements to existing ODE models, by creating

a spatio-temporal modelling and undertaking biological experimentation in conjunction with mathematical modelling. The biological experiments have pointed to a link between cell colony confluence and β-catenin levels. This is an area which can be explored using new mathematical models to help direct new meaningful experiments to further understand the link.

Chapter 5

The Cancer Stem Cell Hypothesis

5.1 Introduction

Stem cells are an essential part of all complex multicellular organisms. They allow for a small number of unspecialised cells to give rise to many differentiated cells types and are important for many different functions. A simple example of this is embryo development. Differentiation from a single zygote allows for the creation of every type of cell in the body. Stem cells are also necessary in adult tissues. After embryogenesis, the stem cells become specialised for different parts of the body. There are specific stem cells for every major organ in the body. These adult stem cells have the characteristics that they are able to renew, regenerate and maintain the population of tissue cells. This is known as tissue homeostasis and relies on the proliferation or quiescence of stem cells depending on the need for mature cells [Moore and Lemischka (2006)].

The idea of stem cells has been extended in recent years to include cancer. This hypothesises that there is a stem cell niche that can create and maintain a population of tumour cells [Chen et al. (2011); Clevers (2011)]. The clinical relevance of this is immense because if the cancer stem cells can be identified and targeted in a cancer patient the chances for survival would be greatly improved.

This chapter develops mathematical models that investigate the cancer stem cell hypothesis. Section 5.2 describes an ordinary differential equation model of the healthy hematopoietic system with the inclusion of leukemia [Stiehl and Marciniak-Czochra (2010, 2012); Nakata et al. (2012)]. The key parameter discovered in this model is the fraction of self-renewal, which is the percentage of daughter cells that stay in the same stage of maturation as their mother cell. Section 5.3 contains a description of a cellular automaton model of a solid neoplasm which shows how the competition between cancer stem cells and normal cancer cells may relate to cancer dormancy [Enderling et al. (2009)]. Section 5.4 develops a novel discrete model in CompuCell3D with a view to extending it to include more inter- and intra-cellular processes in the cancer stem cell hypothesis. Finally, a novel partial differential equation model is developed in a similar manner in section 5.5.

5.2 An ODE model of leukaemia

There are no known morphological or biochemical characterisations available for stem cells. Therefore, the studies of stem cells in the blood system by Marciniak-Czochra et al. [Stiehl and Marciniak-Czochra (2010, 2012); Nakata et al. (2012)] were based on the following assumptions.

1. Stem cells have a capacity for self-renewal. This means they are able to maintain the size of their population by producing offspring with stem cells properties.

2. Stem cells are multi potent, which means they are able to produce offspring with different biological properties.

3. Stem cells are non specialised so they cannot perform specific functions within the organism.

For a detailed mathematical model, more assumptions were needed. It was also assumed that the process of maturation from a stem cell to a fully mature cell is made up of a sequence of discrete stages, none of which may be skipped. The possibly of moving backwards through the stages (dedifferentiation) is neglected.

There was also the question of how do cells at different stages of the maturation process interact. Marciniak et al. proposed that the behaviour of cells is regulated by one feedback signal and that the cells in each maturation step are controlled by the density of cells in the stage and the strength of the signal. Therefore, the behaviour of the cells at one stage and the influx of cells from the previous stage are independent. The concentration of the signalling molecules was controlled by the density of mature cells in the form of negative feedback. This means that the higher the density of mature cells the lower the signal concentration.

5.2.1 The mathematical model

Stiehl and Marciniak-Czochra (2012) presented an Ordinary Differential Equation (ODE) model of the hematopoietic (blood forming) system with leukaemia. An ODE model

is suitable for this purpose because the number of cells in the hematopoietic system is too large to examine each cell individually. Also, since blood is a liquid it is possible to treat the entire system as a 'well-mixed' vat. The model involves a healthy hematopoietic line, $c(t)$, and a leukaemic line of cells $l(t)$. Each line has stem cells which progress through discrete maturation stages as progenitor cells before becoming fully mature. There are n steps for the hematopoietic line and m steps in the leukemic line.

In each maturation stage, the hematopoietic cells will divide and the offspring may belong to the same stage or they may progress to the next stage. The fraction of daughter cells that remain in the same stage as the mother cell is called the fraction of self-renewal. The proposed formula for self-renewal of a population of cell in a maturation stage was given by

$$f_n(s(t), c_n(t)) = (2a^c_{n,max}s(t) - 1)p^c_n c_n(t),$$

where $p^c_n(t)$ is the proliferation rate of the cells in maturation compartment n at time t, $a^c_i(t)$ is the fraction of self-renewal and s(t) is the signal concentration. This function is monotonically increasing in s. Different functions for f_n were considered in Marciniak-Czochra et al. (2009).

The influx of cells in to a maturation stage from the previous one was described by

$$g_n(s(t), c_{n-1}(t)) = 2(1 - a^c_{i-1}(t))p^c_{n-1}(t)c_{n-1}(t),$$

where $a^c_{i-1}(t)$ is the fraction of self-renewal at the previous maturation stage, $p^c_{n-1}(t)$ is the proliferation rate of cells at the previous maturation stage and $s(t)$ is the feedback signal strength.

The feedback signal for the healthy hematopoietic system alone was given by the equation

$$s(t) = \frac{1}{1 + kc_n(t)} \in (0, 1],$$

where $c_n(t)$ is the density of mature cells. This is an attempt to model the negative feedback regulation for the formation of healthy blood cells. If more mature blood cells are required then the concentration of signalling molecules, called cytokines, will stimulate their formation. The exact mechanism for this is not fully understood because the increase in progenitor cells, when the cytokine concentration increases, may be caused by greater proliferation or less apoptosis.

Lastly, a death rate for cells at each maturation stage, $d_n^c(t)$, is included in the model. For simplicity in numerical simulations, the death rate is considered to be zero or constant.

The same dynamics were used for the leukaemic cell line. However, only one signal was used for both cell lines. Therefore, the signal should be changed to include the effect of mature leukemic cells. This was achieved by adding in further negative feedback from the leukaemic cell lines which led to the signal equation

$$s(t) = \frac{1}{1 + k^c c_n(t) + k^l l_m(t)} \in (0, 1].$$

The full system of equations for the hematopoietic system with leukaemia [Stiehl and

Marciniak-Czochra (2012)] is

$$\frac{d}{dt}c_1(t) = (2a^c_{1,max}s(t) - 1)p^c_1 c_1(t) - d^c_1 c_1(t), \tag{5.1}$$

$$\frac{d}{dt}c_i(t) = 2(1 - a^c_{i-1,max}s(t))p^c_{i-1}c_{i-1}(t) + (2a^c_{i,max}s(t) - 1)p^c_i c_i(t) - d^c_i c_i(t), 1 < i < n, \tag{5.2}$$

$$\frac{d}{dt}c_n(t) = 2(1 - a^c_{n-1,max}s(t))p^c_{n-1}c_{n-1}(t) - d^c_n c_n(t), \tag{5.3}$$

$$\frac{d}{dt}l_1(t) = (2a^l_{1,max}s(t) - 1)p^l_1 l_1(t) - d^l_1 l_1(t), \tag{5.4}$$

$$\frac{d}{dt}l_i(t) = 2(1 - a^l_{i-1,max}s(t))p^l_{i-1}l_{i-1}(t) + (2a^l_{i,max}s(t) - 1)p^l_i l_i(t) - d^l_i l_i(t), 1 < i < m, \tag{5.5}$$

$$\frac{d}{dt}l_n(t) = 2(1 - a^l_{m-1,max}s(t))p^l_{m-1}l_{m-1}(t) - d^l_m l_m(t), \tag{5.6}$$

$$s(t) = \frac{1}{1 + k^c c_n(t) + k^l l_m(t)}. \tag{5.7}$$

Where $p^c_i(t)$ and $p^l_i(t)$ are the proliferation rates in compartment i at time t, $a^c_i(t)$ and $a^l_i(t)$ are the fractions of self-renewal and d^c_i and d^l_i are the death rates in compartment i. s(t) is the feedback signal from the mature cells to cells in lower maturation stages.

5.2.2 Numerical results

The system of ordinary differential equations was solved using the ode45 command in Matlab. The first simulation examined was the case of the healthy hematopoietic system with no leukaemia. Through this it was discovered that the inclusion of a large number

of maturation steps is qualitatively the same as including a low number of steps. This is illustrated in figure 5.1. Therefore, the simulations with a leukaemic cell line are carried out with using 2 maturation stages for both the healthy and leukaemic lines. In this case, the first stage of maturation represents a mix of stem cells and progenitor cells. Looking at the healthy system also allowed the researchers [Stiehl and Marciniak-Czochra (2012)] to find parameter values that would give cell numbers in the correct range, as no direct parameter values had been found experimentally. To find insightful results of the model p_1^c, the proliferation rate of stem/progenitor healthy cells was rescaled to 1 and it was decided that a healthy steady state of between 10^9 and 10^{10} mature healthy cells was desired.

The next step was to look at the inclusion of a leukaemia cell line. The following results all begin with an initial condition of the healthy steady state with a small population of leukaemic stem cells. Figure 5.2 shows the development of a leukaemic steady state, which is where the leukaemia cells dominate the population. This sudden death of healthy cells may be seen in acute leukaemia.

There may also be the possibility that the small mutated population becomes extinct and the system returns to the healthy steady state. Figure 5.3 shows this case and it was achieved by reducing the leukaemic cell line's self-renewal ability and increasing its proliferation rate. The increase in proliferation proved insufficient to compensate for the lower self-renewal. This case describes a mutation that is benign because the number of healthy cells does not change on a clinically relevant scale before the steady state is reestablished.

Lastly, there is the possibility of a coexistence of both cell lines. Figure 5.4 shows a steady state in which the change in the healthy cell count is small and the existence of

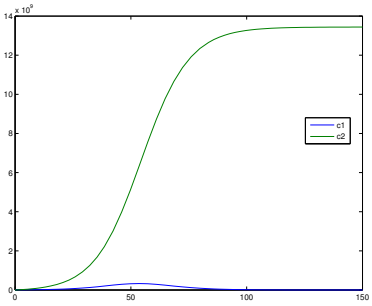

(a) $n = 2$

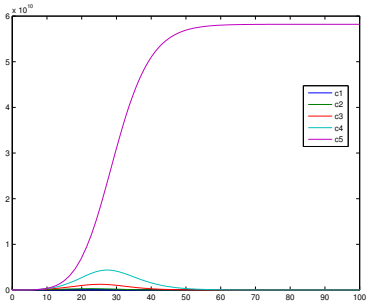

(b) $n = 5$

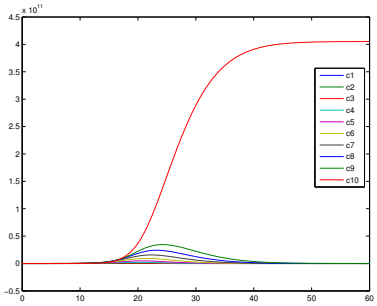

(c) $n = 10$

Figure 5.1: *Simulations of the healthy hematopoietic system with different numbers of maturation steps with initial condition of* $c_1(0) = 1$ *and* $c_j(0) = 0$ *for* $j = 2 : n$. *It can be seen that the healthy steady state always has many mature cells and a very low population of stem and progenitor cells regardless of the number of maturation stages.*

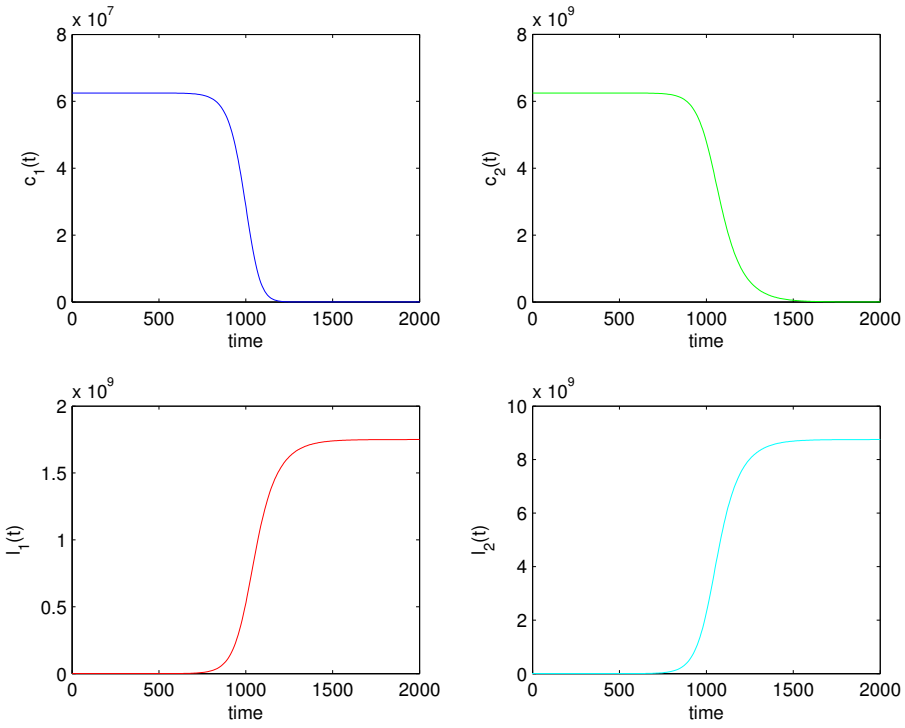

Figure 5.2: *This shows the development of a leukaemic steady state and the extinction of healthy cells. It has an initial condition of* $c_1(0) = 6.25 \times 10^7$, $c_2(0) = 6.25 \times 10^9$, $l_1(0) = 10$, $l_2(0) = 0$ *and has parameter values* $a_1^c = 0.55, p_1^c = 1, d_1^c = 0, d_2^c = 0.01; a_1^l = 0.57, p_1^l = 0.5, d_1^l = 0, d_2^l = 0.1, k_c = k_l = 1.6 \times 10^{-11}$.

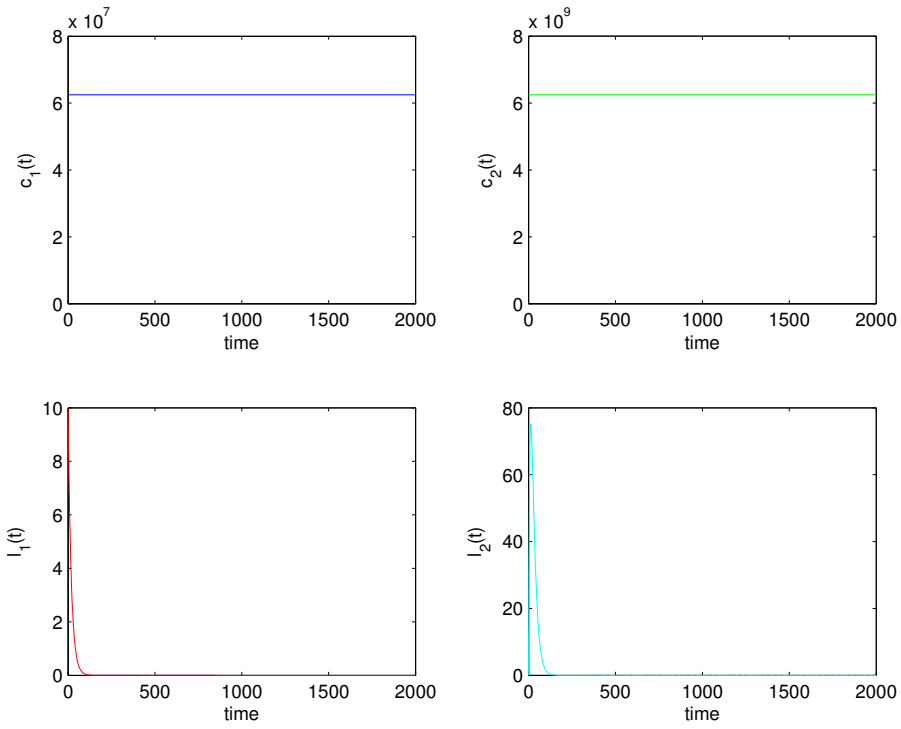

Figure 5.3: *This shows the reestablishment of the healthy steady state after the perturbation of a small number of leukaemic stem cells. It has an initial condition of* $c_1(0) = 6.25 \times 10^7$, $c_2(0) = 6.25 \times 10^9$, $l_1(0) = 10$, $l_2(0) = 0$ *and has parameter values* $a_1^c = 0.55, p_1^c = 1, d_1^c = 0, d_2^c = 0.01; a_1^l = 0.53, p_1^l = 1.5, d_1^l = 0, d_2^l = 0.1, k_c = k_l = 1.6 \times 10^{-11}$.

a tiny population of leukaemic cells. This may describe the case of cancer dormancy [Matzavinos et al. (2004)].

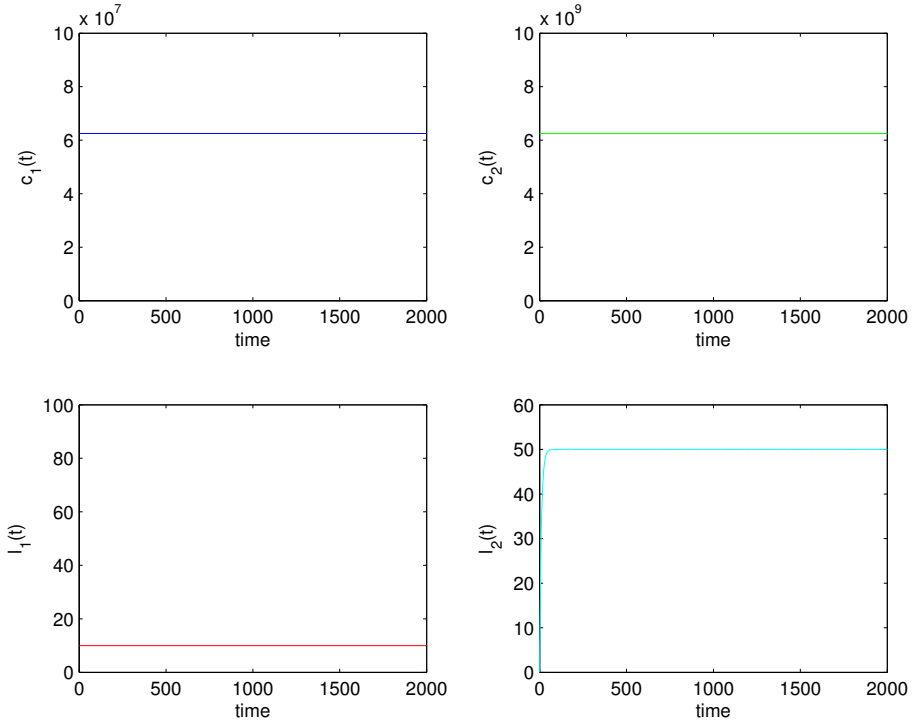

Figure 5.4: *This shows a coexistence of the two cell lines which is not malignant. This is known as cancer dormancy. It has an initial condition of* $c_1(0) = 6.25 \times 10^7$, $c_2(0) = 6.25 \times 10^9$, $l_1(0) = 10$, $l_2(0) = 0$ *and has parameter values* $a_1^c = 0.55, p_1^c = 1, d_1^c = 0, d_2^c = 0.01; a_1^l = a_1^c, p_1^l = 0.5, d_1^l = 0, d_2^l = 0.1, k_c = k_l = 1.6 \times 10^{-11}$.

5.2.3 Discussion

The work of Marciniak-Czochra et al. [Stiehl and Marciniak-Czochra (2010, 2012)] is particularly relevant as it provides evidence for the existence of cancer stem cells in leukaemia. The numerical results in the papers were compared to patient data and they fit together very well. Using the assumptions in these papers it may be possible to extend

this model to look at solid tumours. In this case, spatial concerns need to be taken in to consideration because it is not possible to say that a solid tumour is a 'well-mixed vat'.

5.3 Spatial modelling of solid tumours using a cellular automaton model

While ODE and PDE models are enlightening in stem cell research, they do not show interactions between individual cells or other spatial constraints. Therefore, they do not capture the heterogeneous considerations in a solid tumour. The work of Enderling et al. (2009), described in Section 5.3.1, investigates the competition for space between normal tumour cells and cancer stem cells in an avascular tumour before necrosis.

5.3.1 Mathematical model

The cellular automaton model was composed of a two-dimensional grid of 3500x3500μm. This is further divided into 350x350 lattice points of 100μm^2, with each of these lattice points capable of hosting a maximum of one cell. The behaviour of the cells is based on the following.

Basic Cell Kinetics Each cell has a maximum division capacity $\rho_{\max}$, a migratory capacity μ, and a spontaneous cell death α.

Assumption 1 The tumour population consists of both normal tumour cells and cancer stem cells. Stem cells do not die and can divide symmetrically with probability p_s. Normal cells have a limited proliferation capacity and may die spontaneously.

Assumption 2 Cells are in competition with each other for space and if a cell is completely surrounded by other cells it is considered spatially inhibited and becomes quiescent.

The simulation moves forward in time at discrete steps of 96 minutes. This time step was chosen because it results in a day being broken up into 15 steps. At each step the age of the cells is incremented and they can migrate, if they have enough space, by μ cell widths per day and they can divide, if the maturation age has been reached. The maturation age of every cell is one day and a cell may divide ρ_{max} times. When a cell divides, its proliferation capacity, ρ, is reduced by one. A cell may die if its proliferation capacity has been exhausted or if it is randomly selected to die with probability α. Stem cells are considered to be immortal and therefore have an infinite proliferation capacity ($\rho_{max} = \infty$) and will not die spontaneously ($\alpha = 0$).

To be successful, the cancer cells need to grow and divide to allow the tumour to expand. However, this requires sufficient space and the pressure from other cancer cells may prevent a cell from dividing. To model this, a cell that has every surrounding lattice point occupied by other cells goes into a quiescent state and will be unable to migrate or divide. Therefore, only the edge of the tumour may migrate or proliferate. However, when these proliferative cells migrate away from the tumour or die, there is space created for the cells they were inhibiting, which will result in quiescent cells becoming proliferative.

The spontaneous death term α is the probability of death for a non-stem cells at every time step. This can model several different factors including the immune system response and also treatment with chemotherapy and radiotherapy. It has been hypothesised that cancer stem cells have a stronger resistance to therapy and the immune system

and so setting $\alpha = 0$ for these cells was a reasonable assumption.

This model matches up fairly well with the ODE model presented above. The stem cells in the spatial model represent the stem cells in the ODE model. However, in the work of Enderling et al. (2009) there are no progenitor cells; the stem cells divide asymmetrically into another stem cell and a mature cell or symmetrically into two stem cells.

The key parameter in Marciniak-Czochra's work was the fraction of self-renewal, which determines how many of the daughter cells stay within the same maturation stage as the mother cell, and this may be compared to how many stem cells are produced from a stem cell division. For the spatial model this parameter could be calculated after each stem cell divides and it is determined by the probability p_s.

5.3.2 Results and discussion

The first simulations that were considered began with a single normal tumour cell in an empty space. At first there was exponential growth in the number of cancer cells. However, since the normal tumour cells have a limited replication capacity these tumours were destined to die out. It was shown that if the maximum replicative capacity, ρ_{max}, was set higher then it would produce a larger and longer lasting tumour. For example, when $\rho_{max} = 10$ the tumour would grow to a maximum of roughly 1000 cells and it would disappear after 15 days. However, when $\rho_{max} = 20$ the maximum number of cells was approximately 10000 and it persisted for over 1000 days. From this, it was clear that the absence of stem cells would not allow for a malignant tumour to be formed and this could be compared to the case of a benign mutation from the ODE model above.

The next simulations that were investigated began with a single stem cell that could only divide asymmetrically. In these simulations the maximum number of cells reached was higher than tumours that did not have a stem cell, but they still did not form large enough tumours to constitute a clinical threat. The stem cells were able to give rise to a new tumour cell every time it was not spatially inhibited. The new tumour cell could divide exponentially and form a new cluster but because of their limited replicative potential this cluster would die away. When this happened, the stem cell would have space and would leave the quiescent state to divide to form new clusters of normal tumour cells. It is because of this that the simulations showed the size of the tumour oscillating around a final state. However, there would have to be some perturbation in the system to allow for the tumour to become malignant. The maximum number of cells for $\rho_{max} = 20$ was about 16000 and the system went on to oscillate about 10000 cells.

Only allowing the stem cell to divide asymmetrically is the equivalent to saying that the fraction of self-renewal is exactly 50%. This simulation showed that there must be the possibility for the stem cell population to rise for a tumour to become large enough to be malignant.

The key results that came from simulations which begin with a 'true stem cell', have the ability to divide symmetrically. Enderling et al. (2009) set the probability $p_s = 0.01$, which means that every time a stem cell divides it has a 99% chance of creating a stem cell and tumour cell and a 1% chance of creating two stem cells. The simulations showed that every newly created stem cell gave rise to a new cluster that contributed to the tumour. The results proved counter intuitive because it was shown that a lower maximum proliferative capacity improved the potential for larger tumours. If ρ_{max} was set to a high level then the stem cells would remain in a quiescent state for long periods of time, possibly years. This is the case of cancer dormancy, which was also seen in the

results of Stiehl and Marciniak-Czochra (2012) above. On the other hand, when ρ_{max} was low, the normal tumour cells would die more frequently which gave space to the stem cells. Therefore, more stem cells were created and the tumour grew much more quickly, resulting in a malignant tumour in a clinically relevant time span.

To gain further insight, the next simulations included spontaneous cell death. The parameter α, which was previously set to zero, was set to 0.05, 0.1, 0.15, 0.25 and 0.35. This is the equivalent of saying that every normal tumour cell has a 5%, 10%, 15%, 25% and 35% chance of dying at each time step. The results showed that initially the size of the tumour was smaller than the case with $\alpha = 0$. However, later in the simulation this was reversed. Higher levels of α resulted in a larger growth rate and a larger tumour. This is because the death of cells allows space for other cells, especially stem cells, to migrate and divide. Therefore, more stem cells were created and the tumour grew to a malignant size in a relevant time span.

The spontaneous death of cells may represent several factors including the immune system response and the treatments of cancer. Therefore, it is possible to draw some conclusions about these. If a tumour is treated with chemotherapy or radiotherapy, many of the cancer cells will die. However, it has been seen that after treatment the cancer may come back more aggressively and result in a larger malignant tumour [Wodarz and Komarova (2007)]. This may be explained by these simulations because if the stem cells are not killed with the normal tumour cells then the treatment may only be giving the stem cells more space to migrate and divide.

This model also suggests that the immune system, previously thought to create tumour dormancy [Matzavinos et al. (2004)], may actually facilitate the progression to malignancy. If a tumour is in a dormant state because of the spatial inhibition of its stem cells,

then a large attack by the immune system may cause the stem cells to become active and allow for new clusters of tumour cells to be formed.

5.4 Replicating and extending cellular automaton model in CompuCell3D

The use of ODE and cellular automaton models has given greater insight into the cancer stem cell hypothesis. In an attempt to further our understanding, the software package CompuCell3D [Swat et al. (2009)] has been used to replicate the results of Enderling et al. shown above with a view to include more biologically relevant information. CompuCell3D uses the Cellular Potts Model to simulate cells and their behaviours. This includes cell adhesion, migration, division, secretion and absorption. It is also possible to include intracellular dynamics by the integration of CompuCell3D with Systems Biology Workbench. This allows for the ability to add many features that are not possible with cellular automaton models.

5.4.1 Mathematical model

The implementation of the Enderling et al. model has the same parameters in CompuCell3D except for the following considerations. In the two dimensional model a domain of 200x200 pixels was used. Each simulation began with a single square cell in the centre of the domain with an area of 25 square pixels and it was completely surrounded by medium. CompuCell3D used discrete Monte-Carlo steps to advance time and each Monte-Carlo step represents an interval of 96 minutes as in [Enderling et al. (2009)].

The migration rate in CompuCell3D determines how far a cell can move in each MCS and it corresponds with the parameter μ. Each cell has an adhesion parameter that determines how strongly each cell binds to other cells. This is set to be the same for all cells but this may be changed. Division parameters and conditions are the same as in [Enderling et al. (2009)] except that a cell is divided equally along a random axis. The two daughter cells will then attempt to grow to the size of $25\mu m^2$. The other parameters p_s and α are implemented in the same way as above. The condition for quiescence states that if the entire surface of a cell is completely in contact with other cells and has no contact with the medium then it will become quiescent.

5.4.2 Results in two dimensions

The first case to consider, checking that the model has been implemented correctly, is a single normal tumour cell which cannot die randomly. It has a limited replicative capacity so the population will grow to a certain size before all the cells die. Figure 5.5 gives the number of proliferative tumour cells, quiescent tumour cells and the total cell population for two simulations for different values of ρ_{max}. It shows that as the population increases cells become quiescent before all of the cells die out. If ρ_{max} is higher, then the population will grow to a larger size and will persist for a longer time. Figure 5.6 represents the graphical representation of the two dimension simulation with $\rho_{max} = 10$. There are four times shown: the starting point at MCS 0, the peak of the cell population at MCS 140, the population in decline at MCS 160; and finally the death at MCS 180.

The next case, just as in Enderling et al. (2009), is that of a tumour that begins with a cancer stem cell that only has the potential to divide asymmetrically. The result is in

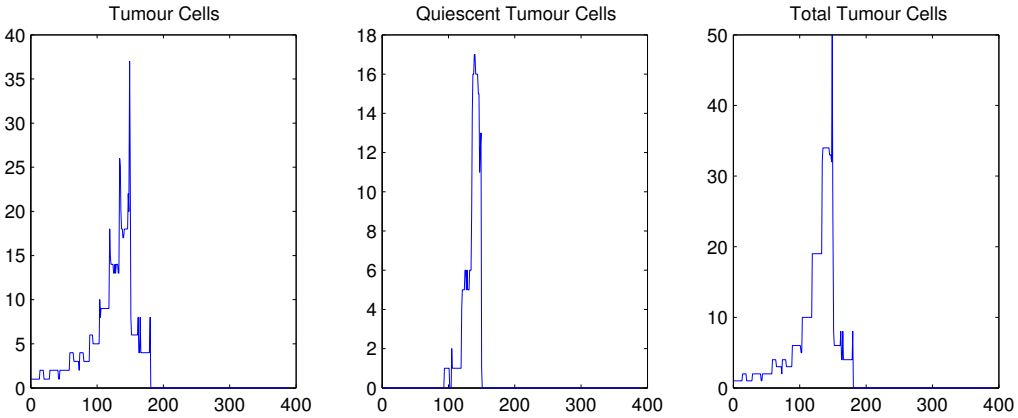

(a) $\rho_{max} = 10$

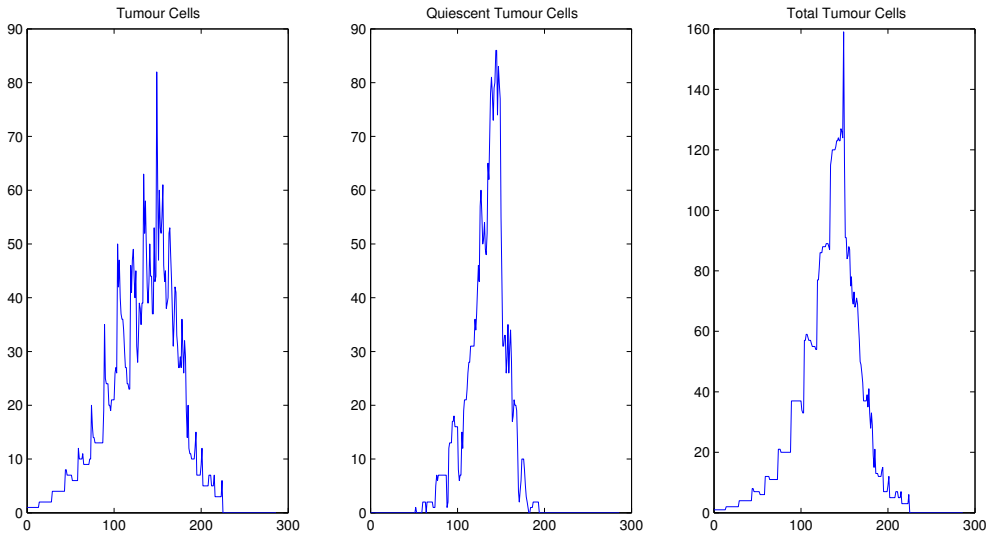

(b) $\rho_{max} = 20$

Figure 5.5: *Two simulations of tumours that are initiated by a single non-stem cancer cell with different replicative potentials. Figure (a) shows the number of proliferative cells, quiescent cells and the total number of cells over time that result from a single cell with* $\rho_{max} = 10$*. Figure (b) shows the same for* $\rho_{max} = 20$*. Neither simulation contains a stem cell so both tumours grow to a maximum size before all cells undergoing apoptosis. The maximum number of cells in (b) is double the maximum in (a) because the initial cell is able to divide twice the number of times.*

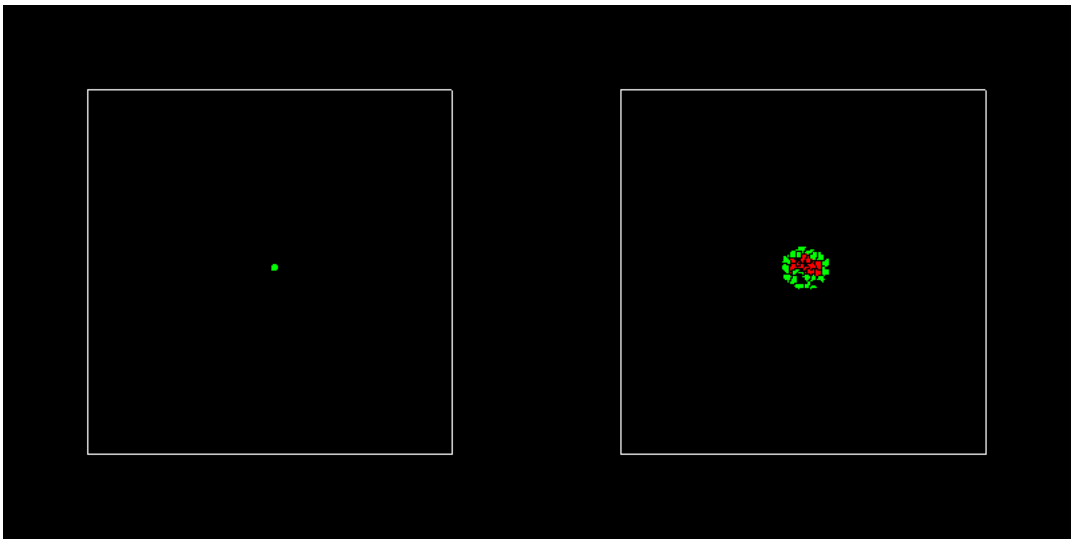

(a) mcs=0 **(b)** mcs=140

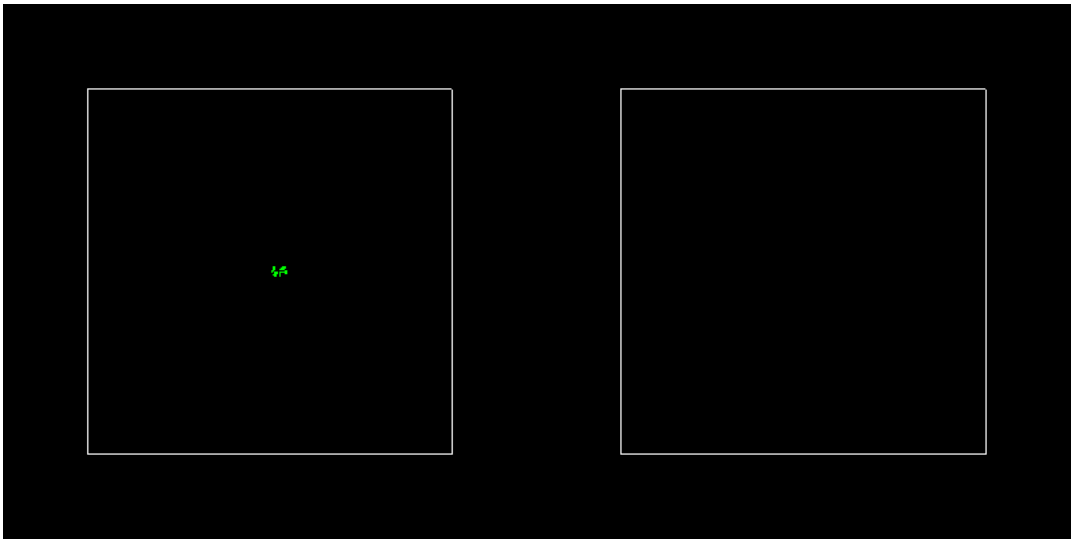

(c) mcs=160 **(d)** mcs=180

Figure 5.6: *The two-dimensional growth of a tumour from a single non-stem cells with* $\rho_{max} = 10$*. Proliferating cells are green, quiescent cells are red and the surrounding medium is black. The initial cell divides until the tumour reaches a maximum size, shown in (b). The cells then become apoptotic when they have divided* ρ_{max} *times until the tumour is gone, as can be seen in (d). This simulation corresponds to Figure 5.5(a).*

figure 5.7 which gives the number of proliferating tumour cells, quiescent tumour cells, total normal tumour cells, proliferating stem cells, quiescent stem cells, total stem cells and the total number of cells in the tumour. It shows the same results as Enderling et al. (2009). The stem cell population is fixed but it can move from proliferative to quiescent and back depending on whether it is inhibited by the normal tumour cells. The peak population is higher than in the case without the stem cell and the eventual population oscillates around 200 cells.

The third case begins with a 'true' stem cell which has the ability to divide symmetrically with the probability p_s. Spontaneous cell death, α, remains set to zero. Figure 5.8 shows a simulation that begins with a single 'true' stem cell that can produce normal tumour cells with a maximum replication capacity of 10. As can be seen, there is an initial exponential growth phase before oscillatory dynamics take over. During this phase the stem cell has not divided symmetrically. However, at roughly 50000 MCS (over 9 years) the stem cell population is increased, causing the tumour to grow resulting in a progression to malignancy. This same progression may be seen if ρ_{max} is set to a higher level but it will take much longer and may not become malignant in the life span of a patient.

The last case from Enderling et al. (2009) was the inclusion of spontaneous cell death. Figure 5.9 shows the case of a true stem cell with $\alpha = 0.01$. As can be seen, the progression to malignancy occurs at about MCS 6000. This is almost 10 times earlier than the case previous case with $\alpha = 0$. Furthermore, the stem cell population makes up a relatively small proportion of the total tumour. If the value of ρ_{max} increased the tumour is more likely to stay in a dormant state for much longer and not make the progression to malignancy. Therefore, a low value of α may correspond to the influence of the immune system on a tumour. For a long time, the immune system picks off tumour cells

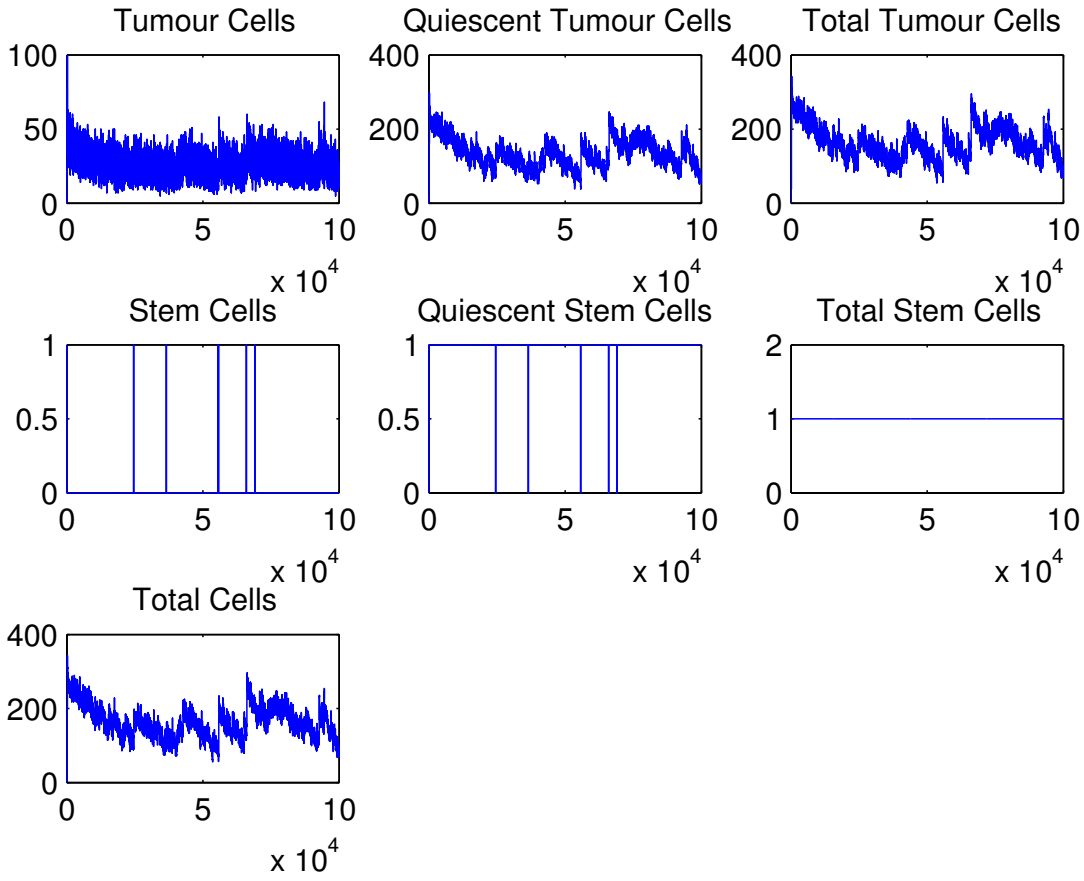

Figure 5.7: *Results of a two dimensional tumour simulation that begins with a single stem cell, incapable of symmetric division over 10000 Monte Carlo Steps with* $\rho_{max} = 10$. *It can be seen that the total number of stem cells remains at a constant value of 1, but it can be proliferative or quiescent depending upon the number of tumour cells around it. The total number of cells is seen to oscillate around 200.*

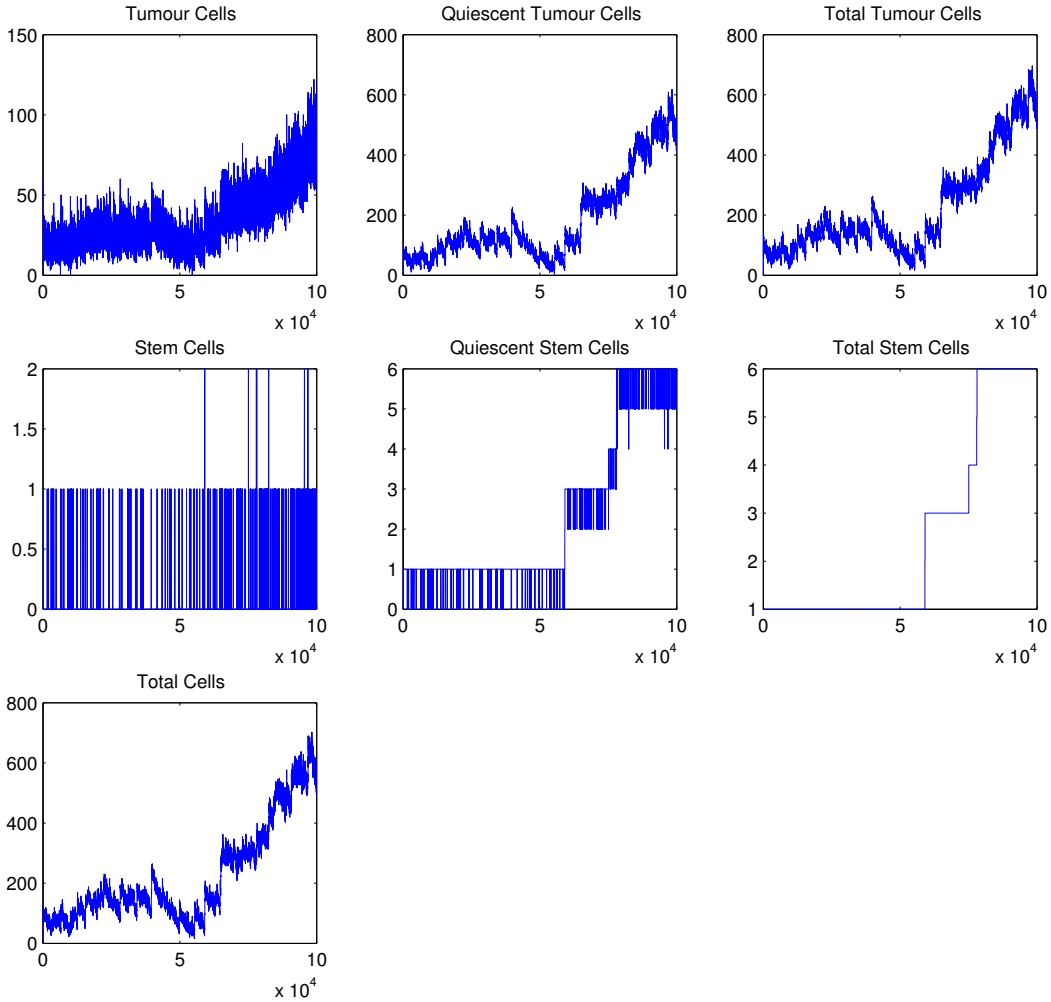

Figure 5.8: *The number of cells in a two dimensional simulation that is initiated by a single 'true' stem cell, capable of symmetric division, over 10000 Monte Carlo Steps with* $\rho_{max} = 10$*. The total number of cells is seen to oscillate for over 5000 MCS in much the same manner as seen in Figure 5.7. However, the stem cell population is increased by symmetric division, which means that the total tumour population is able to grow.*

until eventually the cancer stem cells are able to divide often enough and create a new stem cell and allow the progression to malignancy. This model predicts that for this scenario it is the stochastic nature in which the stem cells interact with the other cells and the immune system that define how a tumour in a dormany state may progress to a malignant tumour in a clinically relevant time.

Another parameter variation of this case is to examine what happens when α is large. Figure 5.10 shows the results of a simulation with $\alpha = 0.35$. As can be seen, the total tumour population is initially much lower than simulations with low values of α. However, later in the simulation the total number of cells suddenly grows at an extreme rate. It should also be noted that that stem cells make up the majority of the tumour. Since they are immune to spontaneous cell death they are not spatially inhibited and are allowed to divide many more times than seen previously. This simulation may show the effect of chemotherapy or radiotherapy in which the treatments are not able to kill the stem cells but are deadly to normal tumour cells. For a long period of time the treatment is able to subdue the tumour. However, eventually it is able to surge aggressively toward a malignant state.

5.4.3 Extension to three dimensions

The previous section showed that the results in Enderling et al. (2009) can be qualitatively replicated in CompuCell3D. However, a simple extension to this model is to expand the domain into three dimensions. Changing the existing two dimensional simulations to three dimensions is remarkably simple in CompuCell3D, but there is a marked increase in the simulation running times. I worked with a domain of 400x400x400 pixels and began each simulation with a single cubic cell with a volume of 125 cubic pixels

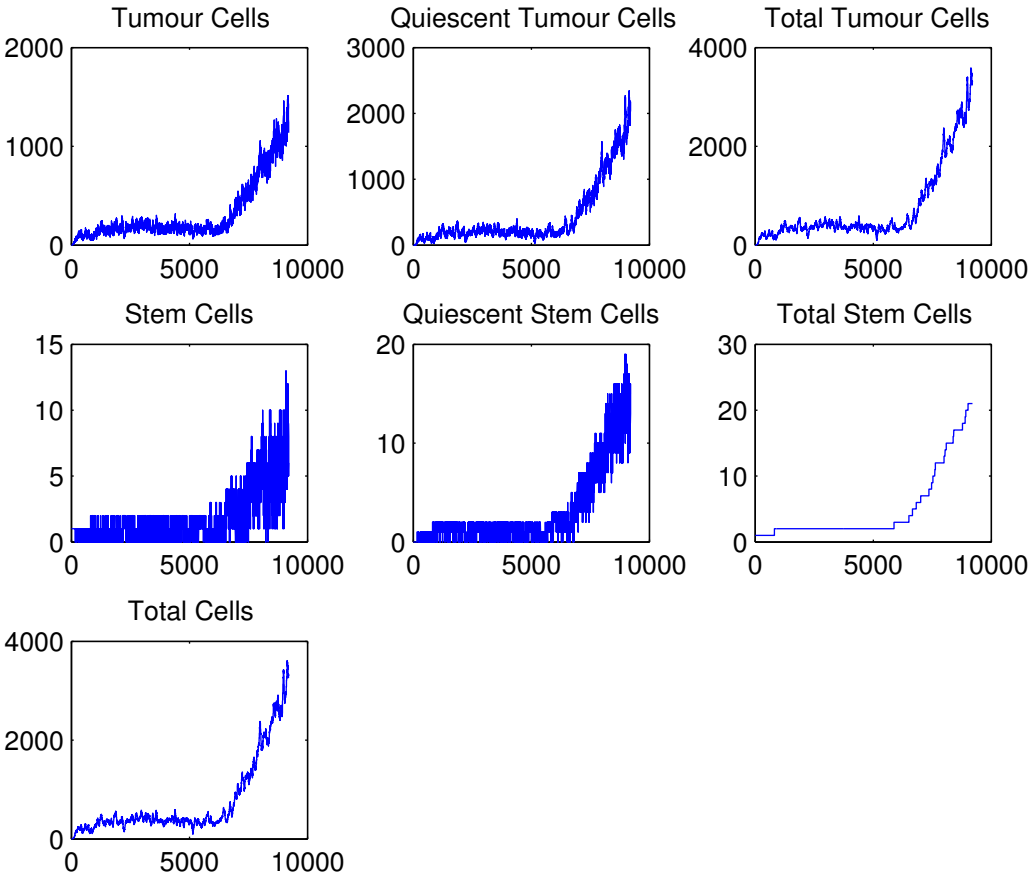

Figure 5.9: *Results of a tumour initiated by a 'true' stem cell over 10000MCS with* $\rho_{max} = 10$ *and a spontaneous death rate* $\alpha = 0.01$. *The total number of cells in the tumour is seen to oscillate for about 5000 MCS before the number of stem cells is able to increase much more than in the case without spontaneous cell death. Therefore, the overall tumour size is several times larger when compared to the simulation in Figure 5.8.*

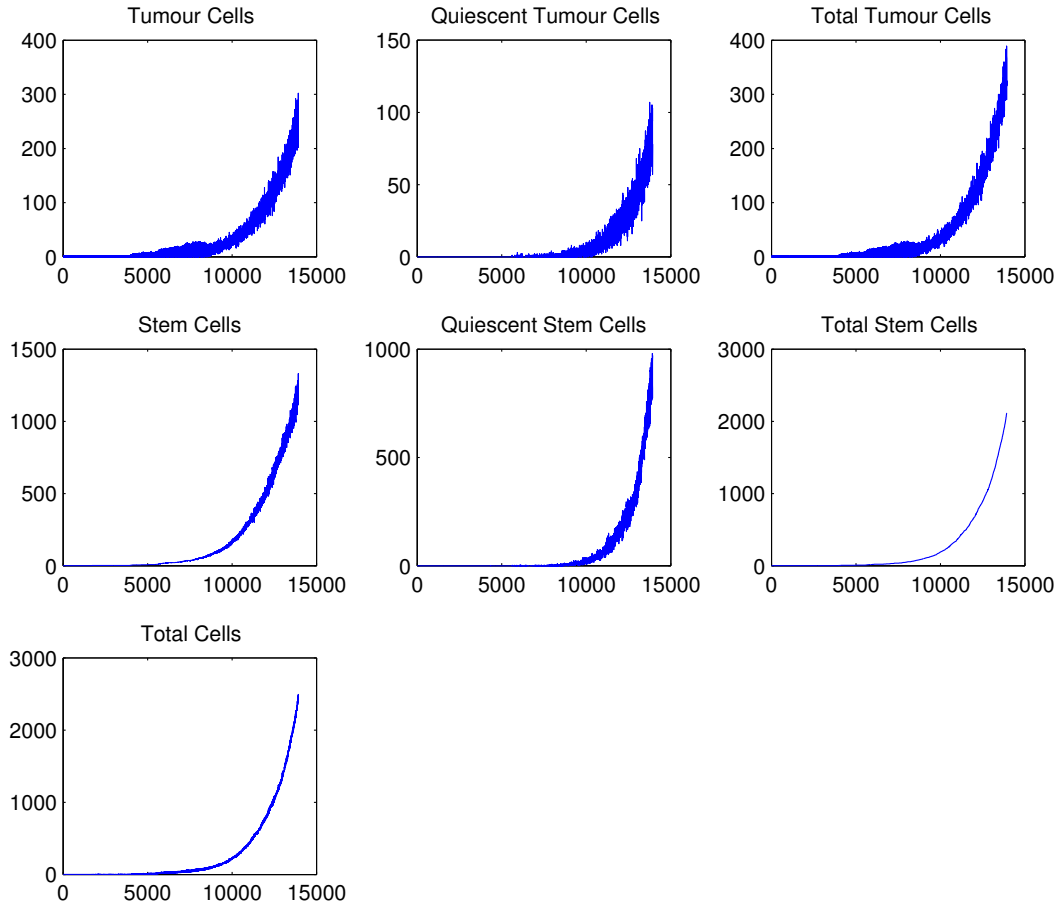

Figure 5.10: *Results of a tumour initiated by a 'true' stem cell over 10000MCS with* $\rho_{max} = 10$ *and spontaneous death rate* $\alpha = 0.35$*. The high death rate of non-stem cells has meant that stem cells are less spatially inhibited which has allowed them to divide more often. Therefore, more symmetric stem cell division has resulted in a very large stem cell population while the normal tumour cell population remained low.*

with the cell surrounded entirely by medium. All of the other processes are implemented in the same way as in the two dimensional case.

It was thought that with extra space in which to migrate perhaps other phenomena might be observed. Figures 5.11 and 5.12 show the results and images of a three dimensional simulation with $\rho_{max} = 10$ and $\alpha = 0.01$. It is possible to compare these results to those of the equivalent two dimensional simulation in figure 5.9. In 3D there is a very short, or possibly non-existent, dormancy period compared to the 2D case. This is because there is more space and the initial stem cells will be in the quiescent state for less time. However, if ρ_{max} is increased, the stem cells will be inhibited for longer and a lengthy dormancy period may be observed. It should also be noted that there is a larger number of cells observed in 3D. Again, this is caused by the lower spatial competition between cells that allows more stem cell divisions.

The larger number of cells simulated in three dimensions may be able to give quantitatively relevant results. However, this greatly increases the computer power required for simulation. A large domain means that CompuCell3D must perform many more calculations for each Monte Carlo Step. An attempt was made to increase the number of cells without increasing the domain by decreasing the size of each cell. Unfortunately, this resulted in strange behaviour by cells because of instabilities caused by small contact areas between cells.

5.4.4 Extensions

There are many areas in which the cancer stem cell hypothesis needs to be explored further. Using the framework of the CompuCell3D it is possible to examine many cellular

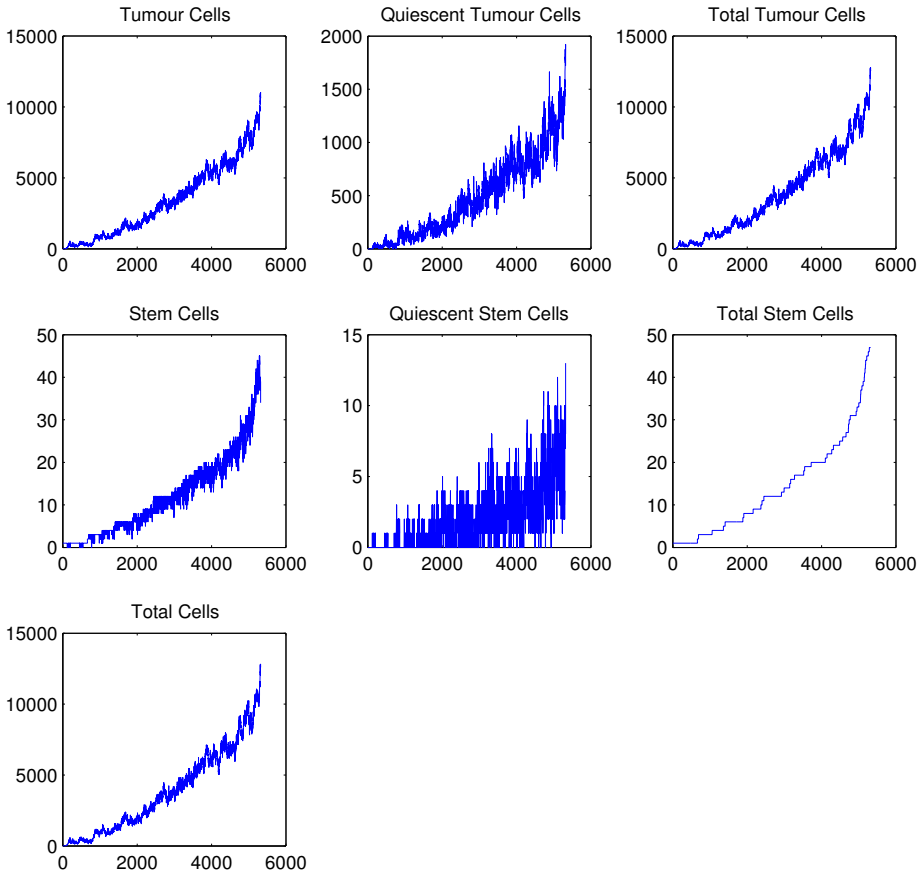

Figure 5.11: *Results of a 3D simulation with* $\rho_{max} = 10$ *and* $\alpha = 0.01$. *It can be seen that the number of stem cells increases very quickly. The stem cell population increase was linear until about 4000MCS when it becomes exponential. This is because there is less spatial inhibition of stem cells in the three dimensions.*

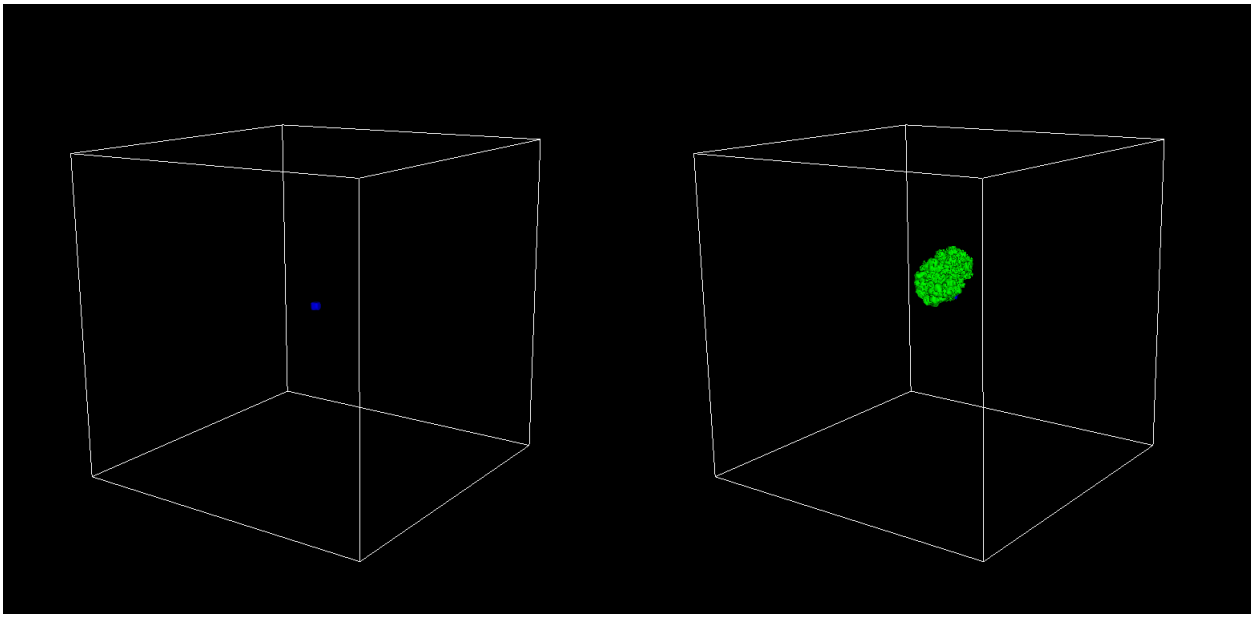

(a) mcs=0 **(b)** mcs=600

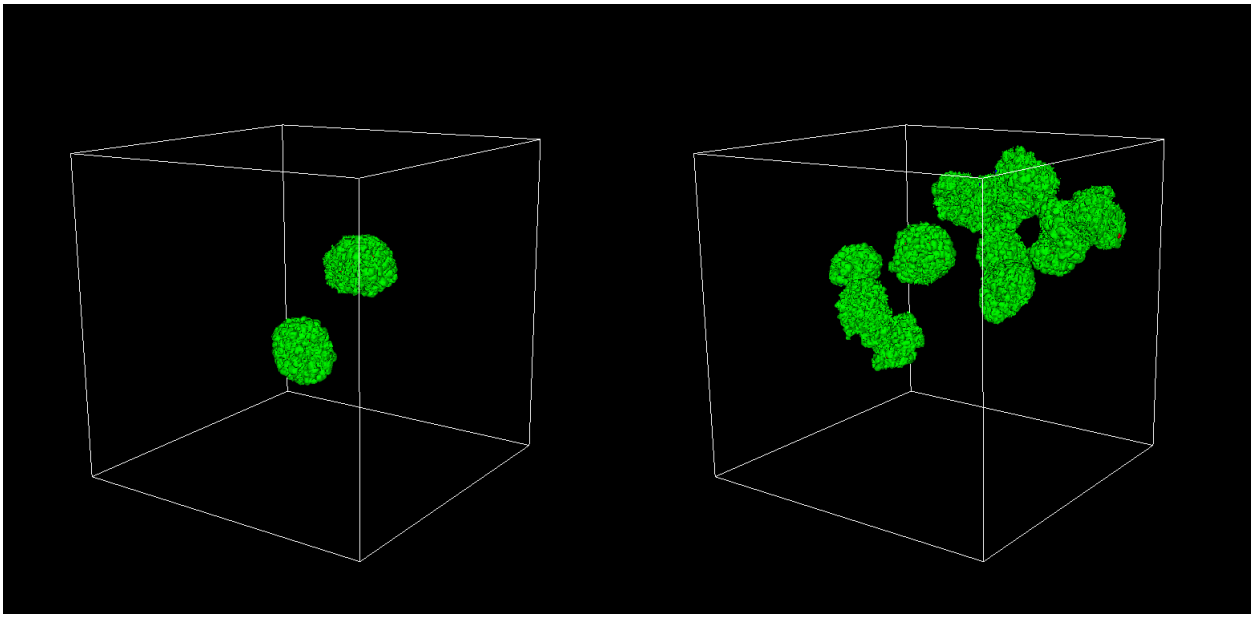

(c) mcs=1070 **(d)** mcs=3070

Figure 5.12: *Images of a 3D simulation with* $\rho_{max} = 10$ *and* $\alpha = 0.01$. *It can be seen that the original stem cell will form a cluster of normal tumour cells. Later, each new stem cell will form its own cluster. Proliferative stem cells are blue and proliferative normal cells are green. The cells in a quiescent state cannot be seen because they are completely surrounded by proliferating cells.*

processes that have not been looked at previously in this context.

It was shown that the spatial inhibition of stem cells plays a key role in tumour dormancy. One of the routes to explore is the possibility that cells in different maturation stages may grow to different sizes. Stem cells are known to be smaller than progenitor and mature cells. This could have a large effect on spatial inhibition because the other cells would be better at competing for the space available.

The simulations in [Stiehl and Marciniak-Czochra (2010, 2012); Nakata et al. (2012)] showed that having more than two differentiation stages was qualitatively the same as including more than two stages. It would be interesting to see if this was the case in spatial models, especially if the cells had different volume potential as described in the previous paragraph.

Using intracellular dynamics it is possible to model many different cellular processes. The inclusion of an individual cell cycle can be used to model cell division in a more realistic manner than a simple break down of 15 Monte-Carlo steps. The cell cycle could depend on nutrient availability and size of the cell. The nutrient availability could also be used to model the quiescent condition to show cells competing for nutrient as well as space. Furthermore, the formation of a necrotic core could be added if the size of the tumour exceeds the oxygen diffusion limit.

The epithelial-mesenchymal transition (EMT) and the reverse process of the mesenchymal-epithelial transition (MET) are important transformations that can have an effect on tumour progression. If a cell undergoes EMT the shape, adhesion and migration rate of the cell is transformed. Mesenchymal cells are less inclined to form contact with neighbouring cells and may break off from the main tumour to metastasise elsewhere in the body. EMT and MET are linked to the Wnt pathway and this can be modelled by a Wnt

gradient and intracellular dynamics involving β-catenin and E-cadherin [Ramis-Conde et al. (2008b)].

The treatment of cancer was discussed and it was shown that a high spontaneous death rate may be used to represent chemotherapy and radiotherapy. In these simulations the probability of death was constant but if this death was carried out at different intervals the treatment may be able to better simulate the different treatments. This could also be used to gain insights into the effectiveness of different treatment regimes.

The ODE model presented above [Stiehl and Marciniak-Czochra (2010, 2012); Nakata et al. (2012)] had two lines of cells. One line to represent the healthy hematopoietic system and another line to represent leukaemic mutations. The current model in CompuCell3D treats the tumour as if it were *in vitro*. It simulates the growth of a single cell to form a tumour in a Petri dish with a medium to provide nutrients. However, it may be possible to carry out simulations of a tumour *in vivo* where the cancer cell was placed in healthy tissue. The competition between cancer cells and healthy cells could be examined with a view to understanding how this affects the cancer stem cell population.

Finally, the initiating cell of a tumour is not always known. A mutation may occur in a healthy stem cell to form a cancer stem cell, but there is also the possibility that a healthy progenitor or mature cell may mutate and gain stem cell qualities. This process is known as de-differentiation because a cell that is in a later maturity stage reverts back to the stem cell stage [Romagnani (2013)].

As has been discussed, the investigation of the cancer stem cell hypothesis may prove vital in understanding the progression of a tumours to malignancy and may improve our ability to treat cancer. This will be an important topic in the future of cancer research.

5.5 PDE model

The cancer stem cell hypothesis was explored in solid tumours using a discrete model in CompuCell3D. While some insight has been gained from these simulations, the model was not able to replicate the number of cells that exist in an avascular tumour (roughly 10^6). Therefore, a spatially-structured, partial differential equation model will be created in this section to simulate a tumour with stem cell and mature cell populations which features spatial inhibition. This continuum model will not describe as many cellular behaviours, but it will be able to simulate avascular tumour growth of the correct size.

5.5.1 Mathematical model

Presented here is a spatially structured model of tumour growth including cancer stem cells and its progeny to examine the competition for space within the domain. A cell is proliferative if it has space in which to move into and divide. Without sufficient space proliferative cells become quiescent.

As well as being proliferative or quiescent, cells will belong to a maturation stage. Stem cells are the most basic of cells with the ability to give rise to different cells types and are therefore the cells at the first stage. When asymmetric division occurs, the daughter cells are of different types. One daughter will be in the same maturation stage as the mother cell and the other daughter will become more specialised and belong to the next maturation stage. Therefore, the cell types included are proliferative cells in stage i, $p_i(x,t)$, and quiescent cells in stage i, $q_i(x,t)$.

The function to represent division of a proliferative cell in maturation stage i is given by [Stiehl and Marciniak-Czochra (2010)]

$$f(t) = (2a_i - 1)\beta_i p_i(x,t), \text{ for } i = 1 \text{ to } n\text{-}1, \tag{5.8}$$

where β_i and a_i are constants and n is the number of maturation stages. This assumes that a cell will divide into two cells at a proliferation rate β_i. The parameter a_i is known as the fraction of self renewal, which determines the fraction of daughter cells that remain in the same maturation stage as the mother cell.

A complementary function to represent the influx of cell from the previous maturation stage is given by [Stiehl and Marciniak-Czochra (2010)]

$$g(t) = 2(1 - a_i)\beta_{i-1} p_{i-1}(x,t), \text{ for } i = 2 \text{ to } n. \tag{5.9}$$

This represents the fraction of daughter cells that have been part of an asymmetric division and have advanced to the next maturation stage.

The next consideration is how to model the decision that cells have to make to become quiescent or proliferative. Each cell must detect its surrounding environment and use this information to decide to remain in its current state or to change. To model the competition for space the following parameters will be used. The rate at which cells change from proliferative to quiescent is

$$\sigma_i(x,t) = r_i(N(x,t) - A) \text{ for } i = 1 \text{ to } n \tag{5.10}$$

and the rate of quiescent cells becoming proliferative is

$$\tau_i(x,t) = r_i(A - N(x,t)) \text{ for } i = 1 \text{ to } n \tag{5.11}$$

where r_i and A are constants and N(x,t) represents the density cells at point x at time t. The function $\sigma(x,t)$ is a relationship in N stating that as N increases, the rate of proliferative cells becoming quiescent increases linearly. Therefore, if the density of cells is high then proliferative cells will run out of space and become quiescent. The constant A defines a critical density at which point there is no more space for cells to divide. The function for the parameter $\tau(x,t)$ is the reversal of $\sigma(x,t)$.

Other forms of these functions can be used. One example uses the heaviside functions

$$\sigma = \begin{cases} 1, & \text{if } N \geq B, \\ 0, & \text{if } N < B, \end{cases} \quad \tau = \begin{cases} 0, & \text{if } N \geq B, \\ 1, & \text{if } N < B. \end{cases}$$

These functions would replicate the discrete case better than equations 5.10 and 5.11. However, these functions were discounted because of their discontinuous nature which results in unrealistic solutions.

For simplicity, the cell death rate has been made constant in time. The constants d_i^p represent the death rates for proliferative cells and d_i^q the death rates for quiescent cells for $i = 1$ to n. It is assumed that stem cells are immortal and therefore

$$d_1^p = d_1^q = 0$$

Proliferative cells, which have free space around them, are assumed to move randomly.

This is represented by random diffusion,

$$D\nabla^2 p_i(x,t) \tag{5.12}$$

where D is a constant. It is assumed that quiescent cells are unable to move because of their lack of space.

A more complicated version of diffusion which depends on the density of the surrounding cells can be represented by

$$\nabla \cdot (D(N(x,t))\nabla p_i(x,t)).$$

An appropriate form of D could be chosen to lower the diffusion of cells if the density of cells increases.

The simulations begin with an initial population of proliferative cancer stem cells in a one dimensional domain and are described by

$$p_1(x,0) = exp(-1000(x-0.5)^2). \tag{5.13}$$

The other variables are initially zero.

$$p_i(x,0) = 0, \text{ for } i = 2 \text{ to } n \tag{5.14}$$

$$q_i(x,0) = 0, \text{ for } i = 2 \text{ to } n \tag{5.15}$$

The following zero flux boundary conditions have been implemented:

$$\frac{dp_i}{dt}(0,t) = 0, \frac{dp_i}{dt}(1,t) = 0, \frac{dq_i}{dt}(0,t) = 0, \frac{dq_i}{dt}(1,t) = 0, \tag{5.16}$$

for $i = 1$ to n.

The set of equations for proliferative cells is

$$\begin{aligned} \frac{\partial p_1(x,t)}{\partial t} &= \frac{\partial^2}{\partial x^2} p_1(x,t) + (2a_1 - 1)\beta_1 p_1(x,t) \\ &-\sigma_1(x,t)p_1(x,t) + \tau_1(x,t)q_1(x,t) - d_1^p p_1(x,t), \end{aligned} \tag{5.17}$$

$$\begin{aligned} \frac{\partial p_i(x,t)}{\partial t} &= \frac{\partial^2}{\partial x^2} p_i(x,t) + (2a_i - 1)\beta_i p_i(x,t) + 2(1 - a_i)\beta_{i-1} p_{i-1}(x,t) \\ &-\sigma_i(x,t)p_i(x,t) + \tau_i(x,t)q_i(x,t) - d_i^p p_i(x,t), \\ &\text{for } i = 2 \text{ to } n-1, \end{aligned} \tag{5.18}$$

$$\begin{aligned} \frac{\partial p_n(x,t)}{\partial t} &= \frac{\partial^2}{\partial x^2} p_n(x,t) + 2(1 - a_{n-1})\beta_{n-1} p_{n-1}(x,t) \\ &-\sigma_n(x,t)p_n(x,t) + \tau_n(x,t)q_n(x,t) - d_n^p p_n(x,t). \end{aligned} \tag{5.19}$$

The set of equations for quiescent cells is

$$\frac{dq_1(x,t)}{\partial t} = \sigma_1(x,t)q_1(x,t) - \tau_1(x,t)q_1(x,t) - d_1^q q_1(x,t), \tag{5.20}$$

$$\begin{aligned} \frac{dq_2(x,t)}{\partial t} &= \sigma_i(x,t)q_i(x,t) - \tau_i(x,t)q_i(x,t) - d_i^q q_2(x,t), \\ &\text{for } i = 2 \text{ to } n-1, \end{aligned} \tag{5.21}$$

$$\frac{dq_n(x,t)}{\partial t} = \sigma_n(x,t)q_n(x,t) - \tau_n(x,t)q_n(x,t) - d_n^q q_n(x,t). \tag{5.22}$$

5.5.2 Numerical results of system with two maturation stages

The system of equations was reduced down to two stages of maturation, which implies that stem cell division can result in a mature cancer cell. The system of equations becomes

$$\frac{\partial p_1(x,t)}{\partial t} = \frac{\partial^2}{\partial x^2} p_1(x,t) + (2a_1 - 1)\beta_1 p_1(x,t)$$
$$-\sigma_1(x,t)p_1(x,t) + \tau_1(x,t)q_1(x,t) - d_1^p p_1(x,t), \tag{5.23}$$
$$\frac{\partial p_2(x,t)}{\partial t} = \frac{\partial^2}{\partial x^2} p_2(x,t) + 2(1 - a_1)\beta_1 p_1(x,t)$$
$$-\sigma_2(x,t)p_2(x,t) + \tau_2(x,t)q_2(x,t) - d_2^p p_2(x,t), \tag{5.24}$$
$$\frac{dq_1(x,t)}{\partial t} = \sigma_1(x,t)q_1(x,t) - \tau_1(x,t)q_1(x,t) - d_1^q q_1(x,t), \tag{5.25}$$
$$\frac{dq_2(x,t)}{\partial t} = \sigma_2(x,t)q_2(x,t) - \tau_2(x,t)q_2(x,t) - d_2^q q_2(x,t) \tag{5.26}$$

and was solved on the one dimensional domain $[0,1]$ together with zero flux boundary conditions and the initial conditions

$$p_1(x,0) = exp(-1000(x-0.5)^2), p_2(x,0) = 0, q_1(x,0) = 0, q_2(x,0) = 0. \tag{5.27}$$

The parameter values can be seen in Table 5.1. The value a_1 is describes the fraction of self renewal first described in Stiehl and Marciniak-Czochra (2010). The remaining parameters have been estimated.

The results, displayed in Figure 5.13, show that there is an initial population of proliferating cancer stem cells. As time progresses the cell types compete for space and form a cluster in the centre of the domain. This gives qualitatively the same behaviour as the

Table 5.1

Parameter	Definition	Value (min^{-1})
a_1	Fraction of self-renewal for stem cells	0.55
β_1	Rate of division for stem cells	1
r_1	Rate that proliferative stem cells become quiescent	1
r_2	Rate that proliferative mature cells become quiescent	1
A	Critical density of cells to determine quiescence	1
d_1^p	Rate of death for proliferative stem cells.	0
d_2^p	Rate of death for proliferative mature cells	0.1
d_1^q	Rate of death for quiescent stem cells	0
d_2^q	Rate of death for quiescent mature cells	0

CompuCell3D simulations in the preceding section.

This reduced form of the full PDE system has shown that it is possible to use a continuum model to describe a lineage- and space-structured tumour. It was able to replicate the behaviours that have been seen in discrete models and can be extended to make it more biologically relevant.

5.6 Discussion

This chapter has developed mathematical models to gain insight into how the cancer stem cell hypothesis can affect cancer growth, invasion and metastasis. Firstly, an ODE model of the blood system was examined to aid the development of a discrete model in CompuCell3D. After seeing the size limitations of the discrete model, a spatially structured PDE model was created to be able to simulate tumours of biologically relevant size.

The ODE model of the hematopoietic system showed that the number of progenitor

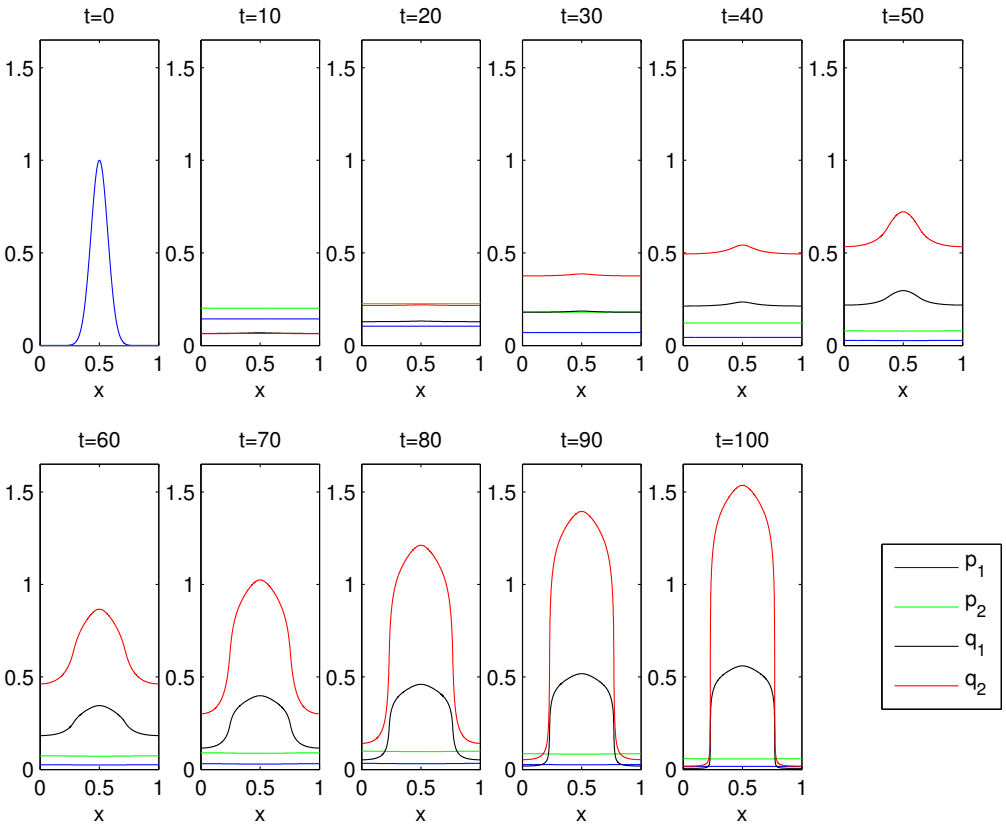

Figure 5.13: *This shows the solution to the reduced system of two maturation stages as time advances. The final time shows quiescent mature cells clustering around quiescent and proliferating cells.*

stages did not make a difference to the overall steady state size of the blood cell population. Therefore, subsequent models in the chapter have only included a stem cell population and a mature cell population. Also, this model showed that the key parameter to study is the fraction of self-renewal, which describes how often a stem or progenitor cell divides symmetrically such that two cells within the same maturation stage are produced. These features were included in the development of a discrete cell model to describe a solid tumour.

CompuCell3D was used to create a model of tumour growth with a stem cell population and a progenitor cell population with the inclusion of spatial inhibition. This was able to show that a stem cell population could give rise to a tumour in a state of dormancy. However, the dormant state was eventually broken when a stem cell divided asymmetrically. The disruption of a dormant state was shown to happen much more quickly if there was spontaneous death of mature cancer cells, which could represent immune response, radiotherapy or chemotherapy. An extension of this model into three dimensions showed that each stem cell was able to generate its own tumour spheroid.

Further extensions of the 3D model were described. The most interesting extension would be the inclusion of a nutrient to form spheroids with a necrotic core, quiescent zone and proliferating rim. This would allow for the exploration of where stem cells reside within an avascular tumour. This would also be able to explore how the stem cells could be important in invasion and metastasis by allowing them to undergo the epithelial-mesenchymal transition. However, the 3D models were only able to simulate tumours with number of cells in the thousands but an avascular tumour has roughly 10^6 cells. Therefore, to be able to model tumours of a biologically relevant size a continuum model was created.

A lineage- and space-structured model of an avascular tumour with spatial inhibition was created using a system of partial differential equations. This was an extension of the ODE model shown at the beginning of the section which described the tumour in one space dimension. This model was able to replicate the findings of the discrete model and extensions can allow it to be more biologically relevant. These possible extensions include: two-dimensional space; nutrient dependent growth, for quiescence and necrosis; interactions with the surrounding tissue; more maturation stages; and the inclusion of more aggressive cell lineages. The advantage of a PDE model is that mathematical analysis may be used to give biological insight, which is not possible in discrete models.

The models developed in this chapter are able to replicate behaviours seen in avascular growth and have shown that cancer stem cells can be the reason for cancer dormancy and invasion and metastasis. However, further extensions can be implemented to explore the importance that cancer stem cells have in these processes.

Chapter 6

Discrete Model of Tumour Growth with Age and Size Structures

This chapter will present a discrete, multi-scale model of tumour growth *in vivo* using the Glazier-Graner-Hogeweg technique. This will be used to simulate the effect that oxygen dynamics in the domain can have on individual cells, which have separate age and size structures. Mitosis will be dependent on several factors. The local oxygen concentration in the microenvironment will decide if a cell is: proliferative, allowing it to proceed through the cell cycle and grow in size; or if it is quiescent, in which it stops many cellular process to wait for a better supply of nutrients. The tumour should reach a steady state because the effect of angiogenesis is not included.

This model is then extended to include a cancer treatment using a chemotherapy drug. The drug will be secreted from blood vessels and diffuses throughout the domain in a similar manner to oxygen supply. This will happen in several doses to replicate the effect of the treatment.

6.1 The multiscale model

The multi-scale simulations in this chapter are created using the CompuCell3D platform with SBML solver. This section will describe how each aspect of the models is implemented.

6.1.1 Cellular rules

The multi-scale simulations will take place in a two dimensional domain made up by a 300 pixel by 300 pixel grid. Each pixel can form part of a cancer cell, a blood vessel or the non-cancerous surrounding tissue. The surrounding tissue is considered to be homogeneous. The presence of healthy cells, extracellular matrix and other components are not explicitly modelled. Components of the model on the tissue scale are the dynamics of oxygen and anti-cancer drugs. These are governed by reaction-diffusion equations with zero flux boundary conditions in which pixels can form sources or sinks.

Cells are known to have a diameter of between 10μm and 20μm [Alberts (2008)]. A newly divided cell will have a diameter of 10μm and must reach a diameter size of 20μm before it can go through mitosis. Each pixel will represent a 2μm by 2μm square so that a newly divided cell will have a diameter of 5 pixel widths. However, as cells grow and move, the shape of cells will vary to make it difficult to gauge the cell size by diameter. Therefore, it is assumed that the area of cells will range between 25 pixels and 50 pixels for an area of between 100 and 200 square microns.

The cancer cells will be differentiated into four subtypes: proliferative, resting, quiescent and necrotic. Proliferative cells are fully oxygenated and have space around them

in which to grow and move. This is the ideal microclimate for a tumour cell to proliferate, progress through the cell cycle and grow in size until division. Mitosis occurs by dividing the cell in two along a randomly oriented axis. When a cell has enough oxygen supply but is completely surrounded by other cancer cells it is spatially inhibited and is said to be in a resting state. Therefore, the cell cycle will be able to progress but the cell will not be able to grow any further. As the microclimate is not ideal for division the cell cycle will not be able to progress beyond a gap phase and will remain in this resting state until space is created through cell migration, apoptosis or necrosis. When the oxygen level at the centre of a cell falls below a threshold value, χ_Q, it will suffer from hypoxia and enters a quiescent state, removing it from the cell cycle and preventing growth. If the oxygen level falls further below the threshold required to maintain a quiescent state, χ_N, the cell will become necrotic. The necrotic cells decrease in size until they are removed from the domain to create space for neighbouring cancer cells to grow and divide. The negative effects of necrosis are not taken into account as this is not the focus of the study.

6.1.2 Age

This section will describe three different methods of modelling the age structure of cells. The first is the simplest method which entails counting the number of Monte Carlo steps that each cell exists for before it divides. The second is a basic method for modelling the cell cycle by counting the number of steps that each cell is in each phase. The third is a presentation of ordinary differential equation models that generate oscillatory dynamics of the cell cycle.

The most basic of all methods is a counter which records the number of Monte Carlo

steps until a cell can divide. This was used in the models in Chapter 5 where each cell would attempt to undergo mitosis after 15 Monte Carlo steps. This idea can be extended to include the definition of a 'young' cell and an 'old' cell. A ' young' cell is one which has recently undergone division and an 'old' cell is one which is approaching division. These definitions will allow for the examination of how each cell will react to changes in the local oxygen supplies. However, a more biologically relevant way to categorise the age of cells is the use of the cell cycle.

The method to represent age used in the models of this chapter is an extension of the simple model described in the previous paragraph. The difference is that the cycle is broken into the distinct cell cycle phases: G1, S, G2, and M. Therefore, each newly divided cell begins in the G1 phase and after a predetermined number of Monte Carlo steps the cell enters the S phase, followed by G2 and M phases. Once in the M phase the cell will divide. The advantage of this method is that it can be seen when the cells react differently to external stimuli depending on which phase the cell is in. Also, it computationally inexpensive and easy to keep track of the number of cells in each phase.

The range of values for which a cell will remain in each stage of the cell cycle are shown in Table 6.1. To illustrate this model of the cell cycle, a simulation of tumour growth

Table 6.1: *Range of times for cell cycle stages*

Cell Cycle Stage	Range of Times(MCS)
G1	20-25
S	3-5
G2	3-5
M	1

was created. Figure 6.1 shows the growth of a tumour from a single stem cell in M

phase, just before it divides. Cells in the G1 are light blue, S are green, G2 are yellow, mitotic cells are red and the surrounding medium is coloured in blue. As can be seen in the figures, most of the cells are in the G1 phase because the length of times spent by cancer cells in the S, G2 and M phases are relatively short [Weinberg (2007)].

To make the representation of the cell cycle more biologically relevant, it is also possible to incorporate sub-cellular mechanisms within each cell. This can be achieved by solving a set of ordinary differential equations which describe the chemical process that governs the cell cycle. Several examples of these are Goldbeter (1991), Gerard and Goldbeter (2009), Tyson and Novak (2001),Tyson and Novak (2003),Tyson and Novak (2004).

6.1.3 Size

As stated above, the model consists of tumour cells which range in size between 10μm and 20μm, which corresponds to areas ranging roughly between 25 and 50 pixels. It is possible for the cells to have a size slightly out with this range because of the constraints set in the cellular potts model. Each cell is given a label to categorise it by its size. The categories chosen are ‘small’, ‘medium’ and ’large’. Small cells are defined as those with an area of less than 35 pixels, medium cells have an area between 35 and 45 pixels and large cells have an area of 45 pixels and above.

The categorisation of cells by size allows for a more realistic representation of oxygen usage for each cell. Large cells will require a higher uptake of oxygen from their environment than small cells to stay in the proliferative state. The size of each quiescent cell will determine how much oxygen is required to prevent apoptosis. These are defined by

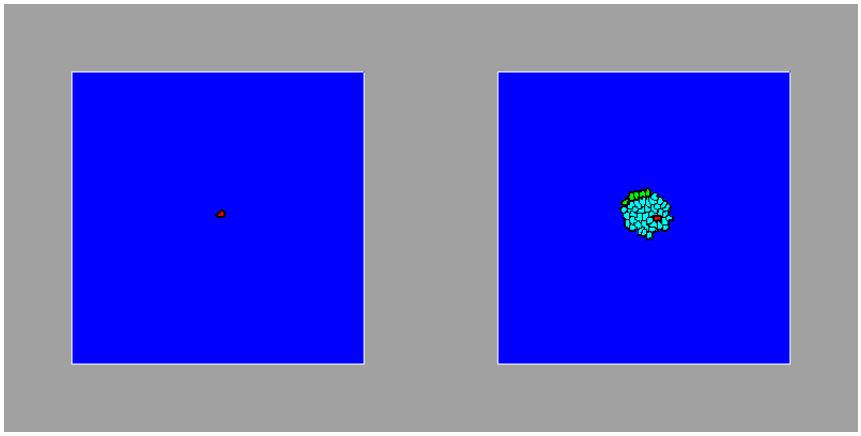

(a) mcs=0 **(b)** mcs=200

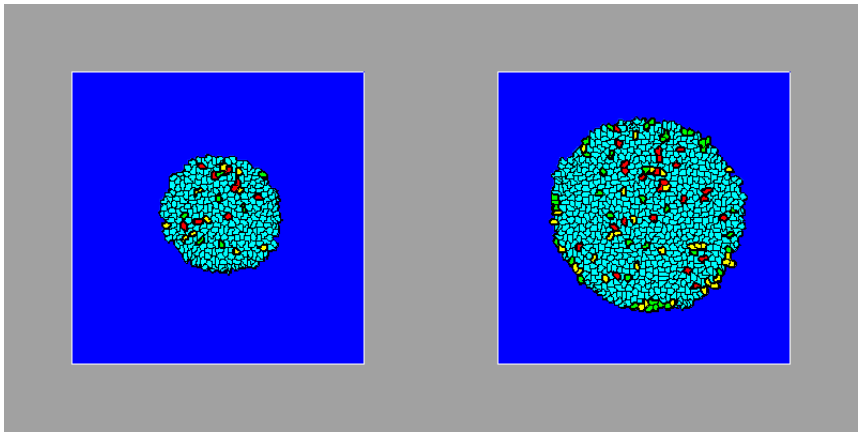

(c) mcs=400 **(d)** mcs=600

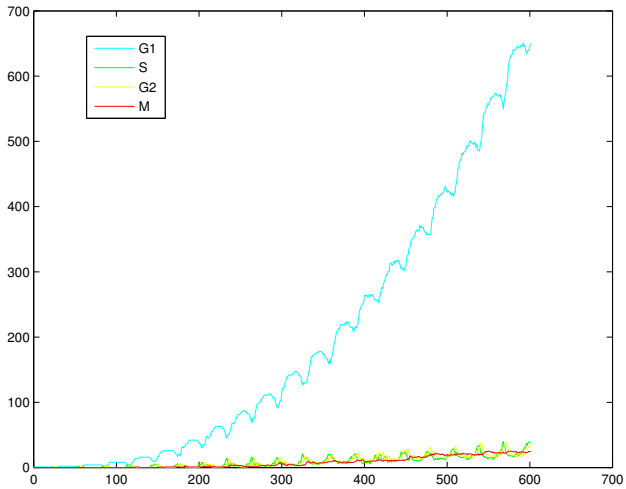

(e) Total number of cells by age in over time.

Figure 6.1: *Figures (a)-(d) show the growth of a tumour over time and the cell cycle stage that each cell is in. Cells in G1 are cyan, S are green, G2 are yellow and M are red. The surrounding medium is coloured blue. Figure (e) shows the number of cells in each stage of the cell cycle as the tumour grows. The figures show that the majority of the cells in the tumour are in the G1 stage.*

the χ parameters.

6.1.4 Modelling oxygen diffusion

The oxygen in the model is represented by a partial differential equation which is solved using the DiffusionSolverFE steppable in CompuCell3D. The governing partial differential equation for oxygen evolution is of the form

$$\frac{\partial c}{\partial t} = D\nabla^2 c - kc + secretion, \tag{6.1}$$

where D is the diffusion rate and k is the decay rate. The term *secretion* and the parameters D and k are determined by their location in the domain. The decay rate k represents the uptake of oxygen by cells and its values are defined as

$$k = \begin{cases} 0.2 & \text{in the medium,} \\ 1.0 & \text{within a proliferative cell,} \\ 0.8 & \text{within a resting cell,} \\ 0.5 & \text{within a quiescent cell,} \\ 0.0 & \text{within a necrotic cell.} \end{cases}$$

The decay rate is seen to be higher in cells that use more oxygen to maintain their functions. This represents a higher uptake of oxygen by the cells. The diffusion rate of oxygen is considered to be lower within the tumour cells than it is in the medium. The boundary condition on the oxygen diffusion is zero-flux at the boundary of the domain.

6.1.5 Adhesion

The adhesion between cells is controlled by the sub-cellular ODE model of E-cadherin/β-catenin, which was seen in chapter 4 [Ramis-Conde et al. (2008b)]. These sub-cellular dynamics used the same parameter values as found in Andasari et al. (2012).

6.1.6 Cell death

Cancer cells are known to acquire the trait of evading apoptosis, also known as programmed cell death. This occurs when a cell actively decides to destroy itself because of irreparable damage or if it is in an environment which does not offer enough support, such as nutrients. However, because cancer cells are able to avoid this phenomenon it will continue to divide despite damage to its DNA and will produce daughter cells with more mutations. Therefore, the cancer cell can only die if it doesn't have access to the necessary nutrients. Without apoptosis, the cell will degrade in a process known as necrosis.

In later simulations, the affect of chemotherapy has been modelled. As a chemotherapy drug makes its way through the body via the blood system, it will be secreted from the blood vessel cross-sections in a similar manner to oxygen described above. From here it diffuses throughout the domain and will make the tumour cells necrotic if it is present in high enough concentrations. However, the chemotherapeutic drugs are known to have a different effect upon cells in different stages of age and size, as will be explored.

6.2 Results

The first simulation in this section is of tumour growth based on oxygen supply from blood vessels with age and size structure. This is followed by mutations in a cell's size and age in relation to oxygen consumption. Finally, the age and size structured model is used to show how chemotherapy treatments can affect tumours.

6.2.1 Tumour growth with age and size structure

The initial scenario presented in this chapter is the demonstration of tumour growth with age and size dynamics and how spatial inhibition and oxygen dynamics have an effect upon it. Following this, the age and size parameters are varied to show how this affects the tumour growth.

The initial set up begins with a random placement of blood vessel cross sections. These are allowed to secrete oxygen in the domain to replicate a piece of tissue within a body. When the oxygen levels have reached a steady state, a single small cancer cell in the G1 phase is placed randomly to represent a mutation of a normal cell within the organism. If the cell is in an area with enough oxygen it will be in a proliferative state and will move through the cell cycle and increase its size. When it has reached the Mitosis phase, and if it is large enough, the cell will divide into two daughter cancer cells. The tumour continues to grow in this fashion.

Figure 6.2 shows the progression of tumour growth from a single cell to a fully formed tumour. The colours of the cells are represented as follows: proliferative cells in light green, resting cells in dark green, quiescent cells in blue, necrotic cells in black, blood

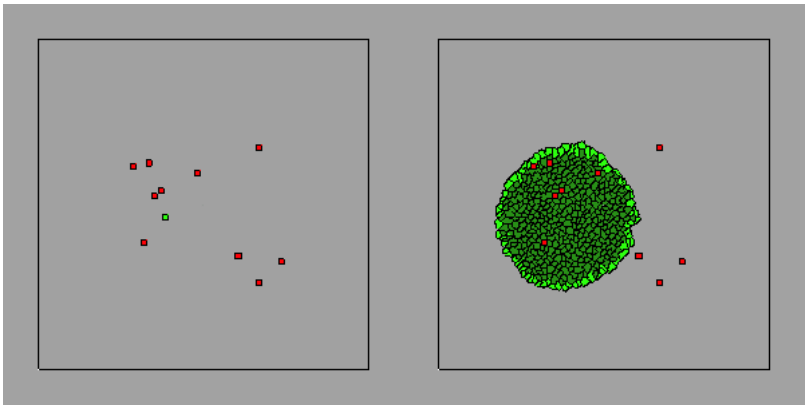

(a) mcs=100 **(b)** mcs=1000

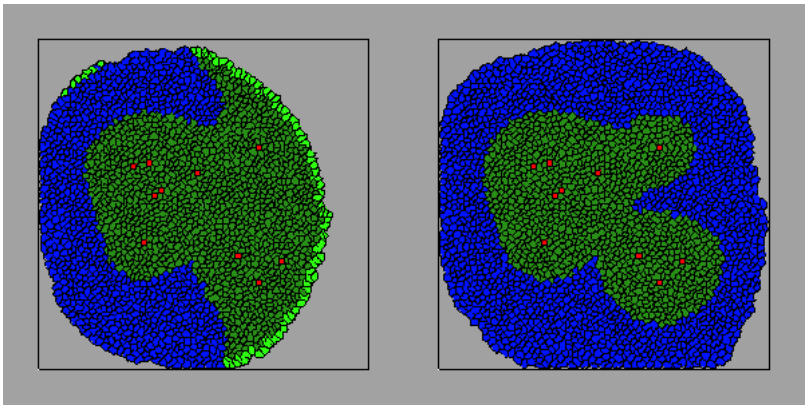

(c) mcs=2000 **(d)** mcs=3000

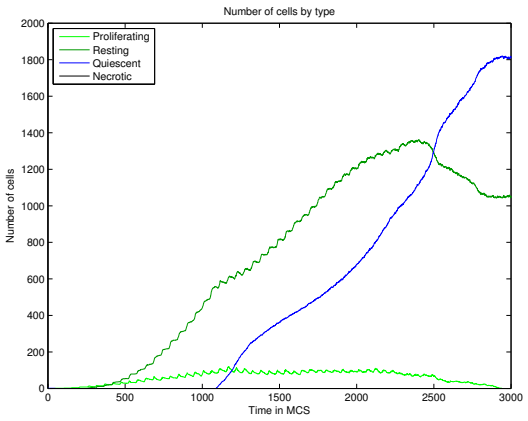

(e) Number of cells over time

Figure 6.2: *The growth of a tumour with age and size structure. Proliferating cells are light green, resting cells are dark green, quiescent cells are blue, necrotic cells are black, blood vessels are red and the surrounding tissue is grey. (a) shows the initial mutation of a tumour cell, which is small and begins in the G1 phase. (b) shows the proliferating rim surrounding resting cells. (c) shows the development of a quiescent zone of cells which is beyond the reach of the oxygen. (d) shows the final size that the tumour is able to grow without angiogenesis. (e) shows the number of cells by type over the time of the simulation.*

vessels in red and the surrounding tissue in grey. Figure (a) shows the initial mutation of a normal cell to a tumour cell, which has been randomly placed within the domain. Figure (b) shows that as the tumour grows, the proliferative cells are present at the edge of the tumour mass. The resting cells in dark green are inhibited by the presence of other cells and will not increase in size. Figure (c) shows that when the tumour expands further, it consumes more oxygen which results in cell cycle arrest, turning the cells into a quiescent state. Quiescent cells consume less oxygen and will wait in this state until the environment improves. However, if the oxygen levels are too low to support the quiescent cells they will become necrotic. Figure (d) shows the state of a fully formed tumour which has reached its maximum size unless it obtains support through angiogenesis, the process by which tumours encourage the body to increase blood supply to the domain by the creation of new blood vessels.

Figure 6.3 displays the size of each cell as the tumour grows. Small cells are cyan, medium sized cells are green and large cells are red. The corresponding graph shows the number of cells in each size category. The majority of the cells are small because as large cells divide the daughter cells eventually become spatially inhibited and are prevented from growing. Therefore, they will remain small unless they gain space.

Figure 6.4 shows the stage that each cell is within the cell cycle. Cells in G1 phase are represented by cyan, S phase in green, G2 phase in yellow and M phase in red. The quiescent cells, in the G0 phase, are represented by a blue. Most of the cells are in the G1 phase because this is the longest part of the cell cycle. The other phases are relatively short in comparison. Also, as shown in Figure 3, most of the cells are small. Therefore, they are unable to progress into the S phase of the cell cycle because they are not large enough to do so.

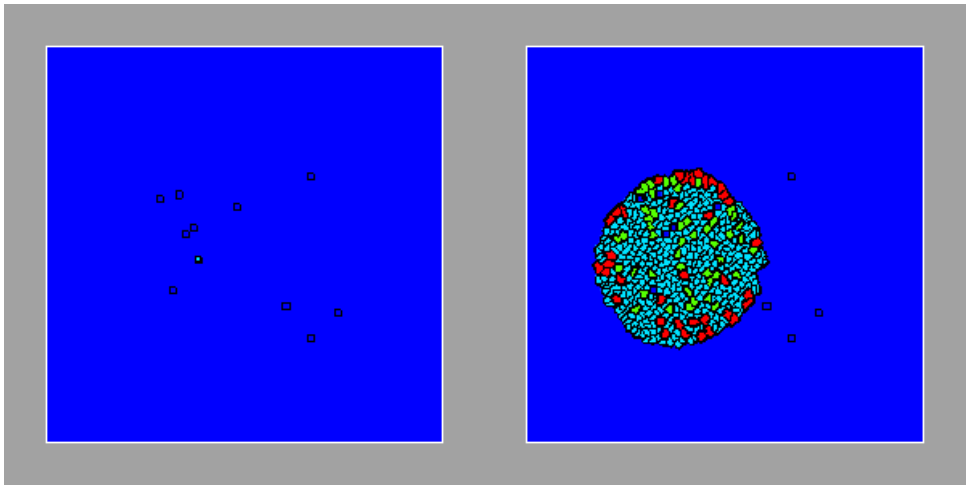

(a) mcs=100 **(b)** mcs=1000

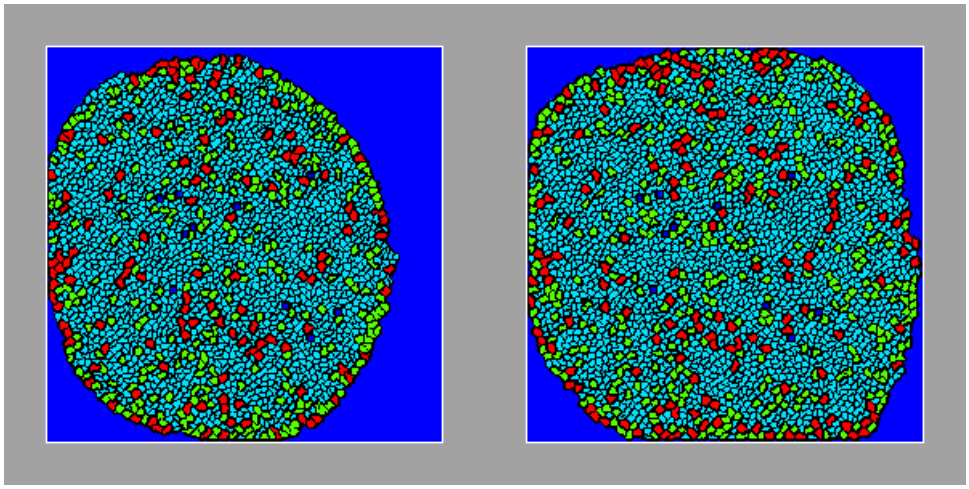

(c) mcs=2000 **(d)** mcs=3000

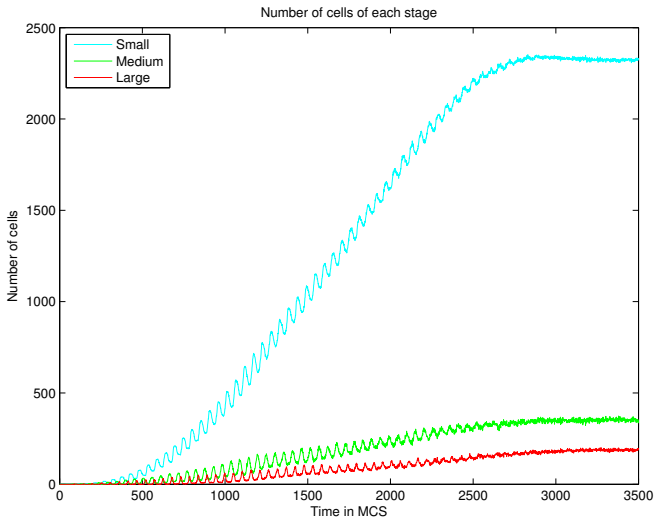

(e) Number of cells over time

Figure 6.3: *Figures (a)-(d) show the growth of a tumour and the size of each cell. Small cells are cyan, medium cells are green and large cells are red. The blue background represents the medium. Figure (e) shows the number of cells of each size as the tumour grows. The figures show that as the the majority of the cells are small because they are spatially inhibited and unable to grow.*

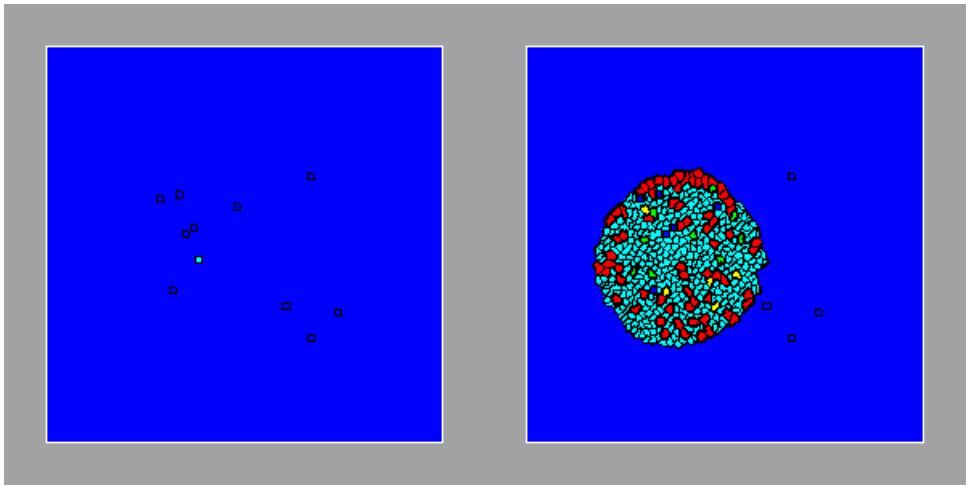

(a) mcs=100 **(b)** mcs=1000

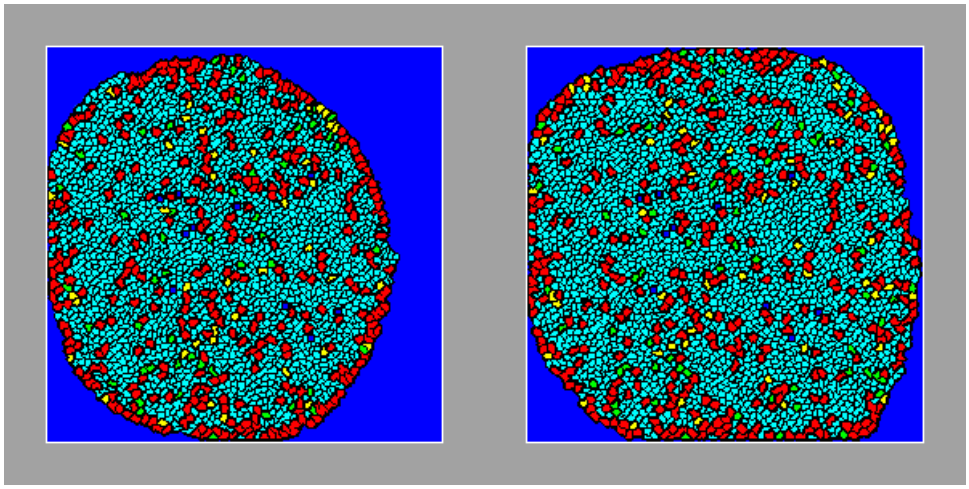

(c) mcs=2000 **(d)** mcs=3000

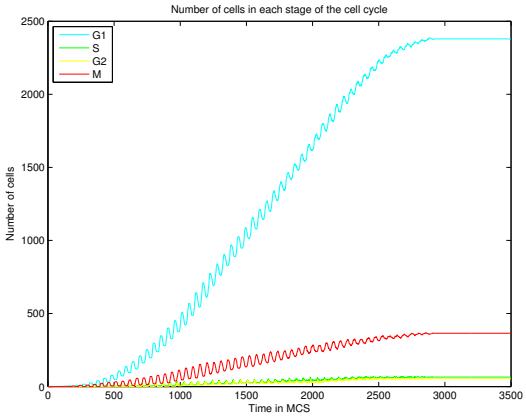

(e) Number of cells over time

Figure 6.4: *Figures (a)-(d) show the growth of a tumour and the cell cycle stage of each cell. Cells in G1 are cyan, S are green, G2 are yellow and M are red. The blue background represents the surrounding tissue. Figure (e) shows the number of cells in each stage of cell cycle as the tumour grows. As can be seen the majority of the cells are in the G1 phase. This is because most of the cells are small and are unable to progress into the S phase in the cell cycle because they are not large enough.*

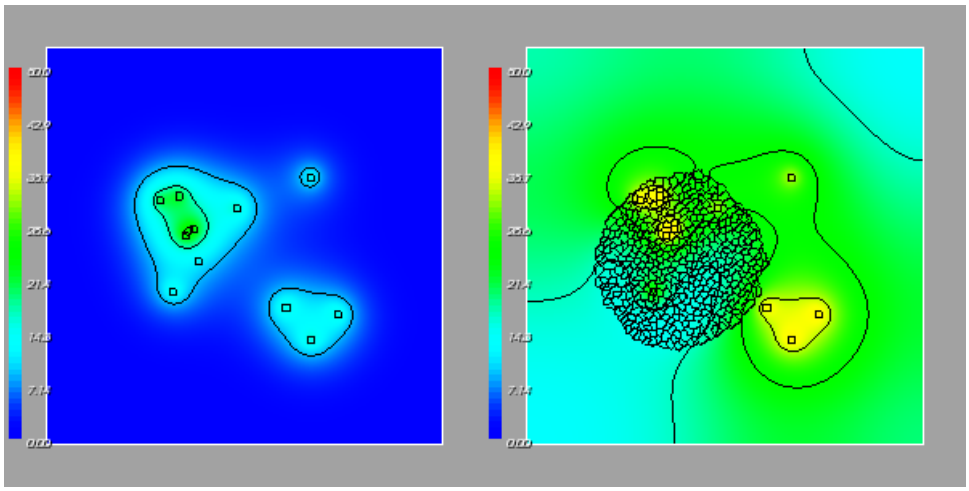

(a) mcs=100 **(b)** mcs=1000

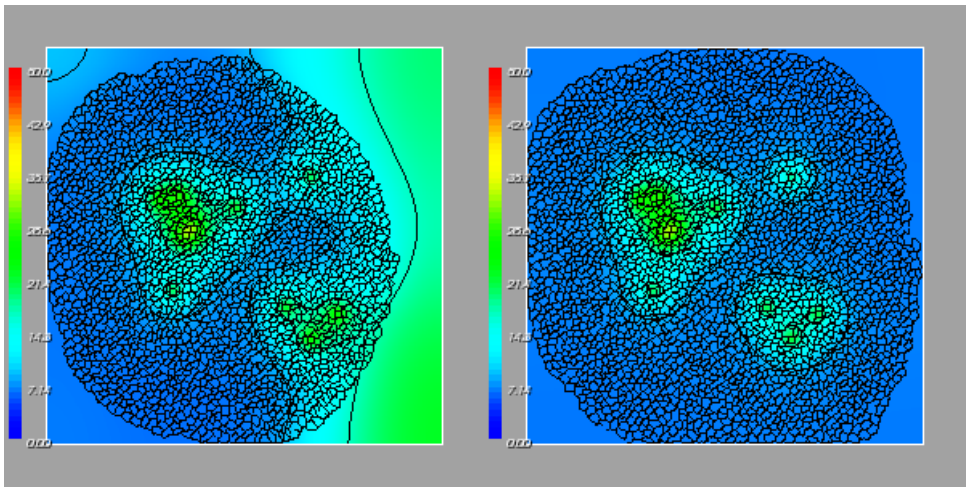

(c) mcs=2000 **(d)** mcs=3000

Figure 6.5: *Figures (a)-(d) depict the oxygen field concentration over time. As the oxygen is secreted from the blood vessels it diffuses throughout the domain. As the tumour takes over the domain it consumes more oxygen than the normal tissue and prevents the oxygen from reaching the edge of the domain.*

Figure 6.5 displays the oxygen levels within the domain. At the starting point of the simulation the domain has oxygen present everywhere. As the tumour grows it consumes more oxygen than the surrounding tissue and patches of the domain have very little oxygen present. The final figure shows that almost no oxygen reaches beyond the tumour.

6.2.2 Size dependent oxygen consumption

It is natural to assume that a large cell has a higher demand for oxygen and other nutrients than small cells. This metabolic need for oxygen for cellular growth and mitosis means that the spread of a tumour depends on the microenvironment around it. In the previous section's simulation, larger cells consume more oxygen than smaller cells because of the way the uptake is calculated in the CompuCell3D finite difference solver. In this section, the threshold oxygen levels for cells, χ_Q and χ_N are varied depending on the size category of the cell. This will assume that a larger cell needs higher oxygen levels at its centre to be able to prevent hypoxia or necrosis. The values used in this simulation are shown in the Table 6.2. As can be seen, large cells require a higher levels of oxygen to be proliferative or quiescent.

Table 6.2: *Oxygen Threshold Parameters by Cell Size*

Name	Description	Value (mM)
χ_{QS}	Hypoxic threshold for small cells.	7.9
χ_{QM}	Hypoxic threshold for medium cells.	8.0
χ_{QL}	Hypoxic threshold for large cells.	8.1
χ_{NS}	Necrosis threshold for small cells.	5.6
χ_{NM}	Necrosis threshold for medium cells.	5.7
χ_{NL}	Necrosis threshold for large cells.	5.8

Figure 6.6 shows the results of tumour growth simulations with the implementation of the χ parameter values shown in 6.2 compared with $\chi_Q = 8.0$ and $\chi_N = 5.7$ for all cells. Altering the χ parameters to depend on size leads to a much different dynamic equilibrium of the tumour than the standard case. Figure 6.6(a) shows that, for $\chi_Q = 8.0$ and $\chi_N = 5.7$, once the tumour has reached its maximum size the number of proliferative and necrotic cells oscillates around 50, resting cells around 1000 and quiescent cells around 1200. These oscillations have a small amplitude and the overall composition of the tumour has little change over time. When the χ parameters are varied by cell size, as shown in 6.6(b), the number of proliferative and necrotic cells oscillates around 50, resting cells around 1100 and quiescent cells around 1050. However, the amplitude of the oscillations of quiescent cells is much larger, moving between 900 and 1200 cells. Also, the number of resting cells is higher than in the standard case. The parameter variations have resulted in a change in the composition of the cells types that make up the tumour mass over time. This was investigated by examining the composition of the tumour by cell size.

Figure 6.7 shows the results of the variation of the χ parameters by cell type and size. As can be seen from the figure, the driving force behind the change in the tumour composition is caused by the number of small quiescent cells. This can be explained by how the cells interact with the oxygen microenvironment. After the tumour has reached a steady state size, proliferative cells near the blood vessels are still able to divide. As the daughter cells grow they consume more oxygen and so are less able to reach the outer edge of the tumour. The resting cells that are furthest away from the blood supply become quiescent and the quiescent cells at the edge of the tumour become necrotic. In the standard case, these two cell types change as a result of higher oxygen consumption occuring at the same time which results in little variation in the overall number of cells

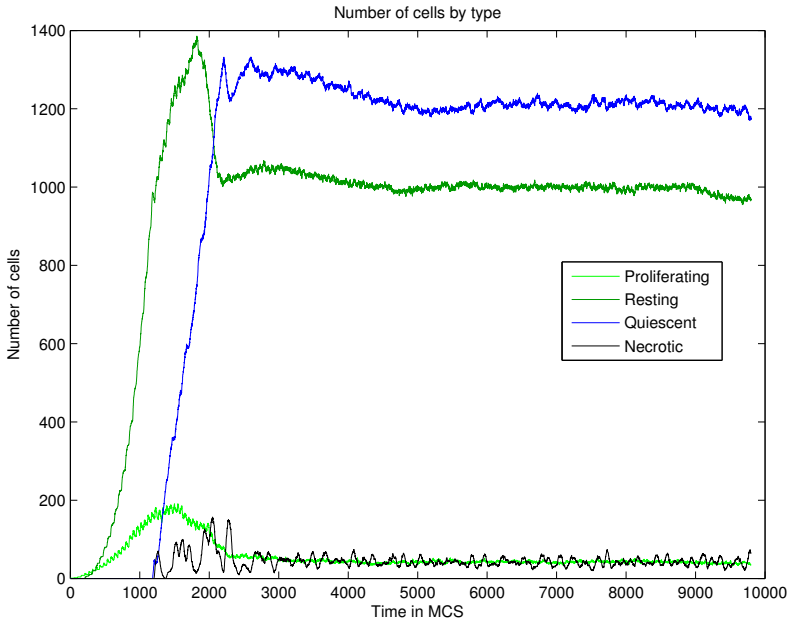

(a)

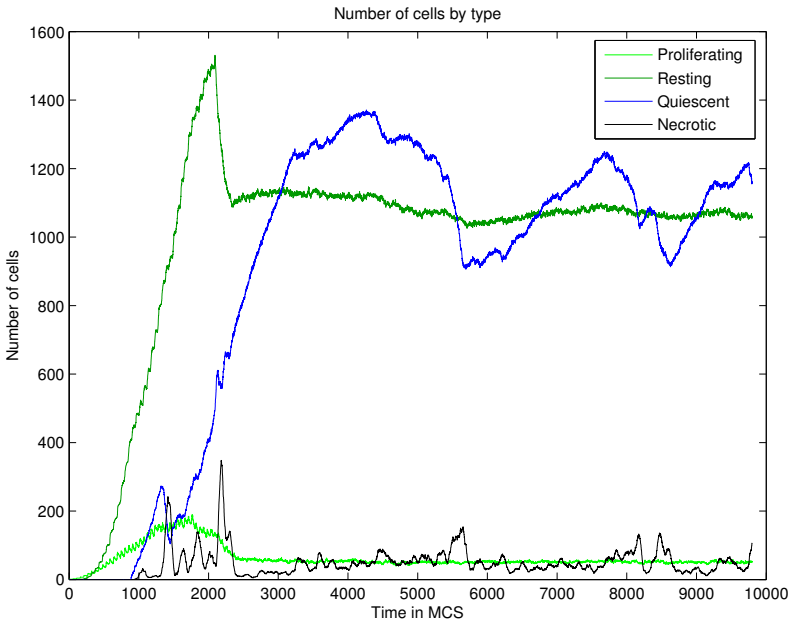

(b)

Figure 6.6: *These figures show a comparison between simulations with different χ parameters, which are the threshold values of oxygen that determine whether cells are proliferative, quiescent or necrotic. Figure (a) shows the number of cells of each type when χ_Q and χ_N are the same for all cells. The tumour quickly grows to its full potential and the number of cells of each type is in dynamic equilibrium. Figure (b) shows the results when the χ values shown in Table 6.2 are implemented. It can be seen that the number of quiescent cells still oscillates around 1100, but it does so with a much greater amplitude.*

by type. However, in the altered case the changes occur at separate times with quiescent cells changing to necrotic before the resting cells become quiescent.

The last point to consider is where, within the tumour mass, cells change from resting to quiescent or quiescent to necrotic. Figure 6.8(a) shows the growth of a tumour without a change to the χ parameters. Here it can be seen that there is very little heterogeneity in the cells types. There is a clear region comprised of proliferative and resting cells which is nearest the blood vessels. This is surrounded by a quiescent region and necrosis occurs at the outer edge of the tumour, further from the blood supply. Figure 6.8(b) shows tumour growth with χ parameters found in Table 6.2. It can be seen that the different regions of the tumour are not mutually exclusive. This is exemplified by the large and medium necrotic cells which are in the quiescent region of the tumour. Also, there are large quiescent cells which are surrounded by resting cells. This greater heterogeneity within the tumour, caused by the size structure, may play an important role in a tumour's development and also how it can react to the surrounding tissue, the body's immune response and its reaction to cancer fighting drugs.

6.2.3 Chemotherapy treatments

This section uses the model of age and size structured tumour growth presented in the previous sections to examine how these structures can have an effect upon chemotherapeutic drug treatments. Firstly, the effect of the chemotherapy drug causing the death of all cells regardless of size and age is presented. This is then followed by an age-structured drug effect in which only cells in the G1 phase of the cell cycle are killed.

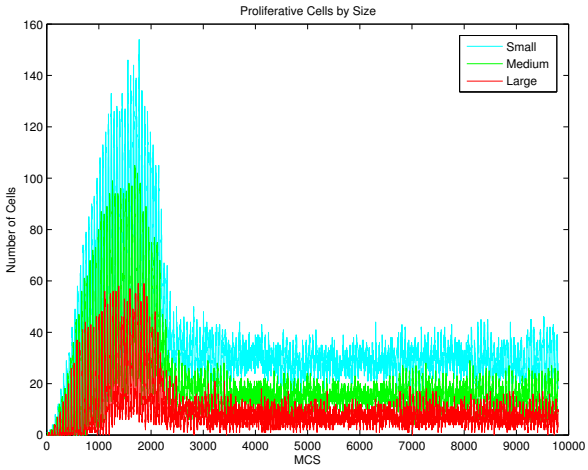

(a)

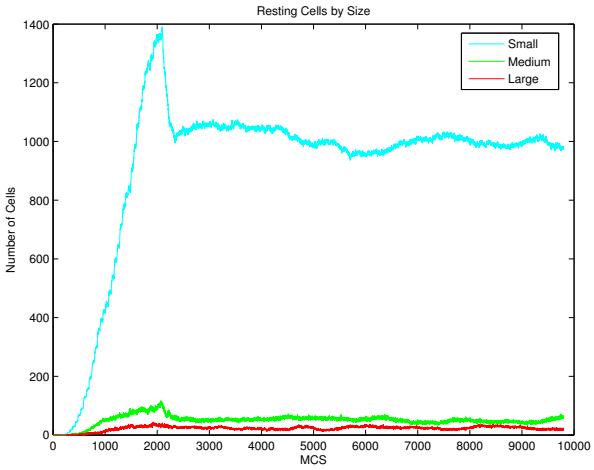

(b)

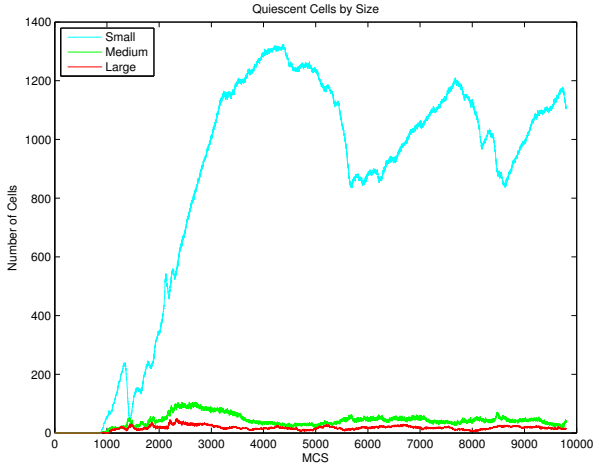

(c)

Figure 6.7: *These figures show the number of cells by type and size over time for the χ parameter values shown in table 6.2. Figure (a) shows the number of proliferative cells of each size over time. Figure (b) shows the number of resting cells of each size over time. Figure (c) shows the number of quiescent cells of each size over time. It can be seen that the variation of the number of quiescent cells shown in figure 6.6(b) is caused specifically by small quiescent cells.*

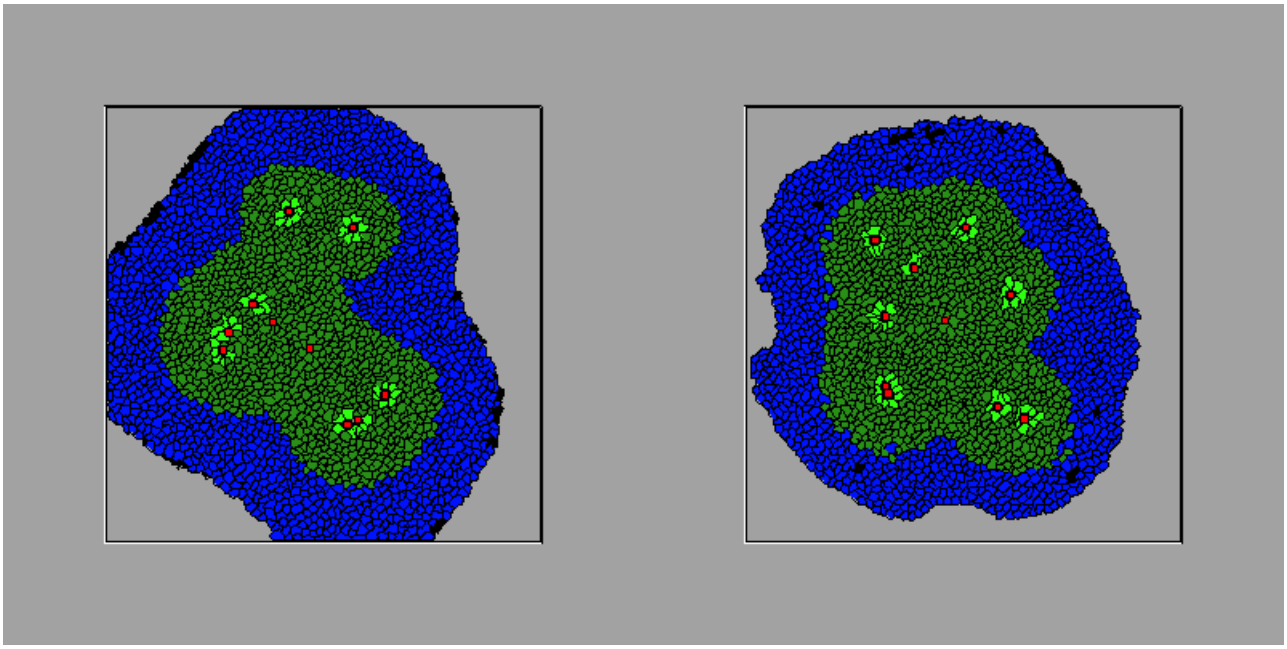

(a) (b)

Figure 6.8: *A comparison of the tumours that are generated with and without the variation of χ values. (a) No change in χ values. (b) The χ values from table 6.2 are implemented. Proliferative cells are light green, resting cells are dark green, quiescent cells are blue, necrotic cells are black, blood vessels are red and the surrounding tissue is grey. In (a) there is a clean division between resting and quiescent cells and necrosis only occurs at the outer edge of the tumour. However, in (b) the tumour has greater heterogeneity because of the use of the size structure. Large quiescent cells can be found amongst resting cells. Small quiescent cells still become necrotic at the outer edge of the tumour but medium and large cells are shown to become necrotic further away from the edge.*

6.2.3.1 A single chemotherapy dose

In this first model, a vascularized tumour is allowed to grow to a steady state size, which happens by 3000 MCS. Figure 6.9 shows how a dose of chemotherapy is modelled on a tumour. The chemotherapy drug is secreted from the blood vessels for 10 Monte Carlo Steps, beginning at 3000 MCS. Figure 6.9(a) shows the concentration of the drug at the end of the dose. The highest concentrations are found at the location of the blood vessels and it can be seen that it has diffused into the surrounding tumour. After a further 10 MCS the drug has diffused even further in to the tumour. 40 MCS later the tumour cells are starting to undergo apoptosis and the drug is allowed to diffuse further into the domain. At 3110 MCS, the drug is now completely decayed away and only the blood vessels and some remaining tumour cells are left in the domain.

This simulation demonstrates how one dose of drug therapy can effectively remove much of the mass of a tumour. The remaining simulations will demonstrate how a course of treatment, featuring several doses, can be used to completely eliminate a tumour or allow for its resurgence.

6.2.3.2 Elimination and resurgence of a tumour

Figure 6.10 shows how a course of chemotherapy can completely eliminate a tumour which has grown to its full potential before the onset of further angiogenesis. It is the case that the drug affects each cancer cell uniformly so that the spatial location of the cells and the diffusion of the drug are the determining factors for cell death or survival. The initial set up was the same as previous models: a single proliferative cell in an oxygenated domain which contained randomly distributed blood vessels. The tumour

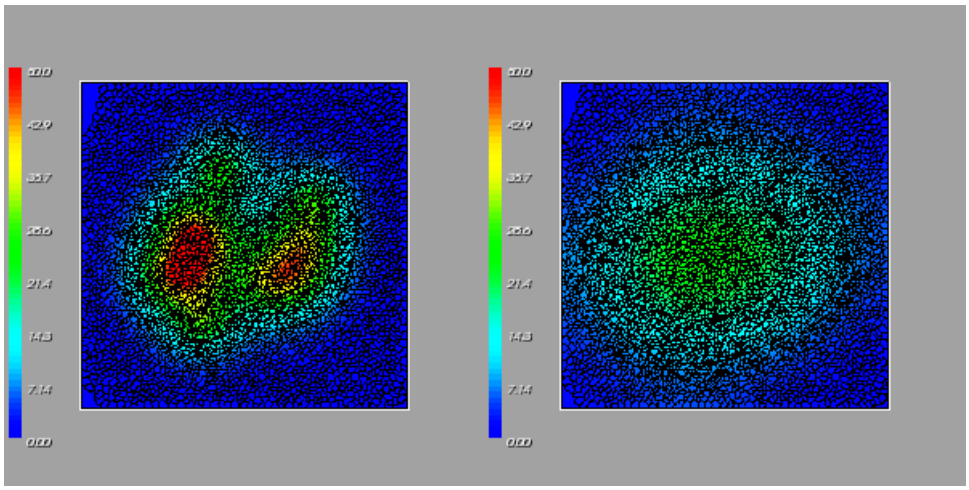

(a) 3010 MCS **(b)** 3020 MCS

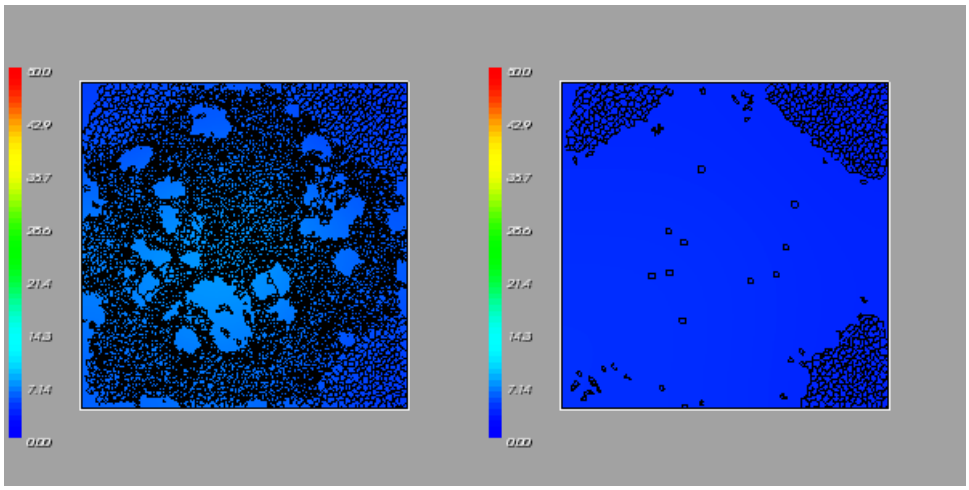

(c) 3060 MCS **(d)** 3110 MCS

Figure 6.9: *Figures (a)-(d) show a single dose of drug therapy on a tumour which has reached its maximum size without angiogenesis. When the therapy begins the drug is secreted from the blood vessels, which can be seen in figure (a). Figure (b) shows how the drug diffuses throughout the domain after the secretion from the blood vessels has stopped. The tumour cells are beginning to be killed in figure (c) and figure (d) shows the end of the treatment when there is very little drug left in the domain.*

then grew to a steady state size and the course of drug therapy began. The therapy was given in doses every 1000MCS. The figure shows that after the first dose, the drug was able to remove most of the tumour. However, because of the density of the tumour cells, the drug was unable to diffuse in high enough concentrations to kill all of the tumour cells. With successive doses, the drug was able to diffuse further from the blood vessels and kill more cancer cells until eventually all of the tumour was eliminated.

Figure 6.11 shows that the result of six doses of chemotherapy treatment that were unsuccessful. As can be seen, the drug cannot reach far enough into the tumour at a lethal dose to prevent a resurgence before the next dose. This can happen if the cancer develops resistance to the drug in question, not enough of the drug is administered or if the doses are too far apart.

6.2.3.3 Age-structured drug death

In this section, the effects of the chemotherapy drug act differently upon cells depending on their stage in the cell cycle. This is because anti-cancer drugs are known to kill tumour cells which are in the G1 phase, the longest phase of the cell cycle. Figure 6.12 shows the results of chemotherapy treatments that kill cells when they are in the G1 phase in a vascularised tumour.

It can be seen that after the first dose of treatment some cells near the blood vessels survived. These remaining cells were able to proliferate in between the doses of therapy, which prevented the drug from reaching further into the tumour population. This resulted in the drug being unable to eliminate the tumour population, resulting in the persistence of the cancer.

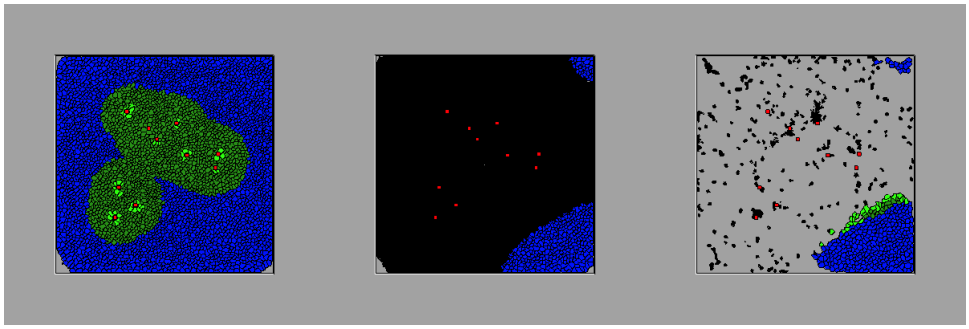

(a) mcs=3000
Steady state before therapy

(b) mcs=3050
First dose

(c) mcs=3200

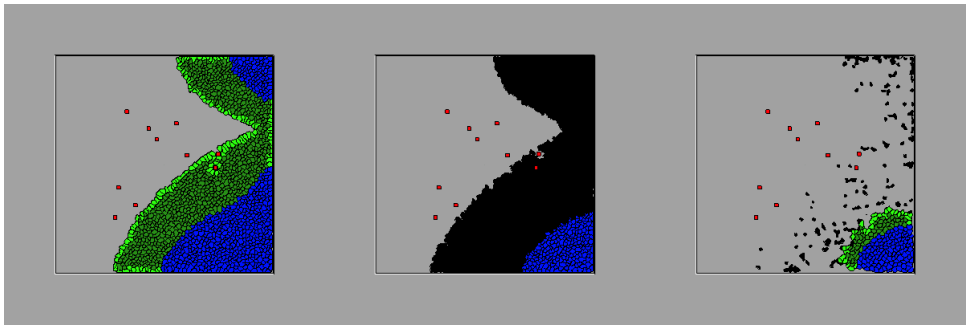

(d) mcs=4000

(e) mcs=4050
Second dose

(f) mcs=4200

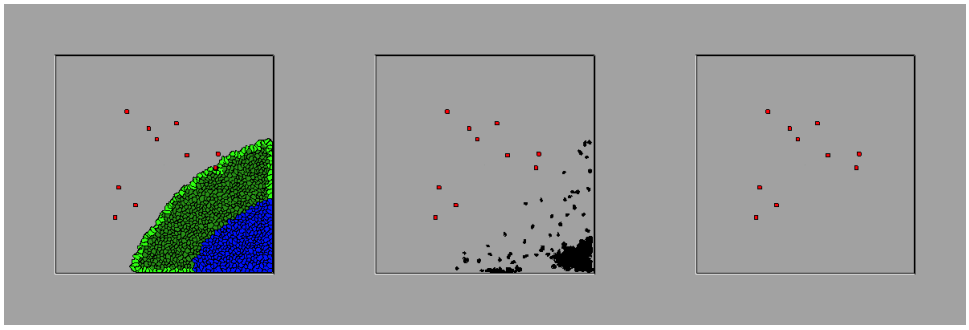

(g) mcs=5000

(h) mcs=5050
Third dose

(i) mcs=5200
Elimination

Figure 6.10: *These figures show how a tumour can be eliminated after three doses of a chemotherapy drug. Proliferative cells are light green, resting cells are dark green, quiescent cells are blue, necrotic cells are black, and blood vessels are red. Figure (a) shows the steady state size of the tumour before drug therapy. Figures (b), (e) and (h) show how far the drug was able to diffuse in the tumour at lethal concentrations. Figures (c) and (f) show the beginning cancer resurgence after the drug dose. Figures (d) and (g) show the size of the tumour just before the next dose of therapy. Figure (i) shows the complete elimination of tumour cells. It can be seen that three doses of therapy were required to completely eliminate the tumour.*

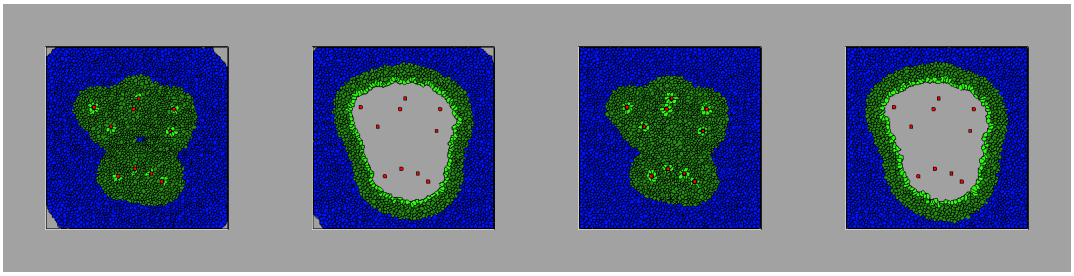

(a) mcs=3000 **(b)** mcs=3130 **(c)** mcs=4000 **(d)** mcs=4140

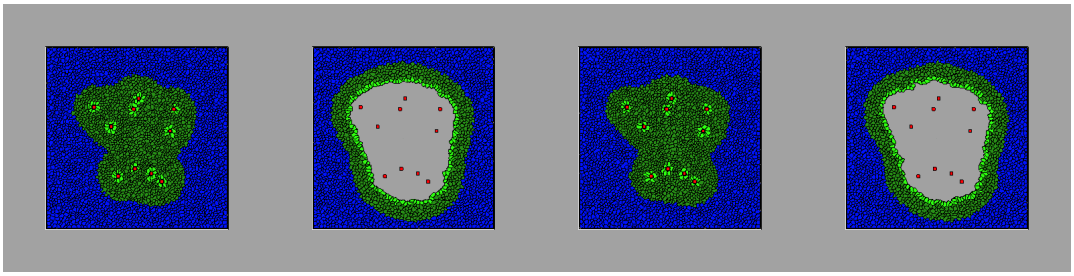

(e) mcs=5000 **(f)** mcs=5130 **(g)** mcs=6000 **(h)** mcs=6130

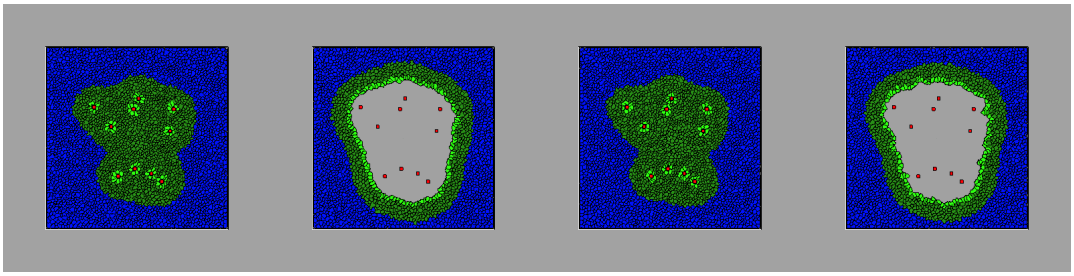

(i) mcs=7000 **(j)** mcs=7130 **(k)** mcs=8000 **(l)** mcs=8130

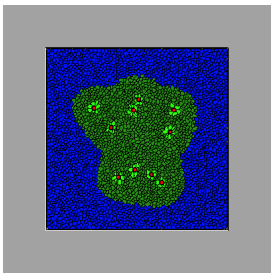

(m) mcs=9000

Figure 6.11: *The results of a course of chemotherapy that was not strong enough to eliminate the drug. Proliferative cells are light green, resting cells are dark green, quiescent cells are blue, necrotic cells are black, and blood vessels are red. Figure (a) shows the steady state before the treatment begins. Figures (b), (d), (f), (h), (j) and (l) show how much of the tumour the drug was able to reach in a lethal dose. Figures (c), (e), (g), (i) and (k) show the regrowth of the tumour immediately before the next dose. Figure (m) shows the final steady state tumour after the course of drug therapy. The resurgence of the tumour cells is seen to be too powerful for the drug.*

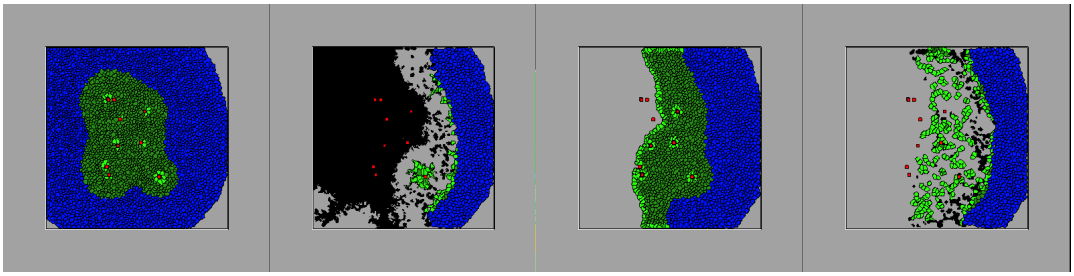

(a) mcs=3000 **(b)** mcs=3130 **(c)** mcs=4000 **(d)** mcs=4140

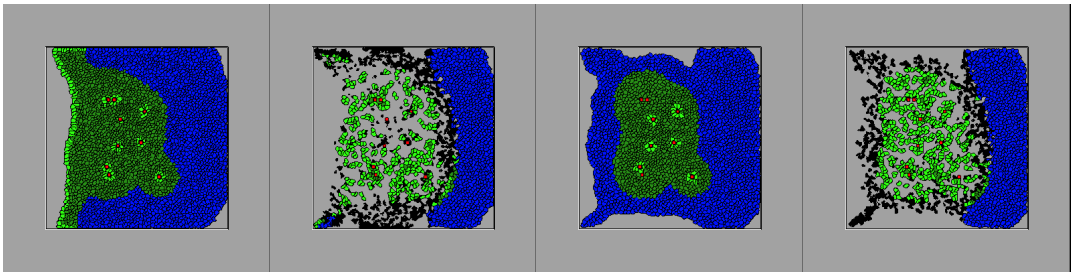

(e) mcs=5000 **(f)** mcs=5130 **(g)** mcs=6000 **(h)** mcs=6130

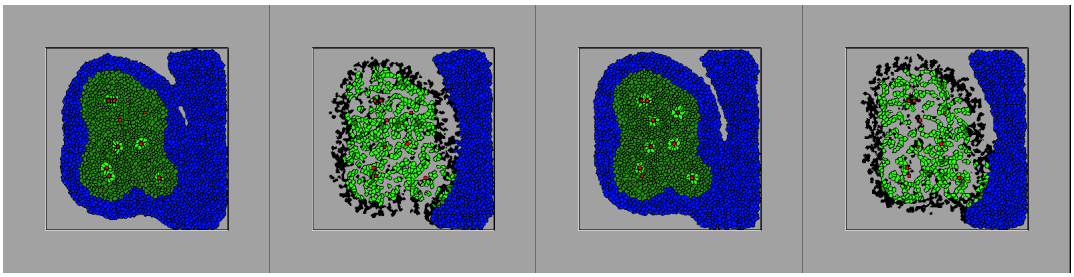

(i) mcs=7000 **(j)** mcs=7130 **(k)** mcs=8000 **(l)** mcs=8130

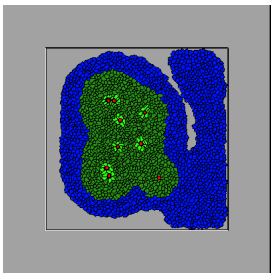

(m) mcs=9000

Figure 6.12: *These figures show the results of a course of chemotherapy in which the drug only kills tumour cells in the G1 phase of the cell cycle. Proliferative cells are light green, resting cells are dark green, quiescent cells are blue, necrotic cells are black, and blood vessels are red. Figures (b), (d), (f), (h), (j) and (l) show how much of the tumour the drug was able to reach in a lethal dose. Figures (c), (e), (g), (i) and (k) show the regrowth of the tumour immediately before the next dose. Figure (m) shows the final steady state tumour after the course of drug therapy. As can be seen, the surviving cells in the S, G2 or M phase of the cell cycle were enough to prevent the elimination of the tumour after six doses of drug treatment.*

6.2.4 Discussion

This chapter presented a multi-scale, discrete model of a vascularised tumour with necrosis and quiescence before the onset of angiogenesis using CompuCell3D. This software described each cell as a group of connected pixels, also called lattice sites. Growth was implemented by increasing the target number of pixels for each cell and the simulation attempted to reach and maintain this volume. The cells were divided into the small, medium and large categories depending upon their volume. Age-structure was given to each cell through the use of an age counter, which increased with each MCS. The age of cells is dependent upon the cell cycle: G1, S, G2 or M. Blood vessels were randomly distributed throughout the domain and oxygen was secreted from them. Each simulation began with a single proliferative tumour cell to represent the cancerous mutation of a healthy cell within the organism.

The first results section showed the growth of a tumour from a single cell, which demonstrated the heterogeneous nature of the cells with regard to age and size. It was found that the majority of cells were in the small size category because of the spatial inhibition which prevented them from growing further. Figure 6.3(d) showed that most of the cells on the periphery of the tumour were in either the large or medium size category, which happened because the proliferating cells on the invasive front entered quiescence. This can be seen in the far left corner of Figure 6.2(c). The cells had enough oxygen provided by the local tissue but eventually used up this supply and were too far from the blood vessels to remain proliferative. This same idea can be seen in age structure. Figure 6.4 showed the cells on the periphery tended to be further in the cell cycle, with the majority of cells in the earliest G1 phase. This was again caused by the induction of quiescence, in which the cell cycle arrested because the microenvironment did not favour division.

This heterogeneity of the tumour population was then explored in other simulations.

The oxygen consumption requirements for cells of different sizes were varied to examine how this would affect the overall growth and invasion of the tumour. The assumption that larger cells required more oxygen was compared to a simulation in which the oxygen requirements were homogenous for all cells. It was shown that the number of proliferative, resting and necrotic cells remained the same, but a large difference was observed in the quiescent population. Large oscillations in the quiescent cell populations were shown to be the result of small cells. The parameter change had created a change in the timing between quiescent cells at the edge of the tumour becoming necrotic and resting cells becoming quiescent. Also, it was seen in Figure 6.8 that it is possible for quiescent cells to be surrounded by resting cells or necrotic cells to be surrounded by quiescent cells. This is important because the necrotic cells can have a destructive effect upon surrounding cells, which is not modelled here.

After the development of the age and space structure, the model was used to explore anti-cancer therapies, through the use of a chemotherapy drug. Firstly, a single dose of chemotherapy was demonstrated, which acted uniformly on all cells. The majority of cells were killed, which can allow the drug to diffuse further in the domain in future doses. However, it also meant that the oxygen supply can reach cells at the edge of the tumour to return them to a proliferative state. Therefore, a course of treatment must overcome the renewed growth of cancer cells to allow it to completely eradicate the tumour cells. The next simulations went on to explore how a course of treatment can eliminate a tumour or result in its resurgence.

The tumour can be eliminated by chemotherapy if the drug is able to reach all of the cells in a lethal dose. However, if the course of treatment is completed but tumour cells still

remain in the tissue the cancer is able to regenerate because of the space and resources available to it. By adjusting the lethality of the drug it was possible to explore how the drug can be used to eliminate the tumour. This has implications for clinical therapy as, with further development of the model to increase biological relevance, it can be used to determine individual treatment plans for patients. Chemotherapy is destructive to several functions in the body and a patient's recovery could be greatly improved by a model which can predict the minimum number of doses required to cure the patient.

The stage of the cell cycle in which cells reside during chemotherapy can have a great effect on the lethality of the drug. Therefore, the next simulations examined how cells in the later stages of the cell cycle can have immunity to the drug and what effect this has on the course of treatment. Cells that were saved from death by the drug were seen to proliferate in between treatments, which led to a quicker re-growth of the tumour cell population and made it difficult for the drug to diffuse to the edge of the domain.

This model has many avenues down which it can be extended. One extension would be to improve the description of the surrounding tissue. This model regards it as a homogeneous entity but it is possible to include many more details. For example, the tumour invasion can be modelled through the secretion of a matrix degrading enzyme. This would mean that the tumour would grow in different shapes, perhaps producing finger-like structures. Chemotherapy may also create more than one tumour mass by separating parts of the original tumour and may lead to metastasis. The effect of necrosis has not been directly included in the model. Here, necrotic cells were created because of a lack of oxygen and the cells would diminish in size until they disappeared from the domain. However, necrotic cells can have a harmful effect upon surrounding tissue which can change how the tumour grows. Another part of the host that could be modelled is the immune response to the tumour. This has been simulated in several continuum models

such as Matzavinos et al. (2004), where it was shown that the immune system can be a factor in cancer dormancy. As cancer cells divide they develop more and more mutations, which lead to more aggressive phenotypes. These phenotypic changes can result in: an increase in motility, a faster cell cycle, reductions in the nutrients needed to pursue division, a resistance to the immune system and a resistance to drugs. Another way to implement multiple cell lines is with the inclusion of stem, progenitor and mature cells, which was seen in the previous chapter.

It is hoped that the development of this type of model can accurately simulate the growth of a tumour *in vivo*. This could be used to test treatments and therapies *in silico*, which could later be used to treat patients. It may also be possible to simulate patient specific tumours, which can lead to individualised treatment plans to cure their cancer.

Chapter 7

Conclusions and Future Directions

This thesis has sought to gain a better understanding of the processes of cancer growth and invasion in the human body through the use of mathematical modelling. The adhesion between tumour cells is known to be an important factor in the invasion processes and, the E-cadherin/β-catenin pathway can govern these cell-cell interactions, discussed in Chapter 4. Chapter 5 focuses on the recent development in the study of cancer which found that, like normal human tissues, tumours may have a stem, progenitor and mature cell lineage structure. This has led to the cancer stem cell hypothesis which may have important ramifications for the development, growth and invasion of tumours. Chapter 6 looks at another heterogeneity within tumours. A cancer population will all be at different stages in the cell cycle and will be different sizes. Therefore, a model of tumour growth was developed with these features in order to study the impact they have on the system.

Chapter 4 explored the E-cadherin/β-catenin pathway within cells and studied how this

intracellular behaviour can be affected by intercellular activities. Firstly, the intracellular reaction kinetics of the pathway found in Ramis-Conde et al. (2008b) were extended to examine its spatio-temporal dynamics. This model included the diffusion and active transport of β-catenin as a way to represent its movement to the boundary upon cell-cell contact, its movement away from the boundary into the cytoplasm and then movement to the nucleus upon cell-cell detachment. The model in one cell was then extended to show β-catenin dynamics within two cells that come into contact with each other. This spatio-temporal modelling of the E-cadherin/β-catenin pathway can be improved by the inclusion of biological data from experiments which uses live immuno-fluorescence imaging to mark the position of proteins within the cells. To better represent the movement of proteins within the cell, it is also possible to include stochasticity to the model.

Later in the chapter, a novel reaction kinetics model of sub-cellular E-cadherin/β-catenin dynamics was developed which included more than one conformation of the β-catenin protein within cells. The different conformations determined whether the protein can perform roles in adhesion, transcription or both. The ODE system was shown to have steady states that corresponded with the presence of Wnt signalling. The results showed that this system, with multiple conformations of β-catenin, was able to replicate previous models. It could also be used to explore how this protein can interact with both adhesion and transcription systems and what effect it can have on tumour invasion.

A further examination of the E-cadherin/β-catenin pathway was done using biological experimentation. Immunofluorescence was used to measure the concentration of β-catenin within cells which were grown to different confluences. Madin-Darby Canine Kidney (MDCK) cells were chosen for experimentation because of their fast growth rate and because they are representative of human epithelial cells. The cells were grown

on plates and were fixed in paraformaldehyde when they reached the desired confluence. Immunostaining was carried out to mark the β-catenin for use in fluorescent microscopy. The images were then analysed with the Volocity software package. The *in vitro* experiment results showed that cells at 100% confluence had a lower percentage of β-catenin in the nucleus and a higher percentage at the membrane than the cells which were grown to 40% confluence. This is because the cells that were at high density were squeezed together and were allowed to form cell-cell adhesion bonds, which replicates an epithelial layer *in vivo*. However, the cells that were 40% confluent were not densely packed together and had more space to migrate and divide. Therefore, the density of cells, and pressure created from it, is an important factor in the sub-cellular E-cadherin/β-catenin dynamics. This idea was implemented later in this thesis using the idea of spatial inhibition. This could be explored further by experimentation using live immunofluorescence imaging techniques to see how the β-catenin dynamics can change over time as the cell density increases.

Chapter 5 explored the cancer stem cell hypothesis in solid tumour growth. As a basis for PDE and discrete models, a lineage structure ODE model of the hematopoeitic system with the inclusion of a leukaemic population of blood cells was examined. Following this, a discrete model of tumour growth with stem cells and mature cells was created in CompuCell3D to explore how a lineage structure can have an effect on tumour growth that is spatially structured. Stem cells took a much longer time to divide but were able do so an unlimited number of times. However, mature cells divided quickly but could only divide a fixed number of times before the cell went through apoptosis. This model was used to show how the spatial inhibition of cancer stem cells by mature cancer cells could result in a steady state tumour size. However, the death of cells by external forces such as the immune system or cancer therapy could result in a loss of spatial inhibition

of the stem cell population which would allow more chances for symmetric division and an overall increase in the tumour size. Therefore, attempts to treat cancer could mean a temporary decrease in the cancer cell population, but allow for the creation of more stem cells which can give rise to a greater population of mature cells when the treatment stops. This model has many possible directions for extension.

The ODE models of lineage structure showed that there was no difference between one progenitor stage and many progenitor stages as the steady states would converge to a large mature population with very small numbers of stem and progenitor cells. However, this assumed that the cells were part of the blood system and were well mixed. However, it would be interesting to examine the case of a cancer cell line with multiple maturation stages in a solid tumour, which has spatial heterogeneity. The inclusion of more than one cell line where one phenotype is more aggressive than the other would allow for a description of cancer invasion driven by stem or progenitor cell mutations. This can give rise to more malignant mature cancer cells. Other modelling features that could be incorporated include: a cell size structure, which can be governed by the maturation stage or not; a more realistic version of the cell cycle to give an age structure; the inclusion of a nutrient field, such as oxygen; a direct representation of the immune system and cancer therapies; vascularised tumour growth; and interactions between tumour cells and the extra cellular matrix. Some of these features are implemented in chapter 6 to a vascularised tumour growth model, but the most interesting addition to this model would be the inclusion of an oxygen concentration. This would allow for the simulation of tumour spheroids with a necrotic core, quiescent zone and a proliferating rim. The model would describe the stem cells on the outer edge of a tumour, rather than in the centre as described here. It could be used to explore how stem cells could be the driving force behind invasion and metastasis.

To explore lineage structure growth in solid tumours further, a PDE model was developed with two cancer cell populations: stem and mature. Each of these cell types were either in the proliferative or quiescent state, which was decided by the local density of cells. The important parameter in this model is the fraction of self-renewal, which determines what percentage of daughter cells are of the same type as the mother cell. This is important because this parameter decides if the stem cell population increases rapidly, slowly or not at all. The results of the PDE model showed that there was a clustering of stem and mature quiescent cells around proliferating rim.

The cancer stem cell hypothesis is an exciting idea that may have many clinical ramifications. If it is true that only a small population of a tumour has unlimited replicative potential then the identification and extermination of these cells must the highest priority. Therefore, it is hoped that the mathematical models presented here can be a first step towards developing treatments which are less invasive and harmful to patients.

In Chapter 6, a discrete model of vascularised tumour growth was created in CompuCell3D. The tumour had cells with an age structure, based on the cell cycle, and a size structure. These were governed by two resources: space, for which cancer cells competed; and oxygen, which was secreted from blood vessels and diffused throughout the tissue. These factors determined whether the cell was in a proliferative, resting, quiescent or necrotic state and resulted in a tumour of a steady state size. However, the variation in oxygen requirements of cells based on size led to greater amplitude of oscillations in the quiescent cell population. This model of tumour growth was extended to include cancer therapy. A cancer drug was secreted from the blood vessels and was allowed to diffuse throughout the domain. If the concentration was above a threshold value it was lethal to the cancer cells. Simulations of the elimination and resurgence of the cancer were shown. Simulations were then run to show how the age structure of cells

can alter the efficacy of the drug. It is hoped that this work can lead to the creation of patient specific models, which can find the best treatment plan for each cancer sufferer.

In conclusion, the work presented in this thesis has aimed to study how the development and invasion of solid tumours can be better understood in an effort to find better patient treatments. However, more work is needed to make these models more biologically relevant, in order to fully validate the results.

Bibliography

Alberts, B. (2008). *Molecular Biology of the Cell*. New York : Garland Science.

Andasari, V., Roper, R. T., Swat, M. H., and Chaplain, M. A. J. (2012). Integrating intracellular dynamics using compucell3d and bionetsolver: applications to multiscale modelling of cancer cell growth and invasion. *PLoS One*, 7(e33726).

Anderson, A. R. A. (2005). A hybrid mathematical model of solid tumour invasion: the importance of cell adhesion. *Mathematical Medicine and Biology*, 22:163–186.

Armstrong, N. J., Painter, K. J., and Sherratt, J. A. (2006). A continuum approach to modelling cell-cell adhesion. *J. Theor. Biol.*, 243:98–113.

Ayati, B. P., Webb, G. F., and Anderson, A. R. A. (2006). Computational methods and results for structured multiscale models of tumor invasion computational methods and results for structured multiscale models of tumour invasion. *Multiscale Model. Simul.*, 1:1–20.

Barker, N., van Es, J. H., and Kuipers, J. (2007). Indentification of stem cells in the small intestine and colon by marker gene lgr5. *Nature*, 449:1003–1007.

Basse, B., Baguley, B. C., Marshall, E. S., Joseph, W. R., v. Brunt, B., Wake, G., and Wall, D. J. N. (2003). A mathematical model for analysis of the cell cycle in cell lines derived from human tumours. *J. Math. Biol.*, 47:295–312.

Basse, B., Baguley, B. C., Marshall, E. S., Joseph, W. R., v. Brunt, B., Wake, G., and Wall, D. J. N. (2004). Modelling cell death in human tumour cell lines exposed to the anticancer drug paclitaxel. *J. Math. Biol.*, 49:329–357.

Basse, B., Baguley, B. C., Marshall, E. S., Joseph, W. R., Wake, G., and Wall, D. J. N. (2005). Modelling the flow of cytometric data obtained from unperturbed human tumour cell lines: parameter fitting and comparison. *Bull. Math. Biol.*, 67:815–830.

Bauer, A. L., Jackson, T. L., and Hirowaka, Y. (2007). A cell-based model exhibiting branching and anastomosis during tumor-induced angiogensis. *Biophys. J.*, 92:3105–3121.

Bauer, A. L., Jackson, T. L., and Jiang, Y. (2009). Topography of extracellular matrix mediates vascular morphogenesis and migration speeds in angiogenesis. *PLoS Comp. Biol.*, 5(e1000445).

Blasco, M. A. (2005). Telomeres and human disease: ageing, cancer and beyond. *Nat. Rev. Genet.*, 6:611–622.

Byrne, H. M. and Chaplain, M. A. J. (1996). Modelling the role of cell-cell adhesion in the growth and development of carcinomas. *Math. Comp. Modelling*, 24:1–17.

Chen, S. Y., Hyang, Y. C., Liu, S. P., Tsai, F. J., Shyu, W. C., and Lin, S. Z. (2011). An overview of concepts for cancer stem cells. *Cell Transplant*, 20(1):113–120.

Cho, K.-H., Baek, S., and Sung, M.-H. (2006). Wnt pathway mutations selected by optimal β-catenin signaling for tumorigenesis. *FEBS Lett. 580*, 580:3665–3670.

Clevers, H. (2011). The cancer stem cell: premises, promises and challenges. *Nat Med.*, 17(3):313–319.

COMSOL, A. (2005). *COMSOL Multiphysics User's Guide*. Stockholm.

Daugherty, R. L., Serebryannyy, L., Yemelyanov, A., Flozank, A. S., Yu, H. J., Kosak, S. T., deLanerolle, P., and Gottardi, C. J. (2014). α-catenin is an inhibitor of transcription. *Proc. Natl. Acad. Sci. USA*, 111(14):5260–5265.

Domschke, P., Trucu, D., Gerisch, A., and Chaplain, M. A. J. (2014). Mathematical modelling of cancer invasion: Implications of cell adhesion variablility for tumour infiltrative growth patterns. *J. Theor. Biol.*, 361:41–60.

Drasdo, D. and Hohme, S. (2005). A single cell based-model of tumor growth in-vitro: monolayers and spheroids. *Phys. Biol.*, 2:133–147.

Dukes, J. D., Whitley, P., and Chalmers, A. D. (2011). The mdck variety pack: choosing the right strain. *BMC Cell Biol.*, 12(43).

Dunn, S. J., Appleton, P. L., Nelson, S. A., Näthke, I. S., Gavaghan, D. J., and Osborne, J. M. (2012a). A two-dimensional model of the colonic crypt accounting for the role of the basement membrane and pericryptal fibroblast sheath. *PLoS Comp. Biol.*, (e1002515).

Dunn, S. J., Fletcher, A. G., Chapman, S. J., Gavaghan, D. J., and Osborne, J. M. (2012b). Modelling the role of the basement membrane beneath a growing epithelial layer. *J. Theor. Biol.*, 298:82–91.

Enderling, H., Anderson, A. R. A., Chaplain, M. A. J., Beheshti, A., Hlatky, L., and Hahnfeldt, P. (2009). Paradoxical dependencies of tumor dormancy and progression on basic cell kinetics. *Cancer Res.*, 69:8814–8821.

Friedl, P. and Wolf, K. (2003). Tumour-cell invasion and migration: diversity and escape mechanisms. *Nature*, 3:362–374.

Friedl, P. and Wolf, K. (2008). Tube travel: The role of proteases in individual and collective cancer cell invasion. *Cancer Res.*, 68(18):7247–7249.

Gerard, C. and Goldbeter, A. (2009). Temporal self-organisation of the cyclin/cdk network driving the mammalian cell cycle. *Proc. Natl. Acad. Sci. USA*, 106:21643–21648.

Gerisch, A. and Chaplain, M. A. J. (2008). Mathematical modelling of cancer cell invasion of tissue: Local and non-local models and the effect of adhesion. *J. Theo. Biol.*, 250:684–704.

Giannini, A. L., Vivanco, M., and Kypta, R. M. (2000). α-catenin inhibits β-catenin signalling by preventing formation of a β-catenin/t-cell factor/dna complex. *J. Biol. Chem.*, 275:21883–21888.

Glazier, J. A. and Graner, F. (1993). Simulation of the differential adhesion driven rearrangement of biological cell. *Phys. Rev. E.*, 43(3):2128–2154.

Goldbeter, A. (1991). A minimal cascade model for the mitotic oscillator involving cyclin and cdc2 kinase. *Proc. Natl. Acad. Sci. USA*, 88:9107–9111.

Gottardi, C. J. and Gumbiner, B. M. (2004a). Distinct molecular forms of β-catenin are targeted to adhesive or transcriptional complexes. *J. Cell. Biol.*, 167(2):339–349.

Gottardi, C. J. and Gumbiner, B. M. (2004b). Role for icat (inhibitor of β-catenin and tcf-4) in β-catenin-dependent- nuclear signaling and cadherin functions. *Am. J. Physiol. Cell Physiol*, 286:C747–C756.

Gottardi, C. J., Wong, E., and Gumbiner, B. M. (2001). E-cadherin suppresses cellular transformation by inhibiting β-catenin signaling in an adhesion independant manner. *J. Cell Biol.*, 153(5):1049–1059.

Greenspan, H. P. (1972). Models for the growth of a solid tumor by diffusion. *Stud. Appl. Math.*, 52:317–340.

Greenspan, H. P. (1976). On the growth and stability of cell cultures and solid tumors. *J. Theor. Biol.*, 56(1):229–242.

Hanahan, D. and Weinberg, R. A. (2000). The hallmarks of cancer. *Cell*, 100(1):57–70.

Hanahan, D. and Weinberg, R. A. (2011). Hallmarks of cancer: the next generation. *Cell*, 144(5):646–674.

Hay, E. D. (1995). An overview of epithelio-mesenchymal transformation. *Acta. Anat. (Basel)*, 154:8–20.

Hayflick, L. (1997). Mortality and immortality at the cellular level. a review. *Biochemistry*, 62:1180–1190.

Hester, S. D., Belmonte, J. M., Gens, J. S., Clendenon, S. G., and Glazier, J. (2011). A multi-cell, multi-scale model of vertebrate segmentation and somite formation. *PLoS Comp. Biol.*, 7(e1002155).

Hinck, L., Näthke, I. S., Papkoff, J., and Nelson, W. J. (1994). Dynamics of cadherin/catenin complex formation: Novel protein interactions and pathways of complex assembly. *J. Cell Biol.*, 125(6):1327–1340.

Huber, O., Bierkamp, C., and Kemler, R. (1996). Cadherins and catenins in development. *Curr. Opin. Cell Biol.*, 8:685–691.

Kalluri, R. and Weinberg, R. A. (2009). The basics of epithelial-mesenchymal transition. *J. Clin. Invest.*, 119(6):1420–1428.

Kemler, R., Hierholzer, A., Kanzler, B., Kuppig, S., Hansen, K., Taketo, M. M., de Vries, W. N., Knowles, B. B., and Solter, D. (2004). Stabilization of β-catenin in the mouse zygote leads to premature epithelial-mesenchymal transition in the epiblast. *Development*, 131:5817–5824.

Kim, D., Rath, O., Kolch, W., and Cho, K. (2007). A hidden oncogenic positive feedback loop caused by crosstalk between wnt and erk pathways. *Oncogene*, 26:4571–4579.

Korinek, V. (1998). Depletion of epithelia stem-cell compartments in the small intestine of mice lacking tcf-4. *Nature Genet.*, 19:1–5.

Lane, D. P. (1992). Cancer. p53, guardian of the genome. *Nature*, 358:15–16.

Lanza, R. (2009). *Essentials of stem cell biology*. Academic Press.

Leckband, D. and Sivasankar, S. (2000). Mechanism of homophilic cadherin adhesion. *Current Opinion in Cell Biology*, 12:587–592.

Lee, E., Salic, A., Kruger, R., Heinrich, R., and Kirschner, M. W. (2003). The roles of apc and axin derived from experimental and theoretical analysis of the wnt pathway. *PLoS Biol.*, 1(1):116–132.

Lodish, H., Berk, A., Kaiser, C. A., Krieger, M., Bretscher, A., Ploegh, H., Amom, A., and Scott, M. P. (2012). *Molecular Cell Biology*. W.H. Freeman and Company, 7th edition.

Macklin, P., Edgerton, M. E., Thompson, A. M., and Cristini, V. (2012). Patient-calibrated agent-based modelling of ductal carcinoma in situ (dcis): From microscopic measurements to macroscopic predictions of clinical progression. *J. Theo. Biol.*, 201:122–140.

Macklin, P. and Lowengrub, J. (2007). Nonlinear simulation of the effect of microenvironment on tumor growth. *J. Theor. Biol.*, 245:677–704.

MacSween, R. N. M. and Whaley, K., editors (1992). *Muir's Textbook of Pathology*. Arnold, London, 13th edition.

Matzavinos, A., Chaplain, M. A. J., and Kuznetsov, V. A. (2004). Mathematical modelling of the spatio-temporal response of cytotoxic t-lymphocytes to a solid tumour. *Math. Med. Biol*, 21(1):1–34.

Merks, R. M. H. and Glazier, J. A. (2006). Dynamic mechanisms of blood vessel growth. *Nonlinearity*, 19:1–10.

Merks, R. M. H., Perryn, E. D., Shirinifard, A., and Glazier, J. A. (2008). Contact-inhibited chemotaxis in de novo and sprouting blood-vessel growth. *PLoS Comp. Biol.*, 4(e1000163).

Mirams, G. R., Byrne, H. M., and King, J. R. (2010). A multiple timescale analysis of a mathematical model of the wnt/β-catenin signalling pathway. *J. Math. Biol.*, 60(1):131–160.

Mirams, G. R., Fletcher, A. G., Maini, P. K., and Byrne, H. M. (2012). A theoretical investigation of the effect of proliferation and adhesion on monoclonal conversion in the colonic crypt. *J. Theo. Biol.*, 312:143–156.

Moore, K. A. and Lemischka, I. R. (2006). Stem cells and their niches. *Science*, 311(5769):1880–1885.

Nakata, Y. N., Getto, P., Marciniak-Czochra, A., and Alarcon, T. (2012). Stability analysis of multi-compartment models for cell production systems. *J. Biol. Dynamics*, 6(1):2–18.

Näthke, I. S., Hinck, L., Swedlow, J. R., Papkoff, J., and Nelson, W. J. (1994). Defining interactions and distributions of cadherin and catenin complexes in polarized epithelial cells. *J. Cell Biol.*, 125(6):1341–1352.

Park, C. H., Bergsaugel, D. E., and McCulloch, E. A. (1971). Mouse myeloma tumor stem cells: a primary cell culture assay. *J. Natl. Cancer Inst.*, 46:411–422.

Pecina-Slaus, N. (2003). Tumor suppressor gene e-cadherin and its role in normal and malignant cells. *Cancer Cell Int.*, 3:17.

Pitt-Francis, J., Pathmanathan, P., Bernabeu, M. O., Bordas, R., Cooper, J., Fletcher, A. G., Mirams, G. R., Murray, P., Osborne, J. M., Walter, A., Chapman, S. J., Garny, A., van Leeuwen, I. M. M., Maini, P. K., Rodriguez, B., Waters, S. L., Whiteley, J. P., Byrne, H. M., and Gavaghan, D. J. (2009). Chaste: A test-driven approach to software development for biological modelling. *Comp. Phys. Comm.*, 180(12):2452–2471.

Polakis, P. (1999). The oncogenic activation of β-catenin. *Curr. Opin. Genet. Dev.*, 9(1):15–21.

Poplawski, N. J., Agero, U., Gens, J. S., Swat, M., Glazier, J. A., and Anderson, A. R. A. (2009). Front instablilities and invasiveness of simulated avascular tumors. *Bull. Math. Biol.*, 71:1189–1227.

Poplawski, N. J., Shirinifard, A., Agero, U., Gens, J. S., Swat, M., and Glazier, J. A. (2010). Front instabilities and invasiveness of simulated 3d avascular tumors. *PLoS One*, 5(e10641).

Powathil, G. G., Gordon, K. E., Hill, L. A., and Chaplain, M. A. J. (2012). Modelling the effects of cell-cycle heterogeneity on tumour response to chemotherapy: Biological insights from a hybrid multi-scale cellular automaton model. *J. Theo. Biol.*, 208(1).

Ramis-Conde, I., Chaplain, M. A. J., and Anderson, A. R. A. (2008a). Mathematical modelling of cancer cell linvasion of tissue. *Math. Comp. Modelling*, 47:533–545.

Ramis-Conde, I., Chaplain, M. A. J., Anderson, A. R. A., and Drasdo, D. (2009). Multi-scale modelling of cancer cell intravasation: the role of caherins in metastasis. *Phys. Biol.*, 6(016008).

Ramis-Conde, I., Drasdo, D., Anderson, A. R. A., and Chaplain, M. A. J. (2008b). Modeling the influence of the e-cadherin-β-catenin pathway in cancer cell invasion: A multiscale approach. *Biophysical Journal*, 95:155–165.

Reya, T., Morrison, S. J., Clarke, M. F., and Weissman, I. L. (2001). Stem cells, cancer, and cancer stem cells. *Nature*, 414:105–111.

Romagnani, P. (2013). Of mice and men: the riddle of tublular regeneration. *J. Pathology*, 229(5):641–644.

Serrels, A., Timpson, P., Canel, M., Schwarz, J. P., Carragher, N. O., Frame, M. C., Brunton, V. G., and Anderson, K. L. (2009). Real-time study of e-cadherin and membrane dynamics in living animals: Implications for the disease modeling and drug development. *Cancer Res.*, 69(7):2714–2719.

Shahriyari, L. and Komarova, N. K. (2013). Symmetric vs. asymmetric stem cell divisions: an adaptation against cancer. *PLoS One*, 8(e76195).

Shirinifard, A., Gens, J. S., Zaitlen, B. L., Poplawski, N. J., and Swat, M. (2009). 3d multi-cell simulation of tumor growth and angiogensis. *PLoS One*, 4(e7190).

Stiehl, T. and Marciniak-Czochra, A. (2010). Characterization of stem cells using mathematical models of multistage cell lineages. *Math. Comp. Modelling*, 53:1505–1517.

Stiehl, T. and Marciniak-Czochra, A. (2012). Mathematical modeling of leukemogenesis and cancer stem cell dynamics. *Math. Model. Nat. Phenom.*, 7(1):166–202.

Sturrock, M., Terry, A. J., Xirodimas, D. P., Thompson, A. M., and Chaplain, M. A. J. (2010). Spatio-temporal modelling of the hes1 and p53-mdm2 intracellular signalling pathways. *J. Theo. Biol.*, 273:15–31.

Sun, Y.-C. (2009). Examination of effects of gsk3β phosphorylation, β-catenin phosphorylation, and β-catenin degradation on kinetics of wnt signaling pathway using computational method. *Theor. Biol. Med. Mod.*, 6(13).

Swat, M., Hestor, S., Heiland, R., Zaitlen, B., and Glazier, J. (2009). Multi-cell simulations of development and disease using the compucell3d simulation environment. *Methods Mol Biol*, 500:361–428.

Swat, M., Thomas, G. L., Belmonte, J. M., Shirinifard, A., Hmeljak, D., and Glazier, J. A. (2012). Computation methods in cell biology. *Meth. Cell Biol.*, 110:325–366.

Tago, K., Nakamura, T., Nishita, M., Hyodo, J., Nagai, S., Murata, Y., Adachi, S., Ohwada, S., Morishita, Y., Shibuya, H., and Akiyama, T. (2000). Inhibition of wnt signaling by icat, a novel β-catenin-interacting protein. *Genes Dev.*, 14(1741-1749).

Tan, C. W., Gardiner, B. S., Layton, M. J., Smith, D. W., and Burgess, A. W. (2011). Wnt signalling pathway parameters for mammalian cells. *PLoS One*, 7(2).

Terry, A. J., Sturrock, M., Dale, J. K., and Chaplain, M. A. J. (2011). A spatio-temporal model of notch signalling in the zebrafish segmentation clock: Conditions for synchronised oscillatory dynamics. *PLoS One*, 6(2).

Turner, S. and Sherratt, J. A. (2002). Intercellular adhesion and cancer invasion: a discrete simulation using the extended potts model. *J. Theor. Biol.*, 216:85–100.

Tyson, J. J. and Novak, B. (2001). Regulation of the eukaryotic cell cycle: molecular antagonism, hysterisis, and irreversible transitions. *J. Theor. Biol*, 210:249–263.

Tyson, J. J. and Novak, B. (2003). Modelling the controls of the eukaryotic cell cycle. *Biochem. Soc. Trans.*, 31:1526–1529.

Tyson, J. J. and Novak, B. (2004). A model for restriction point control of the mammalian cell cycle. *J. Theor. Biol.*, 230:563–579.

van Leeuwen, I. M. M., Byrne, H. M., Jensen, O. E., and King, J. R. (2007). Elucidating the interactions between the adhesive and transcriptional functions of β-catenin in normal and cancerous cells. *J. Theo. Biol.*, 247:77–102.

van Leeuwen, I. M. M., Mirams, G. R., Walter, A., Fletcherand P. Murray, A., Osborne, J., Varma, S., Young, S. J., Cooper, J., Doyle, B., Pitt-Francis, J., Momtahan, L., Pathmanathan, P., Whiteley, J. P., Chapman, S. J., Gavaghan, D. J., Jensen, O. E., King, J. R., Maini, P. K., Waters, S. L., and Byrne, H. M. (2009). An integrative computational model for intestinal tissue renewal. *Cell. Prolif*, 42:617–636.

Wawra, C., Kuhl, M., and Kestler, H. A. (2007). Extended analysis of the wnt/β-catenin pathway: Robustness and oscillatory behaviour. *FEBS Lett.*, 581:4043–4048.

Weinberg, R. A. (2007). *The Biology of Cancer*. Garland Science.

Wodarz, D. and Komarova, N. (2007). Can loss of apoptosis protect against cancer? *Trends in Genetics*, 23(5):232–237.

Wolf, K., Wu, Y. I., Liu, Y., Geiger, J., Tam, E., Overall, C., Stack, M. S., and Friedl, P. (2007). Multi-step pericellular proteolysis controls the transition from individual to collective cancer cell invasion. *Nat. Cell. Biol.*, 9(8):893–904.

Wright, N. A. (2012). Stem cell identification - in vivo lineage analysis versus in vitro isolation and clonal expansion. *J. Pathology*, 227:255–266.